

D. Hasterok^a, J. Halpin^{b,c}, A.S. Collins^a, M. Hand^a, C. Kreemer^d, M.G. Gard^{a,e}, S. Glorie^a

^aMawson Geoscience Centre and Department of Earth Sciences, University of Adelaide, Adelaide, SA 5005, Australia

^bInstitute for Marine and Antarctic Studies, University of Tasmania, Hobart, TAS 7001, Australia

^cThe Australian Centre for Excellence in Antarctic Science, University of Tasmania, Hobart, TAS 7001, Australia

^dNevada Bureau of Mines and Geology and Seismological Laboratory, University of Nevada, Reno, NV, USA

^eGeoscience Australia, Canberra, ACT, Australia

This manuscript was submitted to Earth Science Reviews on March 18th 2022 and revised on 23 May 2022. This is a non-peer reviewed preprint submitted to EarthArXiv. Subsequent versions of this manuscript may differ. If accepted, the final version of this manuscript will be available via the ‘Peer-reviewed Publication DOI’ link on the EarthArXiv webpage for this manuscript. Please feel free to contact any of the authors; we welcome feedback.

Address all correspondence to D. Hasterok (derrick.hasterok@adelaide.edu.au)

New maps of global geological provinces and tectonic plates

D. Hasterok^{a,*}, J. Halpin^{b,c}, A.S. Collins^a, M. Hand^a, C. Kreemer^d, M. Gard^{a,e}, S. Glorie^a

^a*Mawson Geoscience Centre and Department of Earth Sciences, University of Adelaide, Adelaide, SA 5005, Australia*

^b*Institute for Marine and Antarctic Studies, University of Tasmania, Hobart, TAS 7001, Australia*

^c*The Australian Centre for Excellence in Antarctic Science, University of Tasmania, Hobart, TAS 7001, Australia*

^d*Nevada Bureau of Mines and Geology and Seismological Laboratory, University of Nevada, Reno, NV, USA*

^e*Geoscience Australia, Canberra, ACT, Australia*

Abstract

Accurate spatial models of tectonic plates and geological terranes are important for analyzing and interpreting a wide variety of geoscientific data and developing compositional and physical models of the lithosphere. We present a global compilation of active plate boundaries and geological provinces in a shapefile format with interpretive attributes (e.g., crust type, plate type, province type, last orogeny). The initial plate and province boundaries are constructed from a combination of published global and regional models that we refine using a variety of geoscientific constraints including, but not limited to, relative GPS motions, earthquakes, mapped faults, potential field characteristics, and geochronology. These new plate model show improved correlation to observed earthquake and volcano occurrences within deformation zones and microplates, compared to existing models, capturing 73 and 80% of these criteria, respectively. Deformation zones and microplates only account for 16% of Earth's surface area. We estimate 57.5% of the Earth's surface is covered by oceanic crust, which is a slight increase relative to the most recent seafloor age model. The model of last orogenies agrees well with peaks in the globally summed geochronology data. There is room for improvement in future editions of our global plate and geologic provinces model where basins, ice, or lack of geological data fidelity obscure bedrock geology, particularly in the eastern Central Asian Orogenic Belt, much of Africa, East Antarctica, and eastern Australia. Additionally, some province types—ogens, shields, and cratons that are homogenized within our global scheme—can likely be partitioned into smaller terranes with more precise geodynamic attributes. Despite some of these shortcomings, the digital maps presented here form a self-consistent data standard for adding spatial metadata to geoscientific databases. The database is available on GitHub where the geoscience community can provide updates to improve the models and their contempo-

*Corresponding author

Email address: derrick.hasterok@adelaide.edu.au (D. Hasterok)

raneity as new knowledge is acquired. The files are also released in formats suitable for use in Generic Mapping Tools and GoogleEarth.

Keywords: tectonic plate, tectonic province, orogenic system, orogeny, geodynamics, geospatial analysis

Contents

1	Introduction	4
2	Existing Global Models of Tectonic Plates and Provinces	4
3	Method of Construction	8
3.1	Plate Model	10
3.1.1	Plate Type	13
3.1.2	Plate Boundary Type	13
3.1.3	Ocean–Continent Boundary	15
3.1.4	Oceanic Domain	16
3.2	Global Geologic Province Model	16
3.2.1	Province Type	22
3.2.2	Last Orogeny	24
3.2.2.1	<i>Active Orogens</i>	
	· · · · ·	28
3.2.2.2	<i>Neoproterozoic to Mesozoic Orogens</i>	
	· · · · ·	31
3.2.2.3	<i>Paleo- to Mesoproterozoic Orogens</i>	
	· · · · ·	34
4	Model Evaluation	43
4.1	Ocean–Continent Boundary	43
4.2	Plate Boundaries	45
4.3	Plate Model	45
4.3.1	Comparison with Bird (2003)	46
4.3.2	Comparison with Tomography and Volcanism	47
4.3.3	Uncertain Plate Boundaries	51
4.4	Geologic Province Model	53
4.4.1	Comparison with Matthews et al. (2016) and Merdith et al. (2021) . . .	53

4.4.2	Comparison with CrustX models	55
4.4.3	Last Orogeny	59
4.4.4	Uncertain Province Boundaries	62
4.5	Future Improvements	63

5 Summary 64

1. Introduction

The structural architecture, tectonic environment, and temporal evolution of rocks at the surface of the Earth are frequently correlated with the chemical and physical characteristics of the enclosing lithosphere (Gard et al., 2019b; Artemieva, 2019; Tang et al., 2020; Tetley et al., 2020). As a result, it is useful to have spatially accurate maps of geologic provinces and terrane boundaries that encompass a pragmatically uniform set of common geological characteristics for comparative global studies. Such maps also form the foundation for accurate plate reconstructions (Merdith et al., 2021). While there are some regional models of tectonic provinces that are digital (Artemieva, 2006; Laske et al., 2013), there are few accurate global models easily accessible to the geoscience community built on a multiplicity of comparative attributes that approach self-consistency.

In this paper, we present two basic models: (1) a global set of geologic provinces and (2) a model for present-day plate boundaries. Both models are presented in a vector format with accompanying metadata that can be used to improve and simplify the process of global tectonic data analysis and/or modeling across a diverse range of geoscientific phenomena. These models have been produced using a wide variety of geologic and geophysical data and have been partially validated, wherever possible, using igneous and metamorphic age dates allied with additional geophysical datasets. Our hope is these models can be used as a data standard for common classification across the variety of geological databases that currently exist. The global models presented below are freely available in open-source and form a basic digital architecture that can be progressively updated as geological data and interpretations continue to improve.

2. Existing Global Models of Tectonic Plates and Provinces

Previous global plate and province models have been published that incorporate tectonic setting, juvenile age, or thermotectonic age (e.g., Artemieva, 2006; Goutorbe et al., 2011; Laske

25 et al., 2013; Szwilus et al., 2019). Ideally, the digital nature of these maps makes them easy
26 to use and allows one to add desirable attributes to underlying datasets. However, the raster
27 format of these models is often an impediment to accurate spatial analysis at or near province
28 boundaries due to their low resolution and pixelated nature. Even though some plate and
29 province maps include age and province type, it may not be possible to separate individual
30 terranes that potentially have distinctive chemical and physical characteristics. For example, a
31 terrane-type map (e.g., Laske et al., 2013) can be useful for identifying data within a volcanic
32 arc setting, but it can be difficult to separate individual volcanic arcs to compare temporal and
33 spatial geochemical patterns that illuminate the geodynamic character. Furthermore, while
34 some of these maps have been included in peer-reviewed publications as part of global studies,
35 it is unclear to what degree the maps themselves have been examined in detail because the un-
36 derlying geological data used to construct the maps is not available to the geological community.
37 In some cases, it is difficult to obtain digital versions from the authors, making it challenging
38 to validate or improve the models as a geoscientific community and achieve widespread use.
39 As a consequence, some of these maps of global geological provinces are essentially artistic and
40 have opaque underlying rationale that cannot be interrogated.

41 A few global shapefiles of province polygons do exist (Klett et al., 1997; Torsvik and Cocks,
42 2016; Matthews et al., 2016), but they cannot be accurately matched to the province boundaries
43 as they are identified in regional studies. For example, the Klett et al. (1997) proposed geologic
44 provinces were developed to assess global hydrocarbon reserves. Therefore, a narrow perceived
45 attribute rather than broad actual attributes were used to delineate geological provinces. The
46 models by Torsvik and Cocks (2016), Matthews et al. (2016), and Merdith et al. (2021) are based
47 on tectonic blocks as they were developed to perform plate reconstructions (Figure 1b), but they
48 are typically shape-defined by contemporary global geography. Some terrane boundaries agree
49 well with published models (e.g., Africa, McCourt et al. (2013); South America, Ibañez-Mejia
50 et al. (2011)), while others appear greatly simplified and/or do not closely follow geophysical
51 trends for reasons that are not given (e.g., western United States, Hasterok and Chapman
52 (2007)). Furthermore, many models are time diluted. For example, models by Matthews et al.
53 (2016) and Merdith et al. (2021) were developed for reconstructions to 400 Ma and 1000 Ma,
54 respectively. As a result, most Mesoproterozoic and older regions are not divided into separate

55 terranes except where they behave as separate entities during the plate model timeframe, despite
56 a wealth of data that would otherwise allow the organization of these older participants to be
57 illuminated.

58 In addition to the lack of globally a comprehensive and self-consistent scheme for the de-
59 piction of geological provinces, there are still ambiguities and lack of self-consistency in con-
60 temporary plate tectonic maps. [Bird \(2003\)](#) released a widely used plate boundary shapefile
61 (Figure 1a), which built upon the pioneering work by [Minster and Jordan \(1978\)](#); [DeMets](#)
62 [et al. \(1990\)](#). Since its release, several additional microplates have been proposed, generally
63 on the basis of GPS motion data. The new proposed microplates are the Adria Microplate
64 ([Battaglia et al., 2004](#); [Breton et al., 2017](#)), Danakil Microplate ([Eagles et al., 2002](#); [McClusky](#)
65 [et al., 2010](#)), Yakutat Microplate ([Fletcher and Freymueller, 1999](#); [Bruhn et al., 2012](#)), Sierra
66 Nevada Microplate ([Dixon et al., 2000](#); [Schweickert et al., 2004](#)), several microplates around
67 the Caribbean ([DeMets and Wiggins-Grandison, 2007](#); [Sun et al., 2020](#)), and a few microplates
68 on the Somali Plate ([Horner-Johnson et al., 2005, 2007](#); [Saria et al., 2014](#); [Stamps et al., 2021](#))
69 and African Plate ([Njoroge et al., 2015](#); [Wedmore et al., 2021](#)). The Bird model is also missing
70 a few microplates proposed at the time of publication including the Capricorn Microplate and
71 Indo-Australian Deformation zone ([Royer and Gordon, 1997](#)), the Coiba and more recently as-
72 sociated Malpelo Microplates ([Hardy, 1991](#); [Zhang et al., 2017](#)). The Bird model included some
73 plate boundary deformation zones, but many zones of known deformation were excluded from
74 the model (e.g., [Gordon, 1998](#)). Additional improvements can be gained by incorporating more
75 recent kinematic models of strain within plate boundaries to discriminate between discrete and
76 more continuously deforming zones ([Kreemer et al., 2014](#)).

77 Beyond the global models discussed above, there exists a plethora of regional geologic
78 province and terrane maps that are downloadable. Many of these models are more precise
79 because they may incorporate a variety of datasets as constraints (e.g., topography, bedrock
80 geology, seismic tomography, and crustal faults or shear zones), but they are poorly designed
81 for digital processing as they are only available as raster images in papers despite many be-
82 ing created using geographic software. While these depictions are sufficient for presentation
83 in publications, the rationale and metadata are generally not available for scrutiny. Conse-
84 quently, interpreted tectonic boundaries are often inconsistent between publications, especially

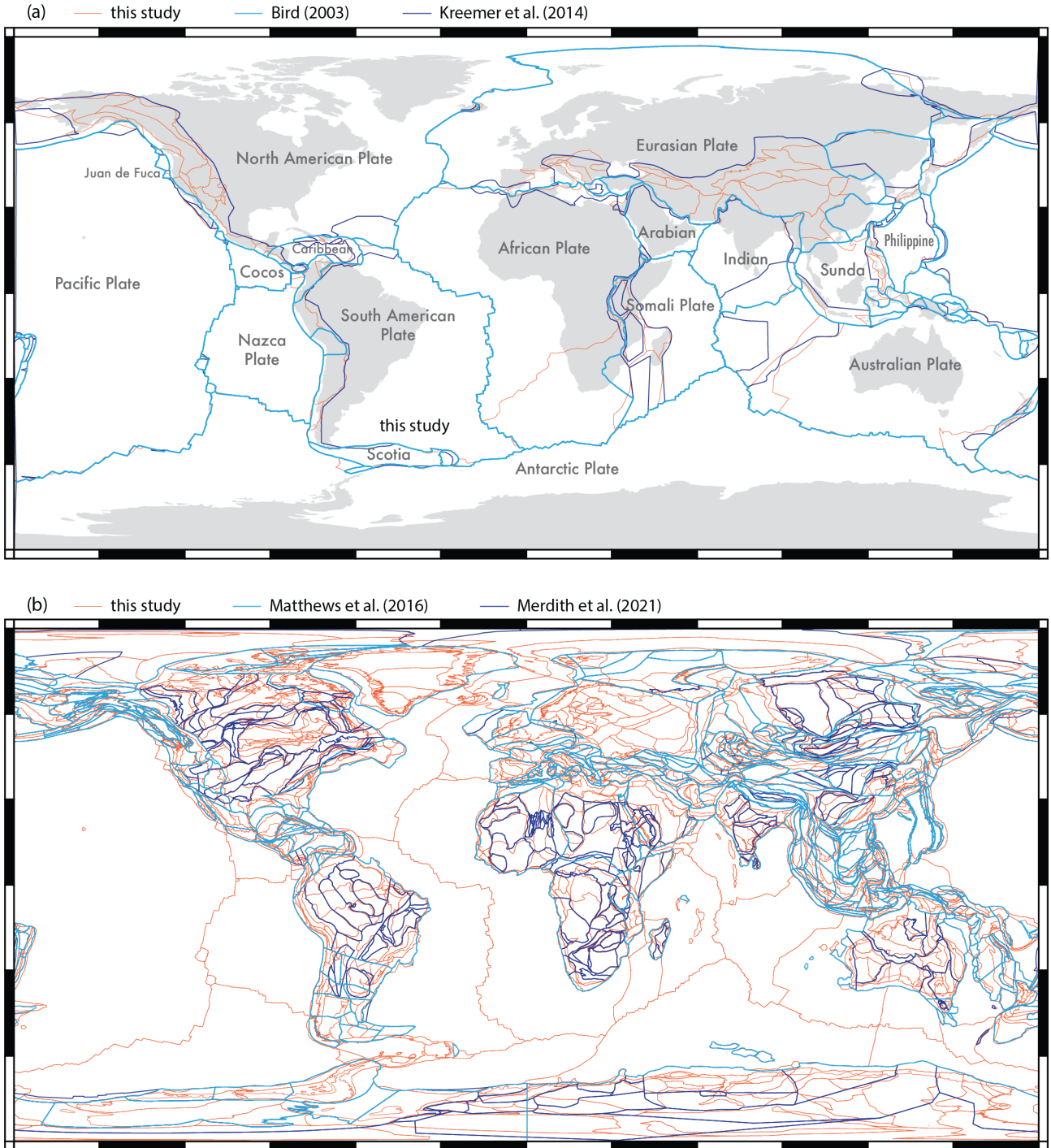


Figure 1: Tectonic plate and geologic province models. (a) A comparison between the [Bird \(2003\)](#) plate model, limit of modeled plate boundary zones ([Kreemer et al., 2014](#)) and the plate model from this study. Note that the limit of the deformation model domain is not an exact limit of the deformation, in many cases wider than the true deformation zone. (b) A comparison between the [Matthews et al. \(2016\)](#) and [Merdith et al. \(2021\)](#) plate models and province models from this study.

when boundaries are envisaged beneath cover. In many publications (e.g., Gee and Stephen-
son, 2006; Xu et al., 2016; He et al., 2018), a province or terrane map is often secondary to
the main point of the paper, and boundary definition may be schematic rather than rigorous
and is commonly simply adopted from pre-existing publications. An obvious example is the
depiction of the Sahara Metacraton (Figure 14 and Figure 1 of Liégeois et al., 2013; Kwékam
et al., 2020, respectively). Furthermore, the locations and level of detail lack continuity be-
tween publications, such that province boundaries cannot be easily matched up between maps
of adjacent regions, even when apparently depicted in the same map projection scheme (e.g.,
wei Zhou and Murphy, 2005; Blayney et al., 2019).

The objective of the work we present here is to try and smooth deficiencies between existing
models for tectonic province and plate boundaries by delineating a set boundaries in a vectorized
format that incorporates attributes derived from geophysical, geochemical and geochronological
data. Our models represent an attempt to extend tectonic boundaries back to ca. 2.3 Ga
and possibly further in some cases, incorporating numerous existing geologic interpretations.
Some of these interpretations are modified slightly to meet additional observational constraints
from global geophysics, geologic maps and geochronology. Our goal is to create an adaptable
and interactive environment that allows the geoscience community to improve delineation of
geological provinces and the behaviors of their boundaries and interiors during Earth evolution.
In particular, we hope creating an interactive data environment will bring more illumination to
the Mesoproterozoic and older Earth, which hosts a significant fraction of metallic resources.

3. Method of Construction

The maps constructed in this study come from four separate shapefiles—also released in
GMT and KML formats for use in Generic Mapping Tools and GoogleEarth, respectively. These
files include the plate polygons, tectonic province polygons, the oceanic–continental crustal
boundary, and plate boundary types. The ocean–continent boundary and plate boundary
types are both developed in conjunction with the plate polygons. Each of these files contains a
number of attributes that include a variety of contextual information. The metadata for each
file are described in Table 1.

Vector format shapefiles have several advantages over the raster maps that dominate the

Table 1: A description of shapefile attributes for the plate and province files released in this study.

Field name	Field description
<i>Plate polygons</i> (plates.shp)	
id	unique polygon identifier
poly_name	unique polygon name
plate	major plate, includes microplates and deformation zones
plate_id	numeric subplate id
plate_code	subplate abbreviation
subplate	separates microplates and deformation zones from major plates
plate_type	rigid plate, microplate, or deformation zone
crust_type	continental or oceanic crust
sea_name	name of ocean or sea
domain	oceanic domain for geochemical grouping purposes
area	polygon area in square kilometers
plate_ref	reference for initial plate polygon
<i>Plate boundaries</i> (plate_boundaries.shp)	
feature_id	unique boundary segment identifier
feature	name of boundary segment
type	type of boundary segment
plate1 and plate2	subplates on either side of boundary segment
level	assigns an integer value, 1 = major plate boundaries and 2 = minor plate boundaries
comment	specific comments about a boundary segment
length	length of segment in kilometers
<i>Ocean–continent boundary</i> (oc_boundary.shp)	
id	line segment identification number
length	length of segment in kilometers
<i>Province polygons</i> (geologic_provinces.shp)	
id	unique polygon identifier
prov_name	unique province name
prov_type	dominant tectonic character of a tectonic province
prov_group	name for multiple polygons with a shared geological history, may contain multiple tectonic styles
lastorogen	most recent significant orogenic event
continent	continent name if on a continent
crust_type	continental, oceanic, or transitional
area	polygon area in square kilometers
comment	specific comments about a province
prov_ref	reference for initial province polygon

existing literature. The polygons and lines created across the four shapefiles are seamless, i.e., they use common boundaries where geologically appropriate. Vectorized data permit multiple attributes to be assigned to each polygon, line, or point, which can be unique. Raster models allow only a single attribute per pixel, often requiring multiple maps (generally from separate studies), which could lead to non-causal juxtaposition of such attributes. For example, slight differences in the boundaries of different attributes from unrelated studies could result in oceanic crust being incorporated into a continental orogenic belt or continental crust being excluded from the same orogenic system. Vector format files are also typically more memory efficient than raster images. Thus the seamless nature of the polygons in this project is a distinct advantage when constructing physical and/or compositional models of the lithosphere.

We recognize the study presented here attempts to do on a global scale, what a large number of studies have done at a variety of subordinate scales. Therefore we are aware of an element of hypocrisy in being somewhat critical of continuity between existing studies. However our goal isn't to be correct, it's to create an environment where decisions about tectonic provinces and their boundaries are globally determined where possible, using the same style of data sets and their interpretation. Where our study differs from predecessors, is the compiled data used is freely available and adoptable by more informed practitioners because the models are available on GitHub (https://github.com/dhasterok/global_tectonics) where community users can correct errors and omission and propose refinements.

3.1. Plate Model

The plate model consists of two separate shapefiles including the plate polygons and the boundary lines (Table 1; Figure 2). The plate shapefiles were created in QGIS using global vector and raster datasets (Table 2). We used the widely-distributed model by Bird (2003) as the initial plate boundaries to construct the shapefile (Figure 1a). Newer models that incorporate proposed past plates and microplates for use with plate reconstruction software such as GPlates were also used for reference (i.e., Zahirovic et al., 2014; Matthews et al., 2016). Although Bird's model is an excellent framework, increased spatial coverage of GPS and an additional 18 years of earthquake observations has improved our ability to recognize additional microplates and identify presently deforming regions. Bird (2003) ignores deformation zones, focusing on rigid plates and microplates. In contrast, our model includes these deformation

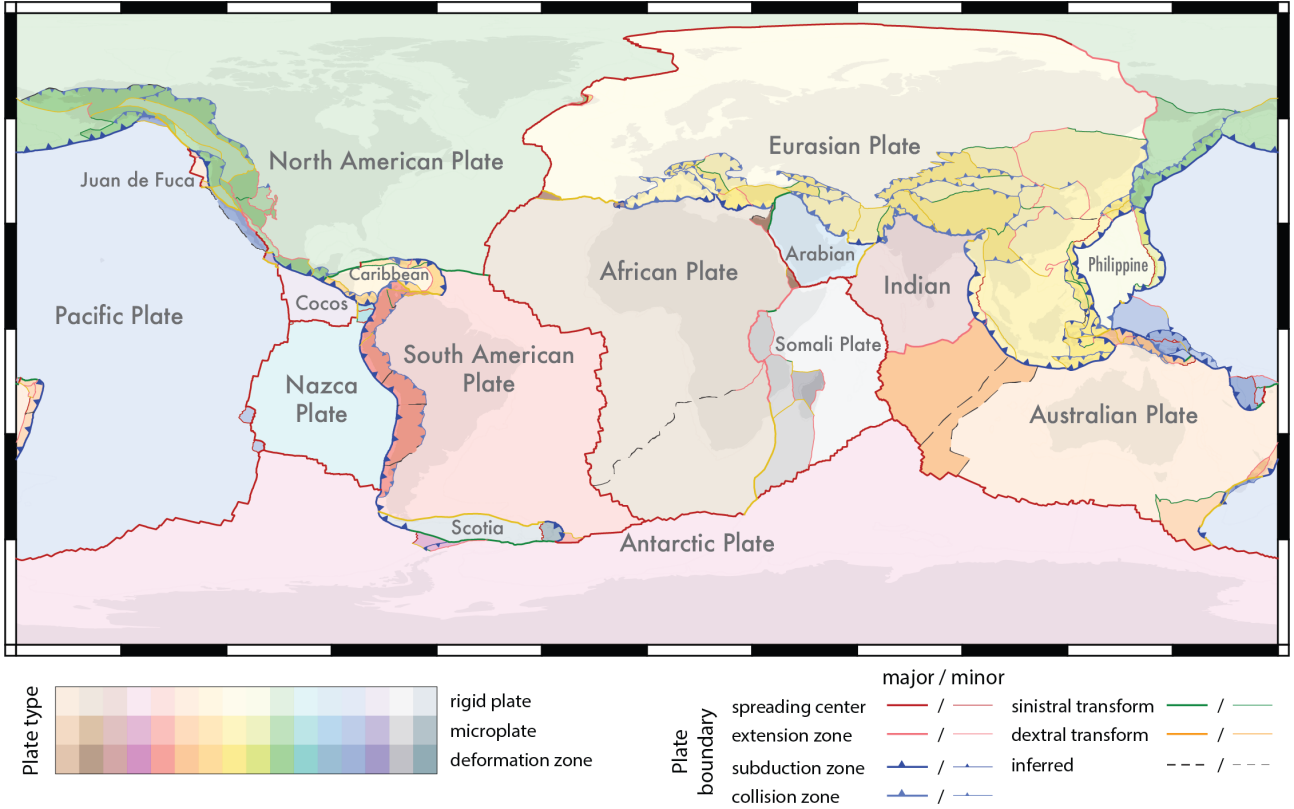


Figure 2: An updated plate model along with the plate boundary types. Microplates and deformation zones are illustrated as darker shades of the same hue as the major plate that they are most closely associated with. Note, geodetic studies often refer to the African Plate as the Nubian Plate, though we opt African as it appears to be more widespread. The case for a San Microplate (southern Africa) is weak, however, we include the proposed boundary in the shapefile (Section 4.3.3).

144 zones as part of the plate boundaries as they accommodate plate motion between the rigid
 145 plates (England and Molnar, 1997; Gordon, 1998; Freymueller, 2010; Kreemer et al., 2003).
 146 The strain-rate model by Kreemer et al. (2014) is also used as an initial constraint on the
 147 boundaries of microplates and deformation zones and as a way to distinguish between the two
 148 (Figure 1). Digital elevation models and global models of active faults have also improved
 149 since Bird’s model (Amante and Eakins, 2009; Styron and Pagani, 2020), which allow for more
 150 accurate and precise positioning of the boundaries.

151 Where there is ambiguity in the location of the plate boundary from topography and its
 152 gradient, the location was chosen to fit with the pattern of recent seismicity (Figure 3). We
 153 found it helpful to compute a spatial histogram of earthquakes because it is easier to identify
 154 zones of high seismicity relative to a simple scatter plot. To produce the histogram, we use global
 155 seismicity M5.5+ for 1970–1990 and M3.5+ for 1990–2020 extracted from the US Geological
 156 Survey’s Advanced National Seismic System (ANSS) global seismic catalog. The earthquake

Table 2: Datasets used to develop and evaluate the plate, plate boundary, and oceanic–continental boundary models.

Region	Data Type	Description	Resolution	Reference
global	plate model	shapefile		Bird (2003)
global	plate model	GPlates shapefile		Zahirovic et al. (2014)
global	plate model	GPlates shapefile		Matthews et al. (2016)
global	earthquakes	1990-2020, <30 km, M3-M5.5		ANSS (2020)
global	earthquakes	1970-2020, <30 km, M5.5+		ANSS (2020)
global	earthquakes	heat map (ANSS data above)	0.1 degree	Global Volcanism Program (2013)
global	volcanic centers			Amante and Eakins (2009)
global	topography	ETOPO1	1 arcmin	
global	topographic gradient ^a	derived from ETOPO1	1 arcmin	Seton et al. (2020)
global	seafloor age	EMC-3D2018_08Sv at 70 km depth	1 arcmin	Debayle et al. (2016), Debayle et al. (2019)
global	shear wave tomography	GEM GAF-DB	2 degree	Styron and Paganini (2020)
global	active faults		various	Kreemer et al. (2014)
global	GPS velocities	computed as a fixed-plate reference frame for each major plate		
global	strain rate		0.25 degree	Kreemer et al. (2014)
Azores Microplate	GPS velocities	global model		DeMets et al. (2010)
Adria Microplate	GPS velocities	case study		Breton et al. (2017)
Alaska and northwest Canada	GPS velocities	case study		Elliott and Freymueller (2020)
Danakil Microplate	GPS velocities	case study		McClusky et al. (2010)
San Microplate	GPS velocities	case study		Njoroge et al. (2015), Wedmore et al. (2021)
Somali Plate	GPS velocities	case study		Saria et al. (2014), Stamps et al. (2021)
Greater Antilles	GPS velocities	case study		DeMets and Wiggins-Grandison (2007), Sun et al. (2020)
Lesser Antilles	magnetics and seismic GPS velocities	case study		Allen et al. (2019)
Coiba and Malpelo Microplates	Seismicity	case study		Zhang et al. (2017)
New Zealand (North Island)	GPS velocities	case study		Shi et al. (2019)
Sierra Nevada Microplate	GPS velocities	case study		Schweickert et al. (2004)
Philippines and East Indonesia	GPS velocities	case study		Zahirovic et al. (2014)
Yakutat Microplate	GPS velocities	case study		Bruhn et al. (2012)

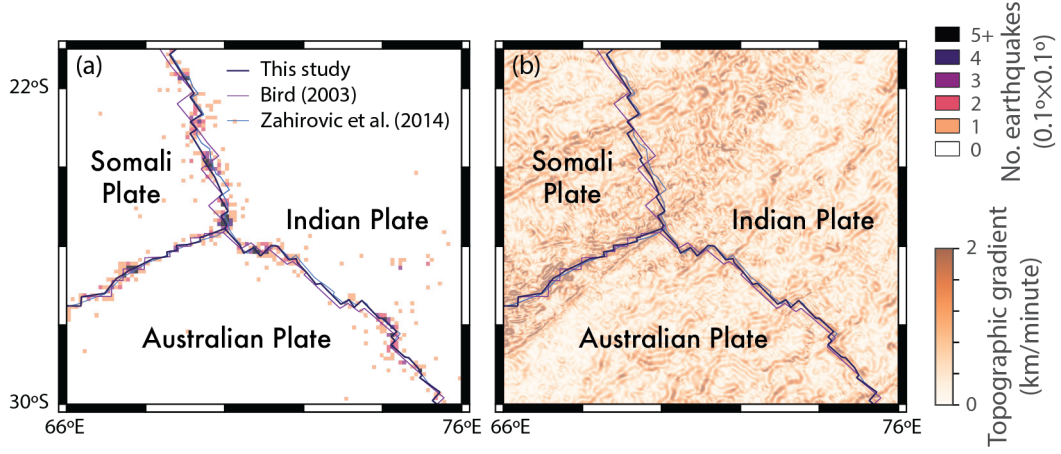


Figure 3: Refining locations of mid-ocean ridges relied heavily on the earthquake catalog, shown as histogram in (a), and topography along with its gradient (b).

157 density accurately traces out much of the mid-ocean ridge systems (Figure 3).

158 *3.1.1. Plate Type*

159 We include metadata with the plate model, including a plate_type field. The following
160 definitions are used to distinguish plate types:

161 **rigid plate**, a region with distinct plate boundaries generally defined by seismicity, little in-
162 ternal deformation, distinct motion relative to several other plates, and generally large
163 area (median 14 million km²);

164 **microplate**, a region with distinct plate boundaries generally defined by seismicity, little in-
165 ternal deformation, motion controlled by surrounding plates, and generally small area
166 (median 0.28 million km²); and

167 **deformation zone**, a zone identified by GPS motions as distinct from, yet controlled by
168 surrounding plates/microplates with significant internal deformation, seismicity, and gen-
169 erally small area (median 0.25 million km²).

170 The microplates and deformation zones are associated with a parent plate for instances
171 where a simpler model is required (Figure 2).

172 *3.1.2. Plate Boundary Type*

173 Plate boundaries are frequently formed by a series of several fault zones that accommodate
174 a portion of the plate motion rather than a single discrete structure. However, there is often
175 one fault zone that accommodates the majority of the motion, which is chosen as the boundary

176 for the plate and plate boundary shapefiles. This choice means that in some cases, the presently
177 most-seismically active fault may not mark the plate boundary as defined here, as it may not
178 have accumulated the greatest displacement. For some extension zones, the deformation is
179 distributed over hundreds of kilometers. In these cases, we chose the boundaries by the major
180 structures that bound the extension.

181 While most models of plate boundaries are limited to three types: convergent, divergent
182 and transform, we opt for six that provide greater contextual information. There are several
183 plate boundary types defined in our model:

184 **subduction zone**, convergent plate boundaries, kinematically active footwall, plate1 field is
185 the upper plate;

186 **collision zone**, convergent plate boundaries, kinematically active hanging wall, plate1 field is
187 the upper plate;

188 **spreading center**, divergent plate boundaries, type reserved for mid-ocean spreading centers
189 (includes transform segments);

190 **extension zone**, divergent plate boundaries, often associated with diffuse extension, plate1
191 field is the upper plate;

192 **dextral transform**, right-lateral transform boundary;

193 **sinistral transform**, left-lateral transform boundary; and

194 **inferred**, unknown boundary types, or location.

195 Our definitions are simplified as they do not include transpressional or transtensional styles,
196 which are classified most commonly as transform boundaries, but these may be considered in
197 future versions.

198 To construct the plate boundary shapefile, we converted the plate polygons to lines and
199 removed duplicate lines. We then split the boundaries so that each line segment represents the
200 boundary between two plates, microplates, or deformation zones (Figure 2). Plate attributes
201 including the boundary type are then added and stylized in QGIS. In order to ensure that
202 thrusts and subduction zone boundaries had the barbs displayed on the upper plate, some lines
203 were topologically reversed in direction.

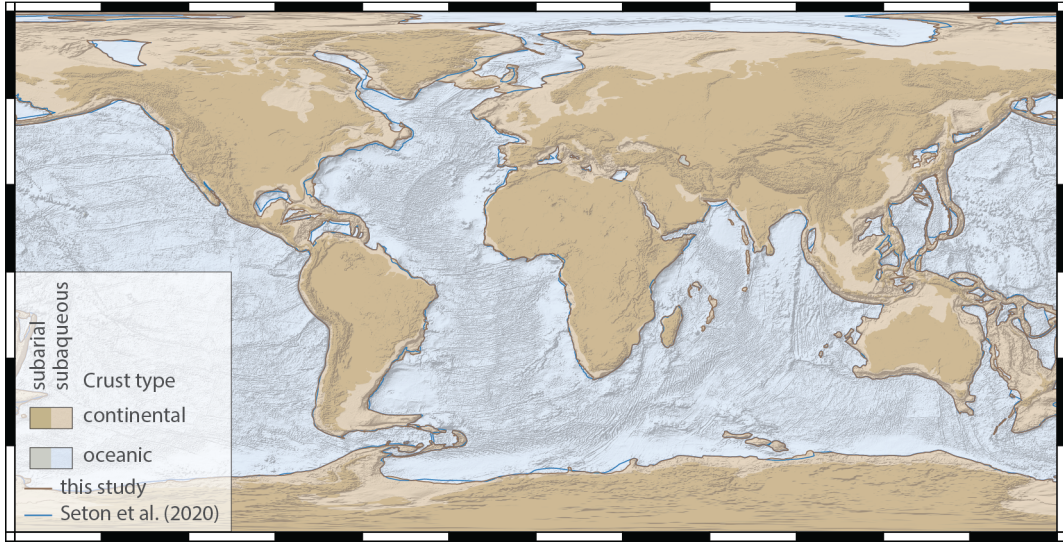


Figure 4: A model of continental and oceanic crustal domains. Plate boundaries as defined in Figure 2.

204 3.1.3. *Ocean–Continent Boundary*

205 We split the plate polygons into continental and oceanic parts because the ocean–continent
 206 boundary is colocated with many plate boundaries. For example, subduction zones generally
 207 form the boundary between plates as well as oceanic and continental regions. However, rifts and
 208 transform boundaries may form boundaries between plates but rarely form ocean–continental
 209 boundaries. Passive margins do not represent plate boundaries but do contain the ocean–
 210 continent transition.

211 A single depth contour cannot be used to identify the ocean–continent transition because the
 212 depth differs from region to region as a result of variations in sediment thickness and isostatic
 213 state. To create the initial model for the ocean-continent boundary, we created a polygon that
 214 defines the global distribution from the global seafloor age model (Seton et al., 2020). This
 215 initial polygon was then modified to provide a better match to the base of steep topographic
 216 gradients (continental slope) computed from ETOPO1 (Figure 4).

217 In reality, the ocean-continent boundary is rarely a sharp discontinuity, rather a transitional
 218 zone that can extend for 10's to 100's of kilometers. However, in many cases it is difficult to
 219 capture at the resolution of this model. Therefore, we place this line at the limit of the transition
 220 on the oceanic side. The province shapefile also includes an additional transitional crustal type
 221 where this boundary is sufficiently wide that it can be easily digitized, though we do not discuss
 222 it further.

223 Intra-oceanic volcanic arcs, such as Izu-Bonin and Marianas, are defined as continental

224 crust. Such arcs are often classified as oceanic crust because they are built upon crust created
225 by seafloor spreading. However, we have reserved the definition of oceanic crust for only
226 regions that have been created by seafloor spreading and not those chemically modified by arc
227 magmatism.

228 The ocean–continent boundary model could be improved with the addition of crustal thick-
229 ness and/or seismic velocity estimates across the ocean–continent transition. Presently, global
230 seismic models are of insufficient resolution to precisely identify the boundary. A compilation
231 of seismic profiles is beyond the scope of the present work.

232 *3.1.4. Oceanic Domain*

233 There appear to be differences in chemistry between ocean basins (domains). For example,
234 [Brandl et al. \(2013\)](#) documents a difference in basaltic geochemistry between the Atlantic
235 and Pacific Oceans, possibly related to temperatures of melt generation. Distinct chemical
236 signatures have long been recognized in the Indian Ocean ([Saha et al., 2020](#)). Back-arc basins,
237 separated from the major oceans by continental ribbons behind subduction zones, tend to
238 contain enriched basalts compared with mid-ocean ridge basalts ([Langmuir et al., 2006](#)). Thus,
239 it is desirable to have a way to quickly divide geoscientific data into these separate domains.

240 For the oceanic-type crustal polygons a mantle chemical domain is included in the plates
241 shapefile attributes table (Table 1). We have separated the oceans into nine separate domains
242 (Figure 5). The domains are intended to make separation of data from the different ocean
243 basins easier for geochemical and geophysical studies. However, the divisions are speculative
244 rather than data driven, specifically the exact boundaries of these chemical domains. The only
245 boundary that has been tested geochemically lies between the Indian and Pacific oceanic mantle
246 ([Pyle et al., 1992](#)). This study used isotopic analyses of Sr, Nd, and Pb to place the Indian–
247 Pacific boundary of Australia along the mid-ocean ridge at approximately 126°E. Similarly,
248 there is also evidence for a more complex chemistry in the seafloor basalts of the Philippine
249 plate compared to the rest of the Pacific ([Hickey-Vargas et al., 2006](#)).

250 *3.2. Global Geologic Province Model*

251 The initial province model was produced by creating a collage of overlapping geological
252 maps from the published literature that varied from the regional to continental scale (Table
253 4). Many of the images were georeferenced in GIS software and vectorized using polygon tools,

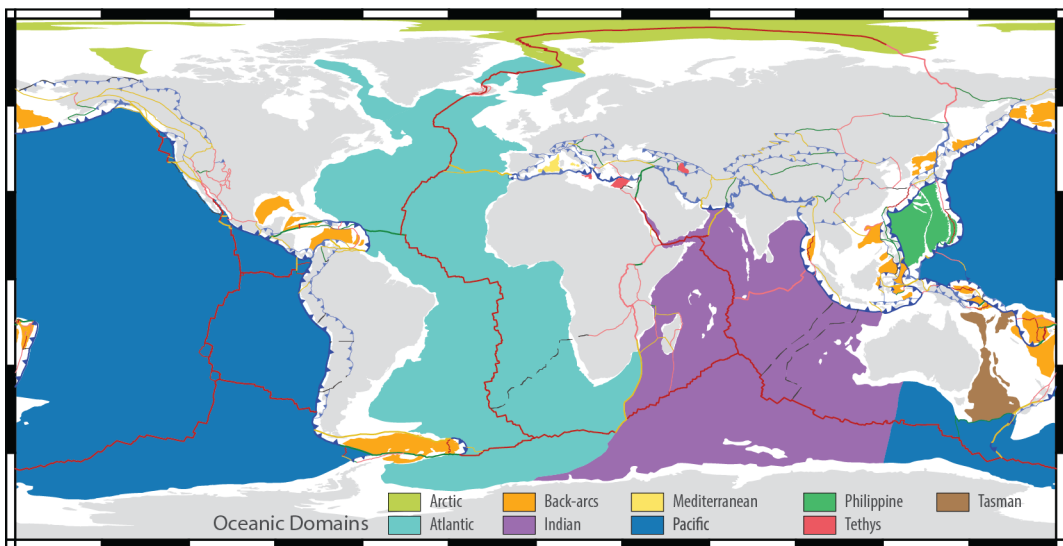


Figure 5: A hypothetical model of mantle chemical domains that source oceanic crust. At present these models are largely untested, but will be refined in future versions using global geochemical datasets.

254 while others were used as a visual reference. Province names are assigned based on commonly
 255 published terms, generally taken from the reference maps themselves (Table 4).

Table 3: Geological and geophysical models used to develop province model.

Region	Data type	Description	Resolution	Reference
global	topography	ETOPO1	1 arcmin	Anante and Eakins (2009)
global	composite gravity	GGM2012	2 arc-min	Balmino et al. (2011)
global	composite magnetics	EMAG2-V3	2 arc-min	Meyer and Saltus (2016)
global	composite magnetics	WDMAMv2	5 km	Lesur et al. (2016)
global	seafloor age		2 arc-min	Seton et al. (2020)
global	volcanic centers			Global Volcanism Program (2013)
global	crustal thickness	Szwilus et al. (2019)	1 degree	
global	active faults	Styron and Pagani (2020)	various	
global	digital lithology	Hartmann and Moosdorf (2012b), Hartmann and Moosdorf (2012a)	0.5 degrees	
global	igneous dates	Gard et al. (2019a)	global geochemical database	Brown and Johnson (2018), updated
global	metamorphic dates	P-T database	DateView	Eglington (2004)
global	metamorphic dates	USGS WEP ^a	1:5,000,000	Persits et al. (1997a)
Africa	surface geology and geologic provinces	USGS WEP ^a	1:2,000,000	Pollastro et al. (1999)
Arabian Peninsula	surface geology and geologic provinces	USGS WEP ^a	1:5,000,000	Wandrey and Law (1998)
South Asia (India)	surface geology and geologic provinces	USGS WEP ^a	1:7,500,000	Schenk et al. (1999)
South America	surface geology and geologic provinces	USGS WEP ^a	1:5,000,000	Gómez-Tapias et al. (2019)
South America	surface geology	CGMW ^b	1:7,500,000	Persits et al. (1997b)
Former Soviet Union	surface geology and geologic provinces	USGS WEP ^a	1:7,500,000	Steinshöner et al. (1999)
China, Southeast Asia, and Australia	surface geology and geologic provinces	USGS WEP ^a	1:2,500,000	Pollastro et al. (1997)
Iran	surface geology and geologic provinces	USGS WEP ^a	1:3,000,000	Pawlewicz et al. (1997)
Europe	surface geology and geologic provinces	USGS	1:7,500,000	Garry and Soller (2009)
North America	surface geology provinces		250 m	Australia (2004)
Australia	magnetic anomaly		830 m	Wynne and Bacchin (2009)
Australia	gravity anomaly			

Table 3: continued.

Region	Data type	Description	Resolution	Reference
Antarctica	bedrock topography	BEDMAP2	1 km	Fretwell et al. (2013)
Antarctica	free-air and Bouguer gravity anomalies	ANTGG	1.0 km	Scheinert et al. (2016)
Antarctica	shear wave tomography	AN1	4 arcmin	An et al. (2015)
Antarctica	magnetic anomaly	ADMAP2	7 km	Golynsky et al. (2018)
Antarctica	mantle gravity anomaly		5 km	Baranov et al. (2017)
Antarctica	crustal thickness	gravity and seismic based	1 degree	Baranov et al. (2017)
Antarctica	crustal thickness	satellite gravity based	0.25 degrees	Llubes et al. (2018)
Antarctica	crustal thickness	seismic methods	4 arcmin	An et al. (2015)
India	Bouguer gravity map		3 arc-min	Geological Survey of India (2006)

^aUnited States Geological Survey (USGS) World Energy Project (WEP).

^bCommission for the Geological Map of the World (CGMW)

Table 4: Published province models used to construct the initial global model.

Region	Reference
	<i>Global</i>
large igneous provinces	Johansson et al. (2018)
modern passive margins	Berndt et al. (2019)
	<i>Africa</i>
Africa	Begg et al. (2009), Hinsbergen et al. (2011)
West Africa	Ennih and Liégeois (2008)
Sahara Metacraton	Liégeois et al. (2013); Şengör et al. (2020)
Mozambique Belt	Chaúque et al. (2019), Goscombe et al. (2020)
Central Africa	Jelsma et al. (2018)
Southern Africa	McCourt et al. (2013), Hanson (2003)
Madagascar	Collins et al. (2003)
	<i>Antarctica</i>
Antarctica	Harley et al. (2013), Stål et al. (2019)
East Antarctica	Golynsky (2007), Harley and Kelly (2007), Elliot et al. (2015), Leitchenkov et al. (2016), Pierce et al. (2014), Pant and Dasgupta (2017), Mulder et al. (2019), Ruppel et al. (2020), Flowerdew et al. (2013), Aitken et al. (2014), Maritati et al. (2016), Maritati et al. (2019), Wang et al. (2020), Ebbing et al. (2021), Jacobs et al. (2015), Dunkley et al. (2020)
West Antarctica	Jordan et al. (2020)
	<i>Asia</i>
Siberian Craton	Tretiakova et al. (2017)
West Siberian Basin	Cherepanova et al. (2013)
Russia, far east	Isbell et al. (2016)
Central Asian Orogenic Belt	Xiao et al. (2015), Janoušek et al. (2018), Ivanov et al. (2014), Windley et al. (2007), Buslov et al. (2001)
North China Craton	Liu et al. (2017)
South China Craton	Wang et al. (2013)
Tian Shan Belts	Charvet et al. (2011)
Tibetan plateau	wei Zhou and Murphy (2005), Blayney et al. (2019)
southeast Asia	Mitchell et al. (2012), Burrett et al. (2014), Zhang et al. (2019), Morley and Searle (2017), Dew et al. (2021)
	<i>Australia and Zealandia</i>
Australia	Foster and Goscombe (2013), Pilia et al. (2015), Abdullah and Rosenbaum (2018)
Zealandia	Stagg et al. (2002), Gallais et al. (2019)
New Zealand	Mortimer (2004)
	<i>Europe</i>
Baltic Shield	Bogdanova et al. (2015), Zhao et al. (2002)
Mediterranean Europe	Schmid et al. (2020)
western Europe	Topuz et al. (2020)
	<i>India and Middle East</i>

Table 4: continued.

Region	Reference
Arabian-Nubian Shield	Johnson (2014)
Iran	Naimi-Ghassabian et al. (2018)
Pakistan	Kazmi and Rana (1982)
India	French et al. (2008)
Sri Lanka	Cooray (1994)
<i>North America</i>	
United States and Canada	Whitmeyer and Karlstrom (2007) , Hasterok and Chapman (2007) , Lund et al. (2015) , Ontario Geological Survey (2011) , Berman et al. (2013b) , Fyffe et al. (2012) , Bjorkman (2017) , Linde et al. (2017)
Greenland	White et al. (2016)
Alaska and Canadian Cordillera	Colpron and Nelson (2011)
Mexico	Sedlock et al. (1993)
Caribbean and Gulf of Mexico	Allen et al. (2019); Davison et al. (2020)
<i>South America</i>	
South America	Ibañez-Mejia et al. (2011) , Chew et al. (2008) , Egydio-Silva et al. (2018)
western South America	Ramos and Aleman (2000) , Eude et al. (2015) , Charrier et al. (2014)

256 Each boundary was then adjusted for seamless fits in the global model using a combination
 257 of geologic maps, active fault databases, geochronology, topography, and geophysical anomalies/models such as gravity, magnetics, and crustal thickness (Table 3). Magnetic anomalies
 258 were the most useful geological dataset for developing the province model as the magnitude
 259 and visual character is often distinctive within a province (Figure 6). We used two global mag-
 260 netic anomaly models to aid with locating province boundaries. Both are constructed from a
 261 combination of airborne and shiptrack magnetics. Because the airborne and ship track data are
 262 recorded at different altitudes and line spacing, this leads to variations in resolution and gaps
 263 filled with very low-resolution satellite observations. Where the resolution is low, it is more
 264 difficult to precisely position the province boundaries (Figure 6), , requiring more emphasis be
 265 placed on the other datasets listed in Table 3.

267 Topography is helpful for identifying the boundaries of many provinces as fault and shear
 268 zones are often expressed topographically. Topographic features are most helpful in active ter-
 269 ranes, but many ancient terranes can also be delineated by the changes in morphology when
 270 the faults/shear zones are no longer immediately apparent. The relatively high resolution of
 271 ETOPO1 (~ 1.85 km at the equator) makes the positioning of boundaries reasonably precise.

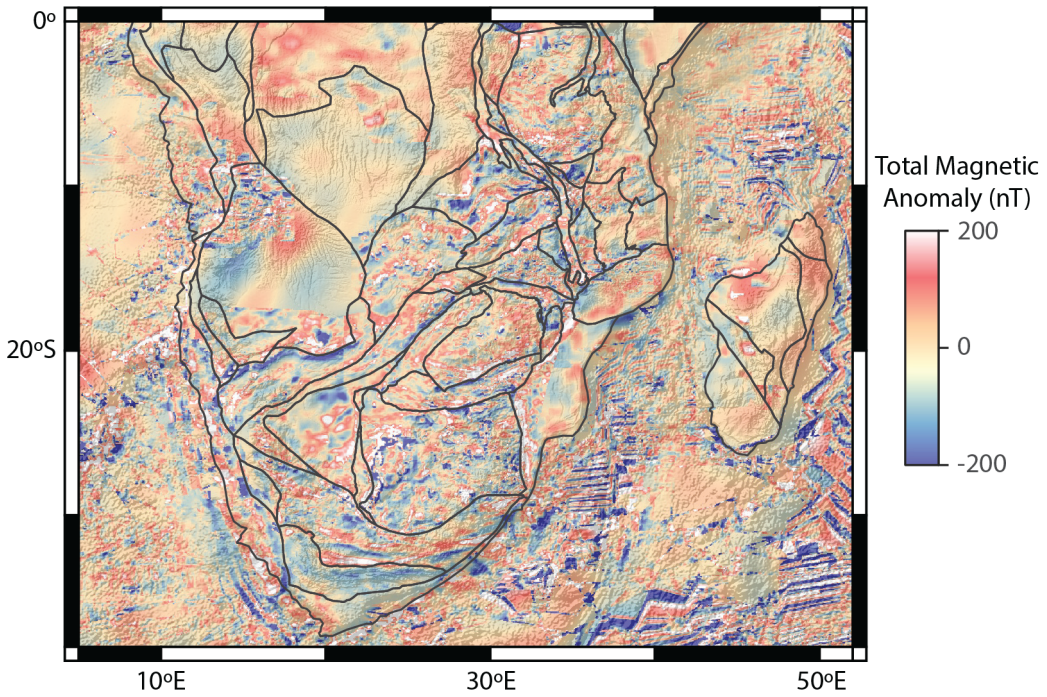


Figure 6: Magnetic anomaly map of southern Africa overlaying topographic relief. The WDMAM_V2 magnetic model has a pixel size of 1.5 minutes, which is approximately 2.8 km at the equator. The model is created from shiptrack, airborne and satellite datasets resulting in variable resolution that is evident in this image and affects the accuracy of province boundaries.

When there is a clear topographic expression at the boundary between provinces, the uncertainties are probably on the order of 3 to 5 pixels (~ 5 to 10 km).

We incorporate a number of attributes ascribed to the province polygons including a province name, province group, tectonic province type, and last significant orogeny (Table 1). The data standards used to define these additional attributes are described below.

3.2.1. Province Type

A geologic terrane captures a set of geologic units that describe a coherent block of crust with a shared geologic history, which can include tectonic setting, magmatic history, and/or metamorphic evolution. While a terrane is less fundamental than a geologic unit or suite, there are often similarities in the physical architecture and chemistry of terranes created in similar tectonic settings (e.g., Ducea et al., 2015; Ueki et al., 2018). However, there are also differences between terranes of similar types that can be uniquely expressed in the architecture, composition, and thermal history (e.g., Furman, 2007; Dilek and Furnes, 2014; Profeta et al., 2015).

To facilitate the analysis of terranes, we include a basic province type attribute with the shapefile. The province definitions are based on the terrane type that covers the majority of

288 a polygon. Most of the terrane definitions we have chosen distinct characteristics within a
289 modern plate tectonic setting:

290 **craton**, predominantly Archean core, contains granite-greenstone belts and other undifferentiated terranes with relatively small area;

292 **shield**, similar to a craton, predominantly Meso- to Paleoproterozoic lithosphere, undifferentiated;

294 **passive margin**, sediment accumulation built on transitional crust between continental and
295 oceanic crust marking half of a tectonically inactive fossil rift;

296 **accretionary complex**, active/subduction margin consisting of sedimentary wedges built on
297 oceanic or continental crust;

298 **basin**, intracontinental sedimentary cover built on preexisting continental crust with uncertain
299 or unknown basement provenance;

300 **foredeep basin**, (foreland basin) thick intracontinental sedimentary basin created during continent-
301 continent collision, basement uncertain;

302 **orogenic belt**, fold and thrust belts created during accretionary, collisional and intracontinental settings that may incorporate a variety of preexisting terrane types, often commingled, making them difficult to differentiate at the regional scale;

305 **narrow rift**, focused extensional terrane with continental basement;

306 **wide rift**, distributed extensional terrane with continental basement;

307 **volcanic arc**, predominantly magmatic arc crust related to subduction, but may contain crust predating the arc and/or interspersed accretionary material in island arcs and in seaward migrating arcs due to retreating trenches;

310 **continental back-arc basin**, a hyper-extended basin either transitional continental or oceanic crust created as a result of upper plate extension in response to subduction rollback;

312 **oceanic back-arc basin**, a back-arc basin where seafloor spreading has been sustained, creating enriched basaltic compositions relative to mid-ocean ridge basalt;

314 **ophiolite complex**, obducted oceanic crust of some variety, excluding volcanic arc-type, but
315 including supra-subduction zone oceanic crust;

316 **magmatic province**, a large intraplate magmatic terrane not clearly associated with subduc-
317 tion or extension processes; and

318 **oceanic crust**, typical oceanic crust not created in a back-arc setting.

319 The focus of the geologic province model is on basement tectonic terranes, hence large
320 igneous provinces (LIPs) are not included in this model as they are superimposed on the
321 basement. LIPs are volcanic features often associated with mantle plumes rather than tectonics.

322 Our model is a tectonic model. We do not discount LIPs as an important aspect of crustal
323 and mantle evolution, but they can obscure the underlying tectonic terranes. In fact, many
324 old LIPs whose volcanics have long been eroded away are recognized only by dike swarms that
325 occupy a fraction of the original surface area (e.g., [Ernst and Bleeker, 2010](#); [Ciborowski et al., 2015](#)). These older terranes retain much of their prior tectonic character beneath the volcanics.
326 Since a good model for LIPs currently exists ([Johansson et al., 2018](#)) so there is no need to
327 recreate one as a separate layer as part of this project. Users who wish to include LIPs can
328 easily incorporate them any spatial analysis.

330 Basins have been ignored except where the character of the underlying basement is unknown
331 (Figure 7). A reasonable resolution (5-arc-minute) sediment thickness model by [Straume et al.](#)
332 ([2019](#)) covers the ocean basins. Australia is covered by a high-resolution, 15-arc-second basin
333 model ([Geognostics, 2021](#)). A 30-arc-second sediment thickness model by [Pelletier et al. \(2016\)](#)
334 covers all continents except Antarctica, but only provides values for regions with less than 50
335 m of sediment thickness. The only available global basin thickness model has a relatively low
336 resolution of $1^\circ \times 1^\circ$ ([Laske and Masters, 1997](#)).

337 3.2.2. Last Orogeny

338 The most recent (last) high-temperature orogenic event to affect a province often has an en-
339 during influence on the present day thermal and physical state of the lithosphere and therefore,
340 its future potential to deform, metamorphose and melt (e.g., [Sandiford et al., 2001](#); [Fossen](#)
341 [et al., 2017](#); [Hyndman, 2019](#)). Here we define the last orogeny as the most recent regional
342 high-temperature thermotectonic event, excluding regions that may have experienced plume-

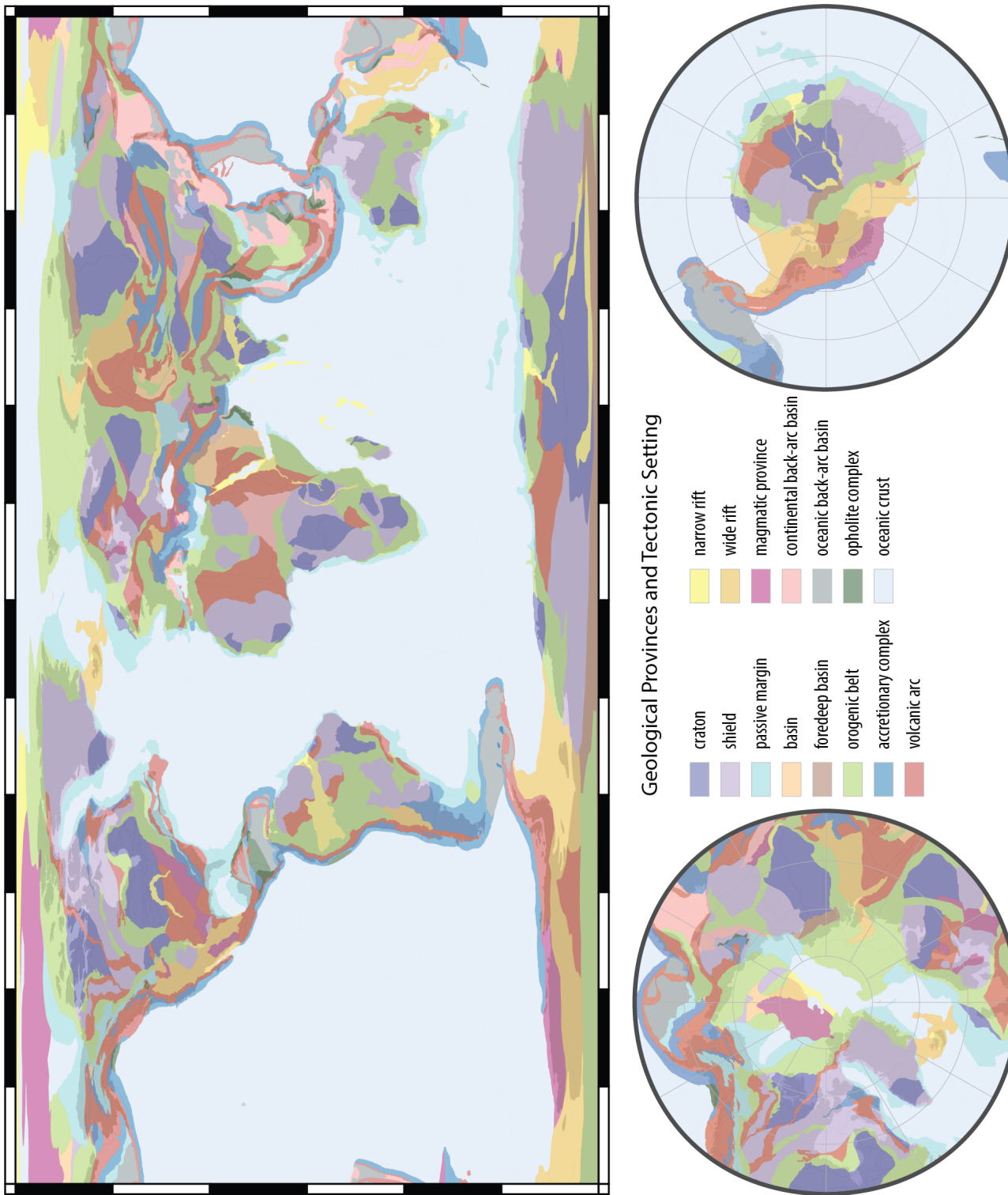


Figure 7: A global model of geological provinces with similar tectonic and compositional histories. Provinces are colored by their dominant tectonic setting. Though the setting may change with time, the provinces are defined by the environment which dominates the majority of rocks found within.

related activity. The most recent thermotectonic event is generally correlated with elevated surface heat flow ([Lucazeau, 2019](#)), and lithospheric buoyancy ([Fischer, 2002](#)), depending on its thermal intensity, it may reset high-temperature thermochronometers ([Wan et al., 2011](#)).

Orogenic systems often span a few hundred million years and comprise multiple, smaller orogenic events that exhibit significant regional variability (e.g., [Ge et al., 2014](#); [de Gromard et al., 2019](#)). For example, orogenic activity may propagate along a system over time as exhibited by protracted continent–continent collision as in the Alpine Himalayan Belt ([Kuhnt et al., 2004](#); [Dilek, 2006](#); [Ustaszewski et al., 2010](#); [Hu et al., 2016](#); [Symeou et al., 2018](#); [An et al., 2021](#)), hence the last orogeny descriptor is not as finely resolved in age as the activity in any given region. Instead, we use the last orogeny term to represent long-lived tectonic/geodynamic systems. These descriptors are often related to consumption of ocean basins ± continental collision; though they can also apply to an intraplate orogeny. In the Phanerozoic, the divisions are generally well-defined, but in the Precambrian, the connection between orogenic systems and now-isolated provinces may be less certain (e.g., [Li et al., 2008](#)). In these cases, the names refer to periods of orogenic activity rather than discrete systems. While this somewhat blurs the meaning of the term, we prefer it over several colloquial orogenic names. It also represents a research opportunity for improving models of orogenies and more accurately capture multiple distinct systems that may overlap in age.

The last orogeny model is built from reviews and large-scale studies of orogenic systems and plate reconstructions, assigning a single orogeny to each province polygon (Figure 8). We then validate the orogeny model against databases of igneous and metamorphic dates. Recently, [Condie et al. \(2021\)](#) attempted to quantify orogens and link them to other global processes by using the ‘number of orogens’ as a measurable quantity. We suggest that this is too arbitrary a parameter and instead we have attempted an ‘orogenic province’ approach where we suggest linking orogens and orogenies based on their interpreted tectonic/geodynamic system. To take the modern Earth as an example, this approach then links the active circum-Pacific orogens into one orogenic province, but separates them from the Alpine-Himalayan system. Understandably, this gets more subjective in deep time, but it provides a framework for building geodynamic models and presents hypotheses that can be robustly tested by new observations.

In the Phanerozoic, the divisions are generally well-defined, but in the Precambrian, the

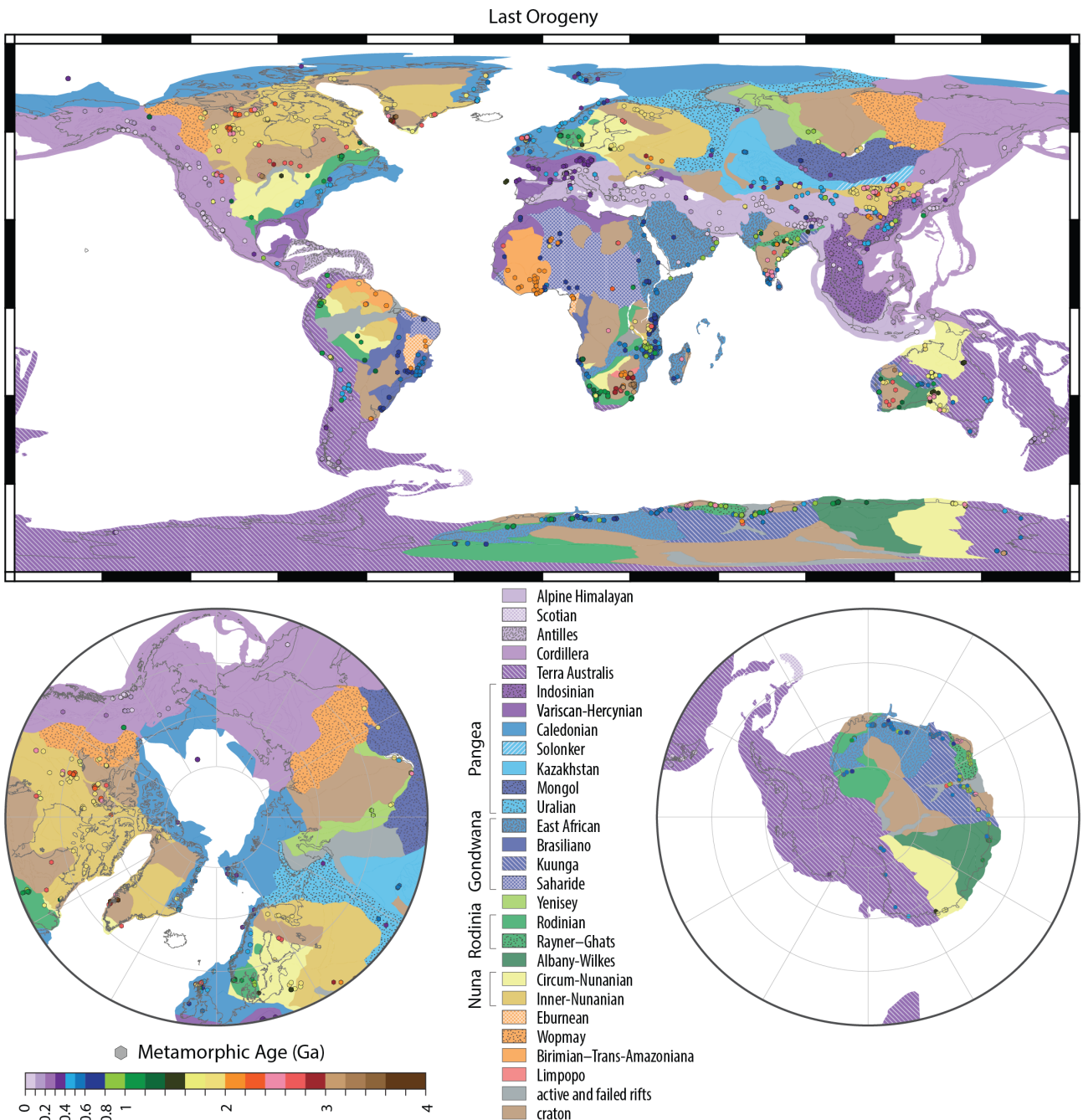


Figure 8: A map of the last orogenic event to affect a province. The colors are approximately related to the age of the orogenic event. The points show locations of observed and estimated metamorphic ages (Brown and Johnson (2018), updated; Eglington (2004)). Classification of the Phanerozoic orogens follows a systems approach as discussed in the main text.

373 connection between orogenic systems and now-isolated provinces is often less certain (e.g. Li
374 et al., 2008). We have used the emerging full-plate tectonic reconstructions of Merdith et al.
375 (2021) and Cao et al. (in prep.) to guide us here (Figure 9). While in many cases we believe
376 these were coherent systems, the names may refer to periods of orogenic activity rather than
377 discrete systems (e.g., Siberian Orogeny as defined below). While this somewhat blurs the
378 meaning of the term, we prefer it over several discrete orogenies with colloquial names. It
379 also represents a research opportunity for improving models of orogenies and more accurately
380 capture multiple distinct systems that may overlap in age. We define each of the orogens below.

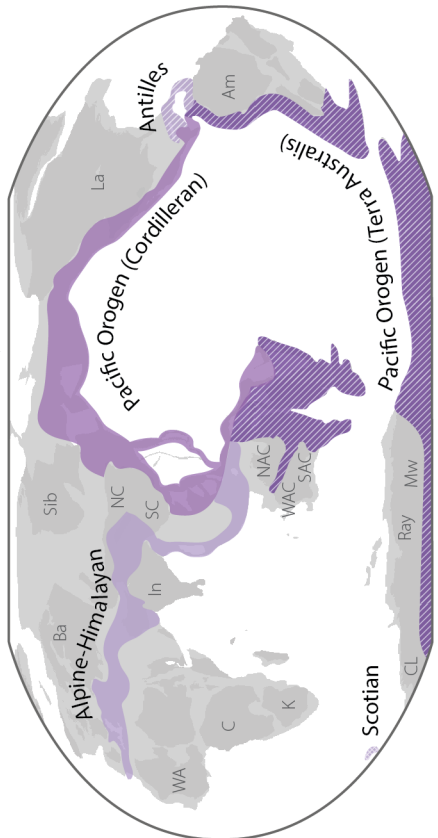
381 *3.2.2.1. Active Orogens*

382 . The Alpine-Himalayan Orogeny includes the collision between several plates with Eurasia,
383 which began ca. 65 Ma. The orogeny was initially driven by the subduction of the Tethys
384 Ocean beneath Eurasia but has continued even as the ocean has closed in many regions. The
385 continent–continent collisions with Eurasia were heterogeneous in time, beginning with the
386 collision of Apulia with Europe ca. 65 Ma (Ustaszewski et al., 2010), India with Tibet ca. 61–
387 59 Ma (earliest suggested timing; Hu et al., 2016; An et al., 2021), Australia with Indonesia ca.
388 25 Ma (Kuhnt et al., 2004), and Arabia with Iran ca. 25 Ma (McQuarrie and van Hinsbergen,
389 2013; Gaina et al., 2015).

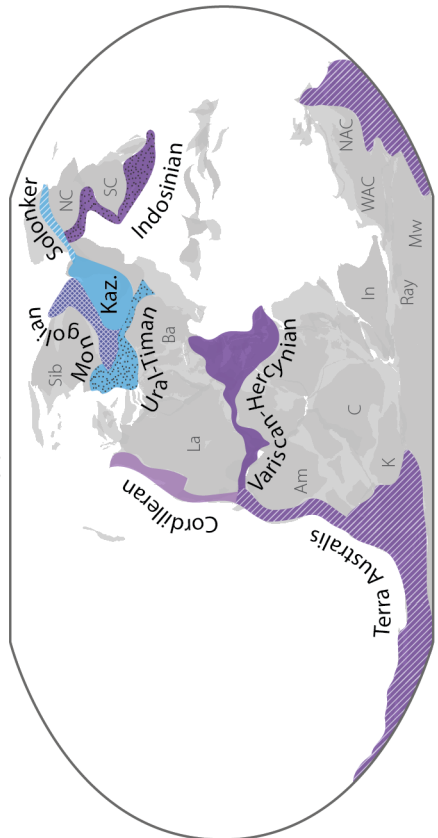
390 The Scotian Orogeny began with the initiation of subduction along the Antarctic and South
391 American Plate margins ca. 80 Ma and continues to the present day beneath the Sandwich
392 Islands (Eagles, 2016; van de Lagemaat et al., 2021). The Scotian Orogeny (Figure 8 and 9a),
393 like the Antilles Orogeny (below), is geodynamically governed by a retreating subduction zone
394 consuming the southwest Atlantic, which has created the Scotia Plate and Sandwich Microplate
395 in its wake.

396 The Antilles Orogeny is a young (ca. 118 Ma to present), active orogenic system in the
397 Caribbean that began in the mid-Cretaceous and created the Caribbean Plate as a result of
398 rapid trench retreat (García Casco et al., 2006). An alternative explanation by Whattam and
399 Stern (2015) suggests plume-induced thinning of the upper plate promoted subduction initiation
400 in the Caribbean ca. 95 to 85 Ma. The orogen is responsible for the creation of three separate
401 arc systems: the Greater Antilles, Lesser Antilles and Aves Ridge (Figure 8 García Casco et al.,
402 2006; Neill et al., 2011; Allen et al., 2019).

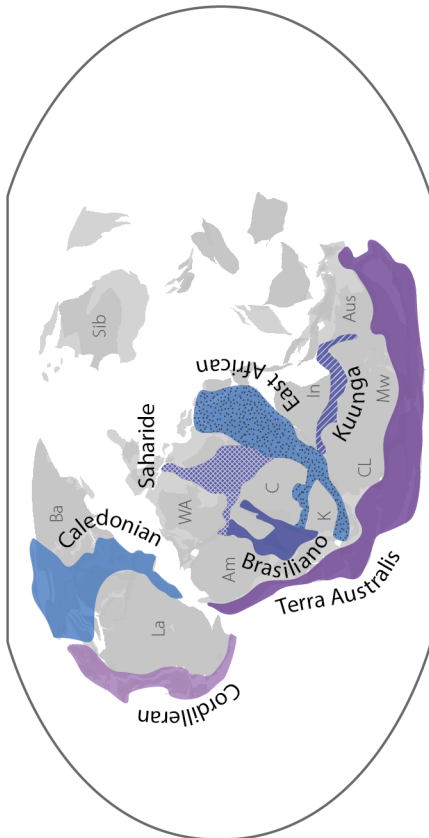
(a) Present Day



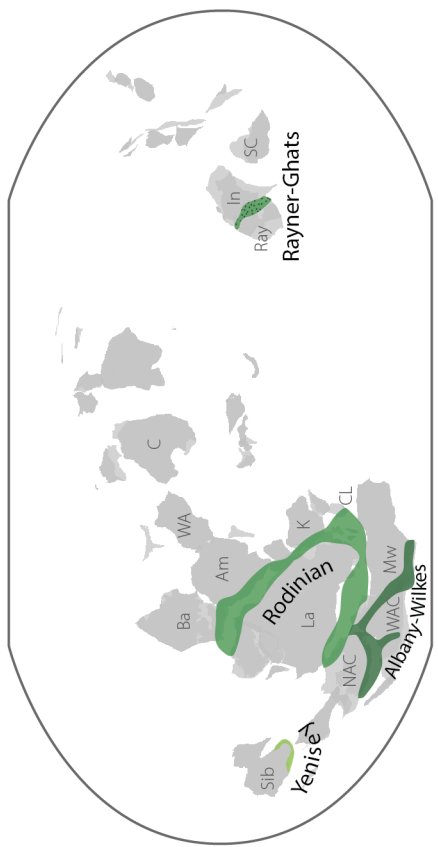
(b) 210 Ma



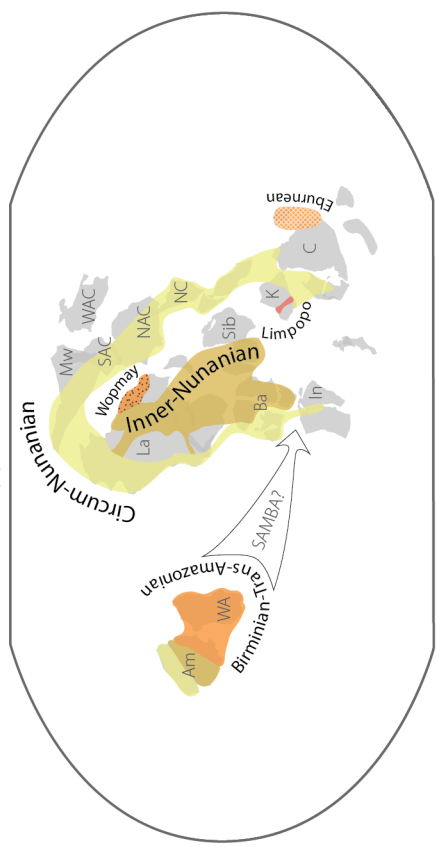
(c) 400 Ma



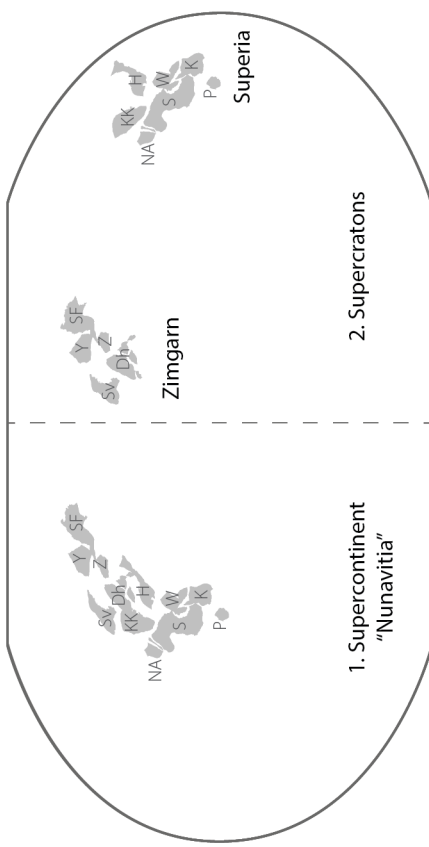
(d) 900 Ma



(e) 1450 Ma



(f) 2410 Ma



1. Supercontinent
"Nunavitia"

2. Supercratons

Figure 9: Reconstructions of orogenic systems at key dates. (a) Present-day shows the five active orogens. (b) Post-Pangea assembly, 210 Ma, keeping the position of Antarctica fixed. (c) Post-Gondwana assembly, 400 Ma, keeping the position of Amazonia fixed. (d) Post-Rodinia assembly, 1450 Ma. Arrow indicates the alternate location of Amazonia and the West African Craton in the SAMBA reconstructions (see Section 3.2.2.3 for discussion). (f) Supercontinent model for Nunavutia at 2410 Ma on the left and supercratons model on the right. Reconstructions (a-d) from [Merdith et al. \(2021\)](#), (e) from [Cao et al. \(in prep.\)](#), and (f) from [Li et al. \(2021\)](#) with terranes that were connected at 2.3 Ga: Grünehogna Craton with the Kaapvaal Craton, Penokean Orogen, North Atlantic Craton and the Nain Province with the Superior Craton; Napier Complex with the East Dharwar Craton; and the Mantiquera Province with the São Francisco Craton. Abbreviations are as follows: Ba, Baltica; C, Congo Craton; CL, Coats Land; Dh, Dharwar Craton, H, Hearne Province; In, India; K, Kaapvaal/Kalahari Craton; KK, Kola-Karelia; La, Laurentia; Mw, Mawson Craton; NA, North Atlantic Craton; NAC, North Australian Craton; NC, North China; P, Pilbara Craton; Ray, Rayner Complex; S, Superior; SAC, South Australian Craton; SC, South China; SF, São Francisco Craton, Sib, Siberia; Sv, Slave Craton; VU, Volgo-Ukrainian Shield; W, Wyoming; WA, West Africa; WAC, West Australian Craton; Y, Yilgarn Craton; and Z, Zimbabwe Craton.

403 The Pacific Orogeny is defined by a set of circum-Pacific subduction zones associated with
404 the destruction of the Pacific, Philippine Sea, Cocos and Nazca Plates beneath the South
405 American, North American, Eurasian, and Australian Plates (Figure 9a to c). In the modern
406 lexicon, this system is often referred to as the Cordilleran Orogeny ([Dickinson, 2004](#)); however,
407 this is too simplistic as the Cordilleran Orogeny either merged with or grew out of the Terra
408 Australis Orogeny ([Muttoni et al., 2003](#)), which is defined by the subduction of the Panthalassic
409 Ocean beneath Gondwana ([Cawood, 2005](#)). We have kept these two orogens separate to preserve
410 the association of Terra Australis with Gondwana, but acknowledge there is little reason to
411 distinguish them geodynamically.

412 The Terra Australis Orogeny began ca. 530 to 520 Ma in response to subduction of the
413 Pacific along the Gondwana margin (Figure 9c; [Cawood, 2005](#); [Chew et al., 2007](#); [Paulsen et al.,
414 2020](#)), which continues through to the present day ([Glen et al., 2016](#)). The orogen includes a
415 series of alternating subduction-related back-arc extensional and collisional events that built
416 eastern Australia, Zealandia, and much of the Transantarctic Mountains ([Fergusson and Hen-
417 derson, 2015](#)). Because the Terra Australis Orogen involved phases of significant extension
418 ([Gaina et al., 1998](#); [Abdullah and Rosenbaum, 2018](#); [Jessop et al., 2019](#)), parts of the oro-
419 gen are no longer active and/or have been separated by seafloor spreading (i.e., Delamerian,
420 Thompson and New England orogens of Australia, Patagonia in South America, Ross Orogen
421 in Antarctica, and the Cape Fold Belt in South Africa). Some authors consider parts of the
422 Terra Australis Orogen to be part of the Cordilleran (Ross Orogen in Antarctica and Southern
423 Alpine Orogen in New Zealand, [Tagami and Hasebe, 1999](#); [Dickinson, 2004](#)) or the Alpine-
424 Himalayan Belt (Zealandia, [Lister et al., 2001](#)). However, we associate these regions with the

425 Terra Australis Orogeny due to (1) their former common Gondwana association and (2) the
426 orogenic system largely predates both the Alpine-Himalayan and Cordilleran Orogenies. In the
427 eastern South Pacific, South America is moving westward over the young oceanic lithosphere
428 ([Schepers et al., 2017](#)). The modern Andes are ca. 66 Ma old ([Capitanio et al., 2011](#)), reach-
429 ing their current heights ca. 14 Ma ([Evenstar et al., 2015](#)); however, some estimates suggest
430 subduction formed a volcanic arc in South America by 530 Ma ([Chew et al., 2007](#)).

431 The Cordilleran Orogeny from Canada to Mexico is long-lived, starting in the late Devonian
432 (ca. 370 Ma) with the collision of the Antler Orogeny and subsequently the Sonoma Orogeny in
433 the Triassic along the western North American margin (Figure 9c; [Dickinson, 2004](#)). At the end
434 of the Sonoma Orogeny, a continental magmatic arc system extended along the western North
435 American boundary ([Dickinson, 2004](#)), some of the remnants of which are still active today in
436 the Cascades, Trans-Mexican Volcanic Belt and Middle America Arc. Subduction has all but
437 ceased along the Canada to Mexico margin as a transform margin developed ca. 50 Ma (Queen
438 Charlotte Fault predecessor, [Rusmore et al., 2010](#)) and ca. 28 Ma (San Andreas Fault, [Atwater](#)
439 and [Stock, 1998](#)) leading to gravitationally relaxation of the orogen ([Liu and Shen, 1998](#)). In the
440 western Pacific, subduction zones are generally in retreat, causing significant upper-plate exten-
441 sion in the back-arcs ([Vaes et al., 2019](#)). We also include the Verkhoyansk-Kolyma Orogeny of
442 far east Russia in our Cordilleran classification (Figure 8), which experienced intracontinental
443 deformation during the mid-Cretaceous in response to compressional forces applied by relative
444 Siberian and Alaskan convergence, but is no longer active ([Oxman, 2003](#); [Filatova and Khain,](#)
445 [2008](#)). The eastern half of the North China Craton also experienced widespread volcanism in
446 the Mesozoic and Cenozoic related to Pacific subduction ([Wu et al., 2019](#)). While there is no
447 metamorphic evidence for resetting of high-temperature thermochronometers, there is ample
448 evidence for significant modification of the lithosphere ([Kusky et al., 2007](#); [Yang et al., 2018](#);
449 [Li et al., 2019](#); [Dong et al., 2021](#)).

450 3.2.2.2. Neoproterozoic to Mesozoic Orogens

451 . The Indosinian Orogeny, ca. 310 to 200 Ma, resulted from the closure of the Paleo-Tethys
452 and Paleo-Pacific oceans in the late Paleozoic and early Mesozoic and led to the formation of
453 much of East Asia ([Lepvrier et al., 2004](#); [Morley et al., 2013](#); [Arboit et al., 2016](#); [Gao et al.,](#)
454 [2017](#); [Dew et al., 2021](#)). Specifically, the orogeny involves the collision of South China with

455 North China, Indochina with South China, and the Sibumasu Terrane with Indochina and the
456 intervening Sukhothai arc terrane (Arboit et al., 2016; Gao et al., 2017; Dew et al., 2021). It
457 is responsible for the accretion and amalgamation of much of East Asia (Figure 9b).

458 The Variscan-Hercynian Orogeny is defined by the closure of the Rheic Ocean ca. 290 Ma
459 (Matte, 2001; Nance et al., 2012). The orogeny spans the period from ca. 360 to 280 Ma (Edel
460 et al., 2014; Žák et al., 2014) and extended from north and western Mexico to Florida in North
461 America, the Iberian Peninsula to the Tornquist zone in Europe and included parts of north
462 and west Africa (Figure 9b; Catalán et al., 2021). The orogeny concluded with the collision of
463 Gondwana with the Carolina Arcs, Meguma, Amorica and Avalonian terranes with Laurussia
464 (Stampfli et al., 2013). In Europe, the orogen involved several additional microcontinents
465 that comprise western Europe (i.e., Iberia and Cadomia). Further east, the orogen merges into
466 the early Alpine-Himalayan Orogen and the late Central Asian Orogenic Belt and Indosinian
467 orogens with the closure of the various strands of the Paleotethys and Paleo-Asian Oceans
468 (Sengör and Natal'in, 1996; Robertson et al., 2004; Xiao et al., 2015; Gardiner et al., 2016).

469 The Caledonian Orogeny comprises a series of orogenic events spanning the period ca. 540 to
470 350 Ma resulting from the closure of the Iapetus Ocean (Figure 9c; McKerrow et al., 2000; Weller
471 et al., 2021). The orogen is typically associated with deformation from northeastern Greenland,
472 Svalbard and western Baltica, extending through the British Isles and continuing south in the
473 Appalachian Mountains (Weller et al., 2021). In eastern North America and Baltica, this
474 orogeny ended with the collision of Avalonia with Laurussia (Nance et al., 2012). We have
475 also included the Arctic Innuitian (Ellesmerian) Orogeny in our Caledonian Orogeny definition
476 due to its proximity in space and time to the Caledonian system sensu stricto (Barnes et al.,
477 2020), though the Innuitian occurred near the end of the Caledonian and is nearly orthogonal
478 in strike. While portions of the Innuitian Orogeny were overprinted in the early Tertiary by
479 the Eurekan Orogeny, this intracontinental deformation was relatively minor and is difficult to
480 distinguish from the earlier Innuitian Orogeny (Gion et al., 2017, and references therein).

481 The Central Asian Orogenic Belt (CAOB; Windley et al., 2007) has been divided into the
482 three separate orogenic systems following the model presented by Xiao et al. (2015), which
483 involves subduction and eventual closure of distinct regions of the Paleo-Asian Ocean from the
484 Tonian until the Triassic. The larger system is divided into (1) the Kazakhstan tectonic collage

and orocline; (2) the Mongolia tectonic collage; and (3) the Tarim-North China system, which we refer to as the Solonker Orogeny (Figures 8 and 9b), that overlaps in age with the more southern Indosinian Orogeny (Xiao et al., 2015; Song et al., 2018). Accretion of the Kazakhstan and Mongolian tectonic collages continued through the Neoproterozoic and Paleozoic and were terminated by the Solonker Orogeny at ca. 270 to 235 Ma that marks the final closure of the Paleo-Asian Ocean (Eizenhöfer et al., 2014; Song et al., 2018, 2021). The CAOB was subsequently reactivated during the Meso-Cenozoic in response to distant events related to the progressive consumption of the Tethys and Mongol-Okhotsk Oceans (e.g., Glorie and Grave, 2016). The Bureja-Jziamusy Terrane also experienced deformation as part of the Solonker Orogen, but was subsequently overprinted by Cordilleran deformation as recently as ca. 95 to 90 Ma (Derbeko, 2013).

The Uralian-Timan Orogeny is the result of several subduction-related magmatic periods spanning the period ca. 610 to 250 Ma (Figure 9b Fershtater, 2012; Pease, 2021). Oceanic arc volcanics associated with the subduction of the Paleo-Asian orogen are recorded in the Pechora arc (ca. 560 Dovzhikova et al., 2004) and blueschists and eclogites in the Urals (ca. 530 Willner et al., 2019). The latter set of magmatic events is related to the subduction and closure of the Paleo-Asian ocean and collision with the Kazakhstan Orocline (Xiao et al., 2015). The Uralian Orogeny extends into the Taimyr Fold belt where compression continued to 220 Ma, after the orogen had ceased elsewhere (Torsvik and Andersen, 2002).

The Neoproterozoic to Cambrian Gondwana-forming orogenies are a set of generally contemporaneous orogens—though they span nearly 700 Ma (1200 to 500 Ma)—culminating in the amalgamation of Gondwana (Figure 9c; Collins and Pisarevsky, 2005; Meert and Lieberman, 2008; da Silva Schmitt et al., 2018; Goscombe et al., 2020; Sengör et al., 2020; Collins et al., 2021b). We have separated these orogenies into the East African, Saharide, Kuunga, and Brasiliiano orogenies in much the same way as the Central Asian Orogenic belt was separated into distinct systems. The East African Orogen (Stern, 1994; Collins and Windley, 2002; Johnson et al., 2011; Fritz et al., 2013; Collins et al., 2021b) runs through Arabia, eastern Africa, Madagascar, southern India and into the Lützow-Holm Bay area of Antarctica. Whereas, we have located the Kuunga Orogen (Meert and Voo, 1997) as being the orogen that separated Neoproterozoic India from Australia/Mawson (Collins and Pisarevsky, 2005), running through

515 NE India, SW Australia and into Antarctica. This is broadly the trace of the Pinjarra Orogen
516 of Fitzsimons (2003) and Prydz-Denman-Darling Orogen of Collins and Pisarevsky (2005), but
517 may include the Mirny Fault (Daczko et al., 2018) and Gamburtsev suture (Ferraccioli et al.,
518 2011) as Neoproterozoic plate boundaries between Indo-Antarctica and Australo-Antarctica
519 (Mulder et al., 2019). Sengör et al. (2020) recently suggested the Tuareg Shield, Arabian-
520 Nubian Shield, and portions of the Saharan Metacraton constitute a single volcanic arc system
521 that was segmented and recombined in a fashion very similar to the Kazakhstan and Mongolian
522 oroclines. We tentatively accept this model for the Tuareg Shield and Saharan Metacraton,
523 but include the younger Arabian Nubian Shield in the East African Orogen (Figure 8), whilst
524 appreciating a likely continuity of orogenesis from one to the other (Blades et al., 2021; Collins
525 et al., 2021a). Our use of Brasiliano Orogen encompasses all the South American Gondwana-
526 forming orogens, as well as orogens along the west coast of Africa that correlate with them
527 (including the West Congo Orogen, the Rokelides, the Gariep Belt and the Kaoko Belt).

528 In the early Neoproterozoic, ca. 880 to 500 Ma, a small subduction-related orogen occurred
529 along the present-day eastern and southern margin of the Siberian Craton (Vernikovsky et al.,
530 2003; Kuzmichev and Sklyarov, 2016), which we refer to as the Yenisey Orogeny (Figures 8 and
531 9). The orogeny coincided with the accretion of the Angara terrane at ca. 870 Ma, (Vernikovsky
532 et al., 2007; Gladkochub et al., 2010). Numerous A-type magmatic dates, ca. 880 to 720 Ma,
533 are interpreted as part of a back-arc basin system (Kozlov et al., 2012; Kuzmichev and Sklyarov,
534 2016) and is consistent with metamorphism recorded during this interval (Gladkochub et al.,
535 2010). The system transitioned to seafloor spreading creating the Isakovka Terrane, an arc
536 ophiolite, ca. 700 to 635 Ma (Vernikovsky et al., 2003; Kuzmichev and Sklyarov, 2016), which
537 later accreted to the continent associated with a 500 to 470 Ma high-temperature metamorphic
538 event in the middle of the orogen (Gladkochub et al., 2010, and references therein).

539 3.2.2.3. Paleo- to Mesoproterozoic Orogens

540 . Today, the Mesoproterozoic and Paleoproterozoic orogens are fragmented and scattered across
541 multiple continents (Figure 8), and in many places, reworked by more recent events (Phillips
542 et al., 2009). This dispersion and tectonic overprinting obscures the orogenic systems with
543 time and makes it more difficult to associate terranes with individual orogens. As a result, we
544 recognise that our orogenic-systems approach becomes more subjective. To retain an orogenic-

systems approach as much as possible, we have used paleomagnetic-based (e.g., Condie et al., 2021) and full-plate tectonic (Merdith et al., 2021; Cao et al., in prep.) reconstructions (Figure 9d to f), while recognising an inevitable shift to a more temporal-based scheme for the pre-Neoproterozoic.

The late Mesoproterozoic to Tonian orogenies include the orogens that assembled Rodinia (Figure 9d), which are now widely dispersed across the globe (Figure 8; Li et al., 2008). Many studies refer to orogenesis during the period 1.3 to 0.9 Ga as Grenvillian-aged (e.g., Tohver et al., 2006; Sheppard et al., 2007; Goodge et al., 2010; Chattopadhyay et al., 2015). However, the conflation of orogen names to mean stretches of time has caused considerable confusion. For example, the term ‘Pan-African’ has been used to mean any orogen that occurred between ca. 800 and 400 Ma (Kröner, 1980), whereas orogens of this age form a number of discrete orogenic systems (see discussion of Gondwana above). Similarly with the term ‘Grenvillian’ (e.g., Krannendong and Kirkland, 2013). Fitzsimons (2000) pointed out that the late Mesoproterozoic to Tonian orogenes that appear to surround Antarctica, in fact, fall into discrete time brackets that relate to three different orogenic systems. Using the reconstruction by Merdith et al. (2021) as a guide, we have separated the orogens of this period into the Rodinian, Rayner-Ghats, and Albany-Wilkes Orogenies as separate systems active between 1.3 to 0.9 Ga.

The Rayner-Ghats Orogeny, ca. 1.1-0.9 Ga, has been interpreted as a distinct orogen outside of Rodinia in recent global plate models (Figure 9d; Merdith et al., 2021). This orogen includes the Rayner Complex in Antarctica (Halpin et al., 2013; Liu et al., 2014; Morrissey et al., 2015), conjugate terranes in India (the Eastern Ghats; Korhonen et al., 2011) and the Central Indian Tectonic Zone (Bhowmik, 2019).

The 1.3 to 1.0 Ga Rodinian Orogeny (Figures 8 and 9d) includes the Grenville and Llano provinces in North America (Whitmeyer and Karlstrom, 2007; Johansson et al., 2022), which, during Rodinia assembly, we link with the 1.1 to 1.0 Ga Namaqua-Natal Belt in southern Africa, the Maud Belt and Coats Land Block in Antarctica, and possibly the eastern South Tasman Rise (Mulder et al., 2018). We also include the ca. 1.1 to 0.9 Ga Laurentia-Australia transform as part of the Rodinian Orogeny that Mulder et al. (2018) connects to Rodinian subduction zones. In South America, the Rondonia-Juruena Province and its continuation underneath the Llanos Basin had a long-lived history of deformation spanning ca. 1.32 to 0.96 Ga (Tohver

575 et al., 2006) with late magmatic activity in the Sunsás Orogen (1.17 to 1.08 Ga; Santos et al.,
576 2008; Nedel et al., 2020; Johansson et al., 2022).

577 The Albany-Wilkes Orogeny, ca. 1.38 to 1.13 Ga, resulted from the collision of the West
578 Australian Craton with the North and South Australian Cratons and the Mawson Craton of
579 Antarctica (Figure 9d; Maritati et al., 2019; Pawley et al., 2020). Mulder et al. (2018) suggests
580 that the Albany-Wilkes Orogen is likely a continuation of the Grenville-Maud system (Rodinian
581 in our lexicon). However, the Albany-Fraser and Wilkes Orogenies may have started on the
582 same broad margin of Nuna/Columbia during break-up through to the assembly of Rodinia
583 (Pisarevsky et al., 2003, 2014; Yang et al., 2020; Kirscher et al., 2020). Most of the Rodinian
584 deformation occurs on the opposite side of Laurentia from East Antarctica/Australia and starts
585 at a later time; hence we consider the Albany-Wilkes to be a separate system. Recent dating of
586 1.38 to 1.275 Ga metamorphism in the Rudall Province and Western Musgravites, respectively
587 (the Parnngurr and Mount West Orogenies; Howard et al., 2015; Payne et al., 2021) extends
588 the early Albany-Fraser orogenesis north and documents collision between the West Australian
589 Craton and the combined South and North Australian Cratons. However, in places these were
590 subsequently overprinted during the Miles (ca. 650 to 625 Ma) and Paterson-Petermann (ca.
591 580 to 530 Ma) orogenies and thus related to the Kuunga Orogeny (Figure 9c). Two meta-
592 morphic events have been dated in the Albany Fraser Orogen, ca. 1.345 to 1.260 Ga and 1.215
593 to 1.140 Ga, resulting from the geometry of the collision between the West Australian Cra-
594 tons and the rest of Proterozoic Australia, with post-Parnngurr orogenic rotation and collision
595 of the West and South Australian Cratons (Clark et al., 2000). The Albany-Fraser Orogen,
596 Coompana and Madura provinces of Australia (e.g., Kirkland et al., 2017; Spaggiari et al.,
597 2018; Pawley et al., 2020) have been linked to their Antarctic conjugates from detrital zircon
598 spectra in offshore sediments and onshore geophysical characteristics (Maritati et al., 2019).
599 The Wilkes Orogen records amphibolite facies metamorphism at ca. 1.305 Ga and granulite
600 facies overprinting associated with charnockite intrusions, ca. 1.20 to 1.16 Ga (Morrissey et al.,
601 2017). The system also includes the 1.380 to 1.275 Ga Parnngurr and Mount West Orogenies
602 (Payne et al., 2021), an intracontinental contractional orogeny between the Yilgarn and Pilbara
603 Cratons. Tectonothermal events are also present in the central Australian Arunta Block (ca.
604 1.13 Ga; Scrimgeour et al., 2005; Morrissey et al., 2011; Wong et al., 2015) and in the Western

605 Australian Capricorn Orogen between the Yilgarn and Pilbara cratons (the 1.321–1.171 Ga
606 Mutherbukin Tectonic Event and the 1.026–0.954 Ma Edmundian Orogeny), which occur as
607 intracontinental far-field orogenesis to the amalgamation of Proterozoic Australia. It is unclear
608 how far the orogen extends into Antarctica due to the extensive ice cover.

609 Between ca. 2.1 and 1.45 Ga two major orogenic systems are associated with Nuna (Fig-
610 ure 9e [Pisarevsky et al., 2014](#); [Condie et al., 2021](#); [Cao et al., in prep.](#)): the Inner-Nunanian
611 Orogeny (ca. 2.1 to 1.7 Ga), which formed the core of the supercontinent; and the accre-
612 tionary Circum-Nunanian Orogeny (ca. 1.85 to 1.45 Ga) that is driven by a subduction girdle
613 surrounding the core. There are several reconstructions for Nuna ([Bispo-Santos et al., 2008](#);
614 [Elming et al., 2009](#); [Johansson, 2009](#); [Zhang et al., 2012](#); [Pisarevsky et al., 2014](#); [D’Agrella-](#)
615 [Filho and Cordani, 2016](#); [Meert and Santosh, 2017](#); [Cawood et al., 2020](#); [Elming et al., 2021](#);
616 [Cao et al., in prep.](#)), and while most are sufficiently similar to yield little difference in the last
617 orogeny designation, there are competing models for the likely participation of Amazonia that
618 will affect our model. In the SAMBA models, first proposed by [Johansson \(2009\)](#), Amazonia
619 (Central Amazonian and Ventuari-Tapajós Belts) is contiguous with the Baltic Shield, ca. 2.1
620 to 1.8 Ga, both of which experienced significant intrusive magmatism during the Nunanian Oro-
621 genies (e.g., [Almeida et al., 2007](#); [Bogdanova et al., 2015](#); [Juliani et al., 2021](#)). In the alternative
622 configuration by [Pisarevsky et al. \(2014\)](#), Amazonia and the West African Craton form a lesser
623 continent separate from Nuna (Figure 9e [Cao et al., in prep.](#)), deforming as part of a separate
624 accretionary margin. We have included the Amazonian Belts as part of the Nunanian Orogenies
625 (Figure 8 and 9e), but acknowledge that they may have evolved as a separate system.

626 The Inner-Nunanian Orogeny, ca. 2.1 to 1.76 Ga, was a major global event related to the
627 closure of the Manikewan Ocean and assembly of the Nuna/Columbia supercontinent ([Corrigan](#)
628 [et al., 2009](#); [Weller et al., 2021](#)). In North America, the Superior Craton collided with the
629 Reindeer Zone and Sask Craton, in a collision that has been compared to India colliding with
630 southern Asia ([St-Onge et al., 2006](#); [Darbyshire et al., 2017](#); [Weller and St-Onge, 2017](#)). On
631 the opposing side of the Reindeer Zone, the core of the orogen, contains a number of terranes,
632 grouped into the Hearne and Rae Cratons, which are sutured together by the Snowbird Tectonic
633 Zone ([Thiessen et al., 2018](#)). Deformation extended across to the Taltson-Thelon Arc (ca. 1.87
634 to 1.84 Ga) between the Rae and Slave Cratons ([Chacko et al., 2000](#); [Whalen et al., 2018](#)).

635 Baltica also experienced widespread orogenic activity as part of the Inner-Nunanian system that
636 is recorded in igneous and metamorphic activity that affected the Kola Block (e.g., [Mikkola](#)
637 [et al., 2018](#); [Daly et al., 2001](#); [Tuisku and Huhma, 2006](#); [Makkonen et al., 2020](#)), which at the
638 time, the present-day northern margin of the Kola Peninsula was adjacent to the eastern margin
639 of northern Greenland ([Evans and Mitchell, 2011](#)). Several reconstructions place the southern
640 margin of the Siberian Craton against the northern Margin of Laurentia at this time ([Condie](#)
641 [and Rosen, 1994](#); [Sears and Price, 2003](#)) and Baltica to its east ([Evans and Mitchell, 2011](#)).
642 However, more recent models suggest it collided post 1.9 to 1.84 Ga after the Anabar and Aldan
643 terranes had accreted to the eastern margin of the Siberian Craton based on geochronology of
644 mafic dike swarms, and post-collisional granitoids ([Donskaya et al., 2009](#); [Ernst et al., 2016](#)).
645 The Inner-Nunanian Orogeny also saw the amalgamation of Volgo-Uralia and Sarmatia, ca.
646 2.1 to 2.0 Ga ([Savko et al., 2015](#); [Baltybaev et al., 2017](#)), and the subsequent collision with
647 Baltica at ca. 1.82 to 1.80 Ga ([Bogdanova et al., 2015](#)). This collision is distinguished from
648 the Circum-Nunanian belts in Baltica that run orthogonal to the Volgo-Sarmatia collision.
649 This collision is distinguished from the Circum-Nunanian belts in Baltica that run orthogonal
650 to the Volgo-Sarmatia collision. The spatial complexity of the Inner-Nunanian Orogeny may
651 result from multiple systems just as the inner Gondwana orogenies, but uncertainties in the
652 geographic positions of many key crustal elements make it difficult to divide further at present.

653 The next few paragraphs discuss the Circum-Nunanian Orogeny and some of the variations
654 in configurations. Some of these variations are slight while others are quite dramatic, but
655 despite these differences the orogens all appear to occur along the exterior of Nuna's core as
656 terranes were accreted. Thus regardless of the accuracy of the geologic connections between
657 terranes, the last orogeny classification remains the same.

658 Wyoming was likely the first accretionary terrane added to Laurentia during the Circum-
659 Nunanian Orogeny, colliding with the Medicine Hat Terrane causing deformation in the Great
660 Falls Tectonic Zone (ca. 1.86 to 1.73 Ga; [Gifford et al., 2018](#)). Also during the first phase
661 of the Circum-Nunanian Orogeny, ca. 1.85 to 1.75 Ga, the Penokean Orogeny was a small
662 deformation event on the southern margin of the Superior craton recorded in metamorphism
663 and accompanying magmatism ([Holm et al., 2007](#); [Vallini et al., 2007](#); [Klier, 2019](#); [Zi et al.,](#)
664 [2021](#)). On the southern margin of Laurentia, a series of exotic terranes, Yavapai (ca., 1.80 to

665 1.70 Ga), Mazatzal (1.70 to 1.65 Ga), and Granite-Rhyolite terranes (1.50 to 1.45 Ga), were
666 accreted over the course of approximately 300 Ma (Karlstrom et al., 2001; Whitmeyer and
667 Karlstrom, 2007; Amato et al., 2008; Mako et al., 2015). The Yavapai and Mazatzal terranes
668 include juvenile arcs, ophiolites and metasediments that were accreted ca. 1.71 to 1.68 Ga
669 and 1.646 to 1.633 Ga during the Yavapai and Mazatzal Orogenies, respectively (Whitmeyer
670 and Karlstrom, 2007; Amato et al., 2008). The ca. 1.49–1.45 Ga Picuris Orogeny occurred
671 during a rare period of orogenic preservation between supercontinent cycles and is relatively
672 limited geographically to southern Laurentia which included parts of Precambrian Australia at
673 the time. The orogeny is identified in the southwestern United States where it deforms older
674 crust and appears not to have juvenile magmatism associated with it (Daniel et al., 2013; Mako
675 et al., 2015; Aronoff et al., 2016). The orogen extends into the northeastern United States
676 (Medaris et al., 2021), where it is progressively overprinted by the Grenvillian Orogeny in the
677 east. On the present-day eastern margin of Greenland, several exotic terranes were accreted to
678 the Kola-Karelia Craton, including Bergslagen-Livonia (ca. 1.89 and 1.84 Ga) and Amberland
679 (ca. 1.84 and 1.83 Ga; Bogdanova et al., 2015).

680 In Australia, extensive plate-margin orogenesis (ca. 1.82 to 1.55 Ga), similar to that inter-
681 preted for SW Laurentia, occurs throughout the South Australian Craton (Kimbang and Kararan
682 orogenies; Hand et al., 2007) and North Australian Craton (Yambah-Strangways-Leibig oroge-
683 nies). These likely formed a continuous accretionary system (Payne et al., 2009; Betts et al.,
684 2008; Betts and Giles, 2006). Extensive intracontinental orogenesis within Western Australia
685 is marked by the 1.82 to 1.77 Ga Capricorn Orogeny (Johnson et al., 2013) and the 1.68 to 1.62
686 Ga Mangaroon Orogeny (Sheppard et al., 2005). The Isan Orogeny (including the Chewings
687 and Olary orogenies) spanned the Paleo-Mesoproterozoic boundary (ca. 1.65–1.55 Ga). The
688 effects of this orogeny dominate the eastern entirety of pre-Phanerozoic Australia (Morrissey
689 et al., 2011; Tiddy et al., 2020; Volante et al., 2020), and extend into the Gawler Craton in
690 southern Australia (Cutts et al., 2011) and into the central North Australian craton (Anderson
691 et al., 2013). This orogeny is envisaged to have occurred as a consequence of collision between
692 Paleoproterozoic Australia (then consisting of the North Australia Craton and the South Aus-
693 tralian Craton with the North China Craton and a large piece of East Antarctica) and Laurentia
694 (Pourteau et al., 2018), and is recorded by the Racklan Orogeny in NW Laurentia (Furlanetto

695 et al., 2013). Orogenic activity coeval with younger Picuris Orogeny are found in the Gawler
696 Craton of Australia (Hall et al., 2018; Morrissey et al., 2019), and in the Mount Isa region of
697 NE Australia (Cave et al., 2022).

698 In Antarctica, ca. 1.7 Ga orogenesis recorded along the coast of the Mawson Craton (Peucat
699 et al., 1999), as well as in the central Transantarctic Mountains (Goodge et al., 2001; Brown
700 et al., 2021), although the extent of this orogenic activity into the interior of Antarctica is
701 unknown, it appears to be an extension of deformation in the Gawler Craton. There is some
702 ambiguity in the connections between Australia, Antarctica and western Laurentia (Wingate
703 et al., 2002), however, the connection of these three bodies is established from paleomagnetics
704 and geologic observations (aforementioned Nuna reconstructions; Whitmeyer and Karlstrom,
705 2007). The difficulty in precisely resolving the connections results from reworking of western
706 North America during the Cordilleran Orogeny and the uncertainties in paleomagnetic poles.

707 The accretionary orogenesis at this time on both the Dharwar-Bastar Cratons (South In-
708 dia) and the Bundelkhand Craton (northern India) is recorded in the Krishna Orogeny of the
709 Ongole Domain (1.68-1.60 Ma; Henderson et al., 2014) and in the Central Indian Tectonic Zone
710 (Bhowmik, 2019), respectively. The two halves of Peninsula India were likely separate conti-
711 nents before the Neoproterozoic. Paleomagnetic reconstructions have placed Southern India
712 conjugate to Antarctica or NE Australia (Zhang et al., 2012); however, more recent models
713 place the Indian continent adjacent to Baltica (Pisarevsky et al., 2003; Cawood et al., 2020).
714 Regardless, the Eastern Ghats appear to have been part of the active accretionary margin of
715 Nuna from 1.85 to 1.60 Ga or possibly as late as 1.45 Ga based on dating of tectonomagmatic
716 activity and an accreted ophiolite terrane in the Krishna Province (Dasgupta et al., 2013).

717 Prior to 1.95 Ga, the North China Craton was a set of microcontinents separated by ocean
718 basins that closed during the same period as both major Nunianian orogenies, completing by
719 1.85 Ga (Zhao et al., 2012), which is recorded in magmatism and widespread metamorphism
720 (e.g., Yin et al., 2014; Cai et al., 2015; Wu et al., 2016; Liu et al., 2017). However, the location of
721 the North China Craton has been subject to extensive debate, with various hypothesis ranging
722 from the northern margin of Siberia (Halls et al., 2000), paired with the Kola-Karelia Craton
723 and (Wilde et al., 2002), positioned between Baltica and Amazonia (Pesonen et al., 2012), or
724 joined with India outboard of the Nuna accretionary margin (Zhao et al., 2011). However,

we prefer more recent models that suggest a long-lived connection with the North Australian Craton on the basis of more extensive paleomagnetic and geologic correlations (Wang et al., 2019; Nixon et al., 2022; Zhang et al., 2022). Much of the North China Craton has similar ages to the Inner-Nunanian Orogen, about half the craton experience widespread magmatism as part of the Cordilleran Orogeny (Wu et al., 2019).

Most models for Nuna do not include the Kalahari Craton; however, the two models that do, place it in opposite hemispheres (Djeutchou et al., 2021; Cao et al., in prep.). A recent paleomagnetic reconstruction by Djeutchou et al. (2021) suggests the Zimbabwe Craton (the northern part of the Paleoproterozoic Kalahari Craton) was juxtaposed against the southern margin of the Superior Craton at 1.88 Ga. Additionally, their model calls for a pair of subduction zones along the south and western margins of the Kaapvaal Craton (the southern part of the Kalahari Craton), reworking the Magondi and Kheis Belts and accreting the Rehoboth Block at this time (Kleinhanns et al., 2013). However, such placement would leave little time for the Kalahari Cratons to rift away from Superior, prior to the arrival of the Mazatzal Orogeny ca. 1650 Ma along a margin that experienced the accretion of at least three major terranes ca. 1850 to 1450 Ma (Yavapai, Mazatzal and the Granite-Rhyolite terranes). The paleomagnetic data and timing dates of deformed terranes are also consistent with a collision between Congo-Tanzanian Craton with the south African cratons, which is consistent with ca. 2.0 Ga, resulting in exhumation of eclogites in the Ubendian-Usagaran Belts (Collins et al., 2004; Tamblyn et al., 2021). Regardless, both interpretations place these deformed and accretionary terranes within the Circum-Nunanian Orogeny.

The Wopmay Orogeny, ca. 1.95 to 1.84 Ga, was a small subduction-related event on the western margin of the present-day Slave Craton in northern Canada (Figure 8 Bowring and Podosek, 1989). East-dipping subduction on the western margin accreted three separate arc terranes, Great Bear, Hottah, and Fort Simpson, to the craton at ca. 1.88 Ga in the short-lived Calderian Orogeny (Hildebrand et al., 2009; Cook, 2011).

The Eburnean Orogeny records the collision between the São Francisco Craton and the Gabon Belt on the eastern Congo Craton margin, (ca. 2.12 to 2.0 Ga; Weber et al., 2016). The orogeny is recorded in a set of tectonomagmatic events (Doumbia et al., 1998; Barbosa et al., 2008; Peucat et al., 2011; Loose and Schenk, 2018; de Carvalho Filgueiras et al., 2020).

755 Although the Eburnean Orogeny was accretionary at the margins of Nuna (Figure 8e), it was
756 geographically isolated and earlier than the majority of Circum-Nunianian orogenesis.

757 Early models of the Limpopo Orogeny suggested it was active between 2.7 and 2.65 Ga
758 as the result of the collision between the Kaapvaal and Zimbabwe Cratons ([Barton and van](#)
759 [Reenen, 1992](#)), which is based on the age of granitoids contained within the thrust sheets.
760 However, metamorphic ages and more recent interpretations suggest it was active ca. 2.0 Ga
761 ([Yin et al., 2019](#)). The Limpopo Orogeny was probably intracontinental due to a lack of arc or
762 accretionary sediments of appropriate age ([Yin et al., 2019](#)).

763 The Birimian–Trans-Amazonian Orogeny occurred during the early stages or just prior to
764 the assembly of Nuna and may have been multiple spatially discrete events between ca 2.3 and
765 1.9 Ga. During this period, the West African Craton records considerable tectonomagmatic
766 activity in sedimentary deposits ([Grenholm, 2019; Grenholm et al., 2019](#)) as it collided with
767 the present-day northeastern Amazonian Craton ([Grenholm, 2019](#)). Both magmatic and meta-
768 morphic events are recorded in Amazonia during this period ([De Roever et al., 2003; Savko](#)
769 [et al., 2015; Baltybaev et al., 2017; Klaver et al., 2015; da Rosa-Costa et al., 2008](#)).

770 In the early Paleoproterozoic (ca. 2.5 to 2.3 Ga), a purported drop in magmatism corre-
771 sponded with several cratonic regions that experienced high-temperature, often contractional,
772 metamorphic events ([Pehrsson et al., 2013, 2014](#)). [Pehrsson et al. \(2013\)](#) hypothesized these
773 events are related to a formation of a supercontinent (Nunavutia), however, a recent paleo-
774 magnetic reconstruction suggested two separate supercratons were also consistent with pole
775 determinations and patterns of dike swarms (Figure 9f; [Liu et al., 2021](#)). The reconstructions
776 of the Siderian are based on paleomagnetic poles from 11 terranes ([Liu et al., 2021; Salmi-](#)
777 [nen et al., 2021](#)); however, less than one-quarter of blocks with igneous dates older than 2.3
778 Ga (Figure 10) are included in the reconstructions. Igneous activity in the interval 2.5 to
779 2.3 Ga is nearly ubiquitous across Archean terranes with the exception of regions covered by
780 ice, sediments, and or Phanerozoic large igneous provinces. As a result, the classification as
781 a super-continent/craton may be premature without the reconstructed positions of additional
782 Archean terranes. Metamorphic dates in this time interval are sparse (Figure 10), but the
783 metamorphic database is incomplete, so it is difficult to make clear inferences at this point. We
784 refer to the regions with significant 2.4 Ga tectonothermal activity collectively as the Siderian

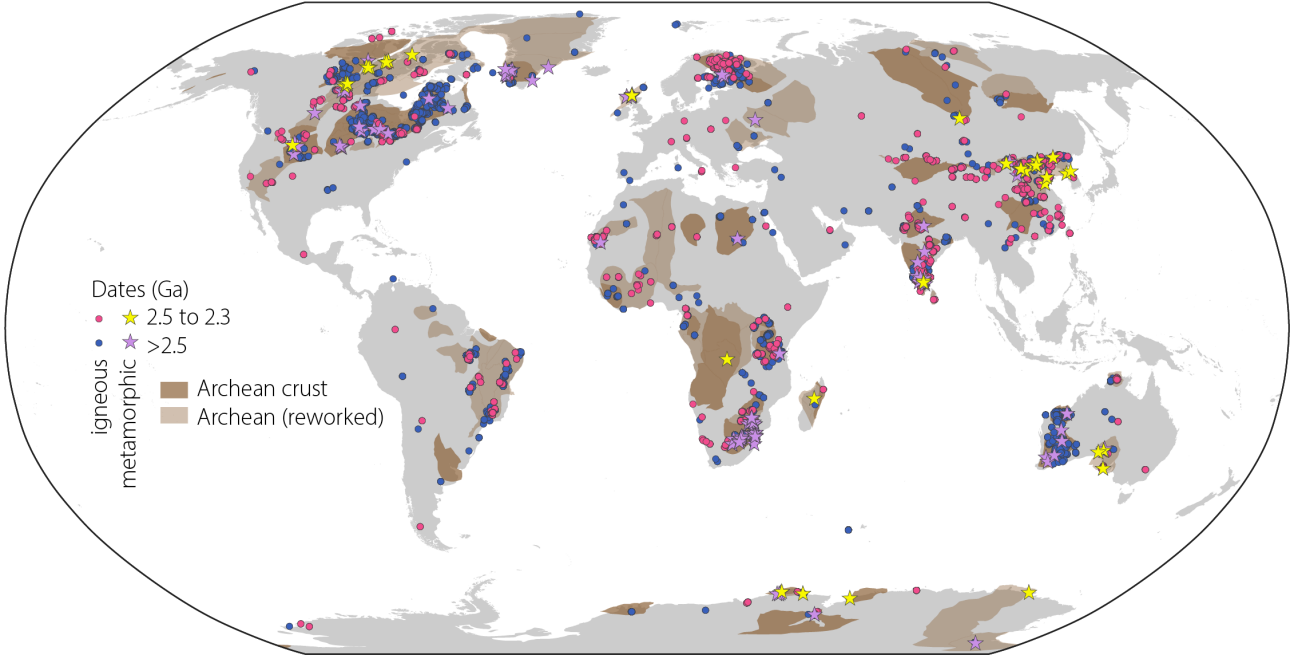


Figure 10: Regions with crust >2.3 Ga with superimposed locations of dated igneous and metamorphic activity. The observed dates are divided into the period 2.5 to 2.3 Ga, and older than 2.5 Ga. Reworked Archean crust is displayed in a lighter shade. Province boundaries from Figure 7 and a few additional Archean basement provinces in North America by Lund et al. (2015). Igneous ages extracted from Gard et al. (2019a) and Puetz (2018); metamorphic ages from DateView (Eglington, 2004) and the expanded metamorphic database by Brown and Johnson (2018).

785 Metamorphic Event, referring to the geologic time period rather than a coherent orogen due
 786 to the present uncertainty in reconstructions. The ca. 2.4 Ga affected terranes are now scat-
 787 tered across all seven continents and many have been reworked (Figure 9f and 10). Some of
 788 the terranes where the Siderian Metamorphic Event has been documented include the Mawson
 789 Craton (Duclaux et al., 2008), the Sask Craton (Chiarenzelli et al., 1998), Arrowsmith Orogen
 790 in Northern Canada (Hartlaub et al., 2007; Schultz et al., 2007; Berman et al., 2013a), the
 791 East Dharwar in India (Clark et al., 2009; Li et al., 2018), and the Sleaford Complex in south
 792 Australia (Halpin and Reid, 2016) and the North China Craton (Liu et al., 2017).

793 4. Model Evaluation

794 4.1. Ocean–Continent Boundary

795 Not counting for topographic relief, we estimate 57.5% of the Earth’s surface is covered by
 796 oceanic crust and 42.5% is covered by continental crust (Figure 4). The seafloor age model by
 797 Seton et al. (2020) covers a slightly smaller proportion of the Earth’s surface with seafloor ages,
 798 57.3%. However, there are a few significant differences between the models.

799 In general, the edges of the seafloor age model by Seton et al. (2020) are easily correlated

with high bathymetric gradients and deep water. However, there are a few regions where locations differ significantly between their model and our ocean–continent boundary. Some of the differences may be due to the quality of magnetic data near the continents where remnant magnetization may be reset by high temperatures beneath insulating sediments or where magnetic data is of insufficient quality and/or density to resolve seafloor ages. A few of the larger differences include the Greenland-Iceland-Faroe Ridge (GIFR), Blake Plateau, Gulf of Mexico, and some microcontinents.

Perhaps the most obvious difference between our model and [Seton et al. \(2020\)](#) is the inclusion of the GIFR as a region of continental crust. In a recent comprehensive paper by [Foulger et al. \(2020\)](#), the authors make a compelling case that the GIFR is a peculiar region with variably extended continental crust rather than the product of anomalous oceanic volcanism. The nearby Jan Mayen microcontinent has been recognized as a microcontinents for decades ([Peron-Pinvidic et al., 2012](#), and references therein), lending credence to the model. The total thickness of the crust approaches 40 km thick beneath the Iceland microcontinent—a value more typical of continental than oceanic crust. The symmetric, linear magnetic anomalies characteristic of seafloor spreading are muddled in this region, possibly indicating a complex history of rifting and volcanism. The upper crust in the region exhibits seismic properties and layer thicknesses typical of oceanic crust (3–10 km), but the middle and lower crustal seismic velocities and densities are better explained by continental material ([Foulger et al., 2020](#)). Therefore, we favor their interpretation in our model.

There are a number of other microcontinents that we have included in our model that are not found in the [Seton et al. \(2020\)](#) model. We have included the Hovgaard Ridge and the East Greenland Ridge in the Arctic Ocean ([Funck et al., 2016](#)). Several microcontinents lie in the Indian Ocean including the Mascarene Plateau, Chagos–Laccadive Ridge, Gulden Draak, and Batavia Knoll ([Torsvik et al., 2013](#); [Gardner et al., 2015](#); [Halpin et al., 2017](#)), which are formerly pieces of Madagascar and India, respectively. We have also included the Bollons Seamount east of the Campbell Plateau in the Pacific ([Davy, 2006](#)).

The Blake Plateau on the Atlantic side of Florida sits at a bathymetric depth of ~1000 m and is underlain by transitional crust ([Dillon et al., 1988](#)). In the Gulf of Mexico, the ocean–continent transition is obscured by sedimentary cover making magnetic data the most useful for

830 identifying the boundary, but the global models are relatively low resolution. However, there
831 are industry magnetic datasets that we do not have access to that yield a much clearer view of
832 the Gulf of Mexico.

833 In the future, incorporation of seismic reflection profiles taken across the ocean–continent
834 transition and improvements in the magnetic datasets may warrant alterations to the ocean–
835 continent boundary.

836 *4.2. Plate Boundaries*

837 There are significant differences in the lengths of plate boundaries by type (Table 5). The
838 total length of all major plate boundaries is nearly five times the Earth’s circumference. Among
839 major boundaries, the total length of divergent boundaries is significantly greater than con-
840 vergent boundaries. The mid-ocean ridge system and associated transforms is \sim 1.6 times the
841 length of subduction zones. Transform boundaries account for the least length of major bound-
842 aries, but this does not include the transforms between mid-ocean ridge segments.

Table 5: Lengths of plate boundaries. Major and minor boundaries are identified in Figure 2.

Boundary Type	Major (km)	Minor (km)
spreading center	87,001	12,663
extension zone	16,608	41,663
subduction zone	52,994	9,688
collision zone	18,295	65,113
dextral transform	20,856	41,663
sinistral transform	13,276	24,099
inferred	0	24,923

843 Including minor deformation zone and microplate boundaries more than doubles the total
844 length of boundaries (Table 5). The latter number may be a bit misleading as the minor bound-
845 aries generally bracket the deformation, while in reality multiple structures may accommodate
846 the motion. Among minor boundaries, convergent and transform boundaries are longer than
847 divergent boundaries. Also in contrast to major boundaries, spreading ridges and subduction
848 zones are less common than extensional zones and thrusts.

849 *4.3. Plate Model*

850 The plate model consists of 16 rigid plates, 54 microplates and 73 deformation zones. The
851 areas of rigid plates span (Figure 11 just over three orders of magnitude from the smallest

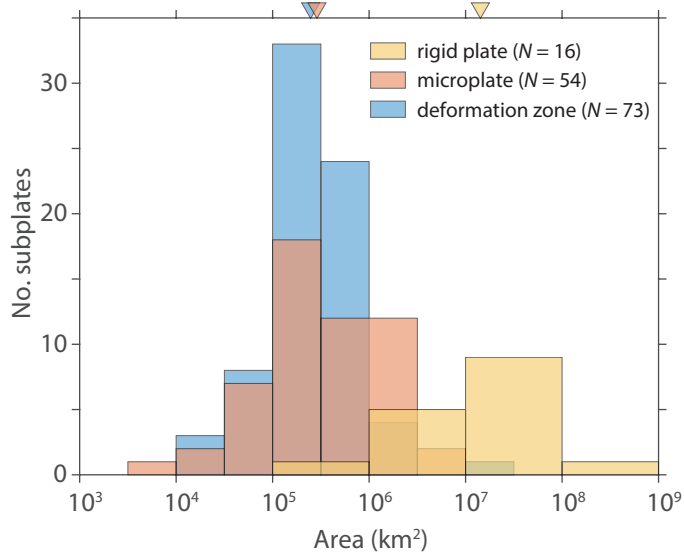


Figure 11: Areas of subplate polygons by type. The triangles are centered about the median area for each type, respectively.

(Juan de Fuca, $0.15 \times 10^6 \text{ km}^2$) to the largest (Pacific, $103 \times 10^6 \text{ km}^2$). The areas of microplates and deformation zones have similar ranges to rigid plates, but the median sizes are nearly two orders of magnitude lower than rigid plates. The subplates are further split into smaller polygons (208) to split oceanic from continental regions.

4.3.1. Comparison with Bird (2003)

The major differences between the [Bird \(2003\)](#) plate model and our model are the microplates and deformation zones (Figure 1a). Most major plate boundaries are very similar to [Bird \(2003\)](#) with some refinement. The [Bird \(2003\)](#) model contains 52 polygons, whereas ours contains 121 regions comprising rigid plates, microplates and deformation zones. Most of these added regions are located in the Alpine–Himalayan Belt and the North American Cordillera. These changes are driven by a significant improvement in the number and quality of land-based GPS coverage; however, several of our additions have long been recognized as plate boundary zones (e.g., [Gordon, 1998](#); [Lowman and Yates, 2002](#); [Freymueller, 2010](#); [Kreemer et al., 2014](#)). Many of these regions have also been previously identified as microplates (case studies in Table 2). In total, we estimate 16% of the Earth’s surface is covered by microplates and deformation zones, divided roughly equally between them whereas the Bird model only includes 6%.

The southern Somali–African boundary has changed considerably with respect to the [Bird \(2003\)](#) model. The [Bird \(2003\)](#) model connects several discrete regions of seismicity in southern

871 Mozambique and central South Africa. However, GPS motions suggest there is little deformation
872 on either side of this boundary (Kreemer et al., 2014). From GPS data, the boundary
873 appears to be further east, near the southern Mozambique coast (Stamps et al., 2021).

874 Another region of significant refinement relative to Bird's model among the microplates and
875 deformation zones of the Philippines and eastern Indonesia. Our model more closely follows
876 several boundaries identified by Zahirovic et al. (2014), which shows better correlations with
877 seismicity and active fault models (ANSS, 2020; Styron and Pagani, 2020).

878 In our plate model, ~80% of earthquakes occur within 100 km of a plate boundary and ~91%
879 within 200 km (Figure 12a). Approximately 73% of earthquakes occur within deformation zones
880 and microplates. For the Bird (2003) model, these percentages are significantly lower. Less than
881 27% of earthquakes lie within Bird's microplates and 65% of earthquakes lie within 100 km of
882 plate boundaries. Therefore, we suggest our new model provides a more accurate representation
883 of the actively deforming crustal regions.

884 The pattern of distance of earthquakes from plate boundaries varies depending on the type
885 of plate boundary. Earthquakes are centered close to spreading centers (Figure 12b), but are
886 more diffuse around transforms (Figure 12f), which occurs because transform plate motion is
887 frequently accommodated by multiple faults rather than a single structure (e.g., Pacific–North
888 American boundary in California, Hauksson et al., 2013; DeMets et al., 2014). In contrast to
889 spreading centers and transforms that identify the centers of deformation, extensional zones
890 and thrusts identify the boundaries of internal deformation so it makes sense that earthquakes
891 are distributed at a greater distance from these boundaries (Figure 12c, e). Subduction zone
892 earthquakes are distributions furthest from their associated plate boundaries (Figure 12d).
893 The more rapid increase in cumulative density of subduction zone earthquakes could be due to
894 our limiting earthquakes to 30 km depth and/or the earthquakes extend far enough into the
895 deformation zone that the opposite boundary becomes the closest (Figure 2).

896 4.3.2. Comparison with Tomography and Volcanism

897 Our plate boundary model correlates well with slow seismic shear-wave velocity slices from
898 40 to 90 km depth, with 70 km displaying the most similarity to the plate boundary zones
899 (Figure 13). Greater than 90 km depth, the mantle beneath the oceans has significantly larger
900 negative velocity anomalies. Greater than approximately 125 km depth, some of the continental

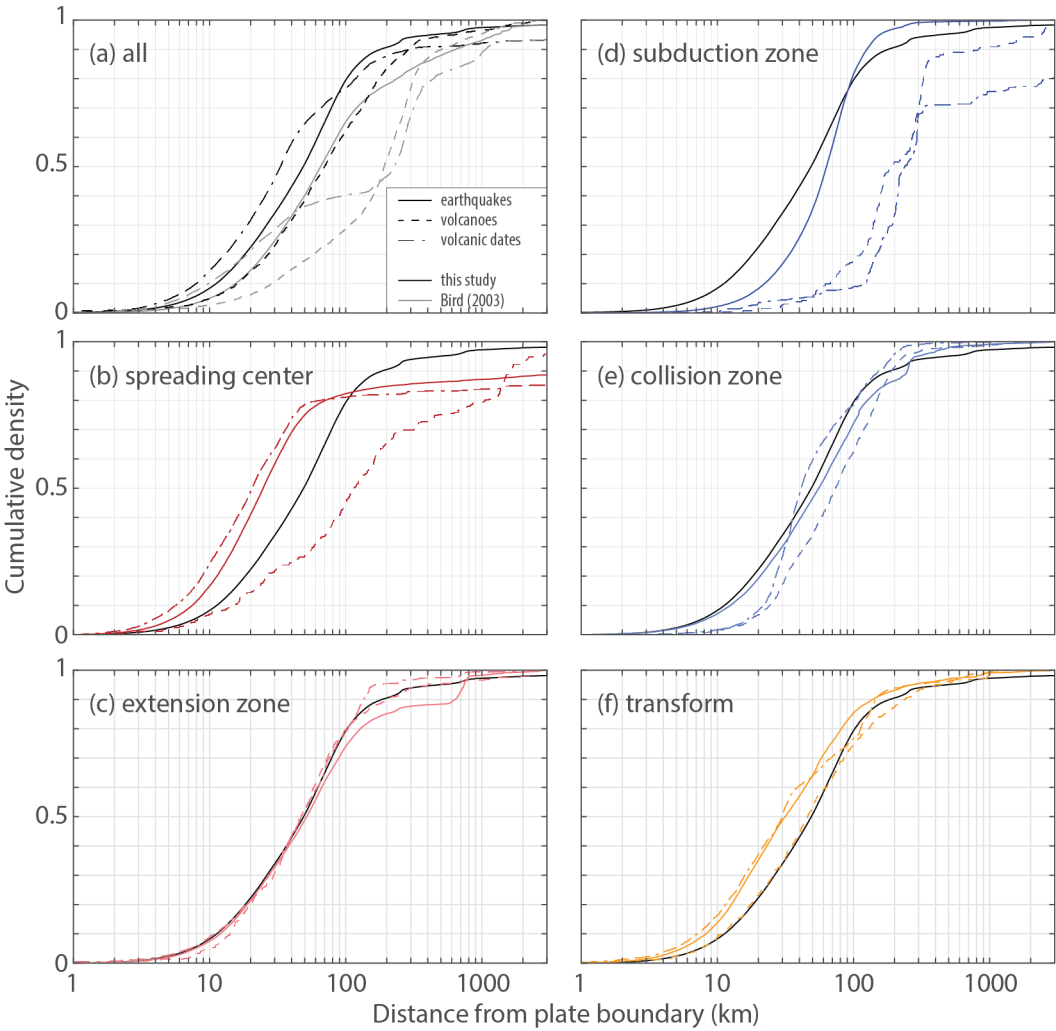


Figure 12: Cumulative distributions of earthquakes and volcanoes by distance to plate boundaries. Each subplot contains CDFs from three datasets: (solid) earthquakes from the ANSS catalog, magnitude 3.0 to 5.5, 1990 to 2020 and magnitude 5.5+, 1970 to 2020 ([ANSS, 2020](#)); (dashed) Quaternary volcanoes ([Global Volcanism Program, 2013](#)); and (dashed-dotted) dates of volcanic samples limited to Quaternary samples [Gard et al. \(2019a\)](#) with duplicate sample locations removed to limit oversampling. (a) Computed using all data in each respective dataset, black lines using our model and grey lines using [Bird \(2003\)](#). (b-f) Computed for listed plate boundary types as classified in Figure 2. The black line on each plot is earthquakes from all plate boundaries as a reference.

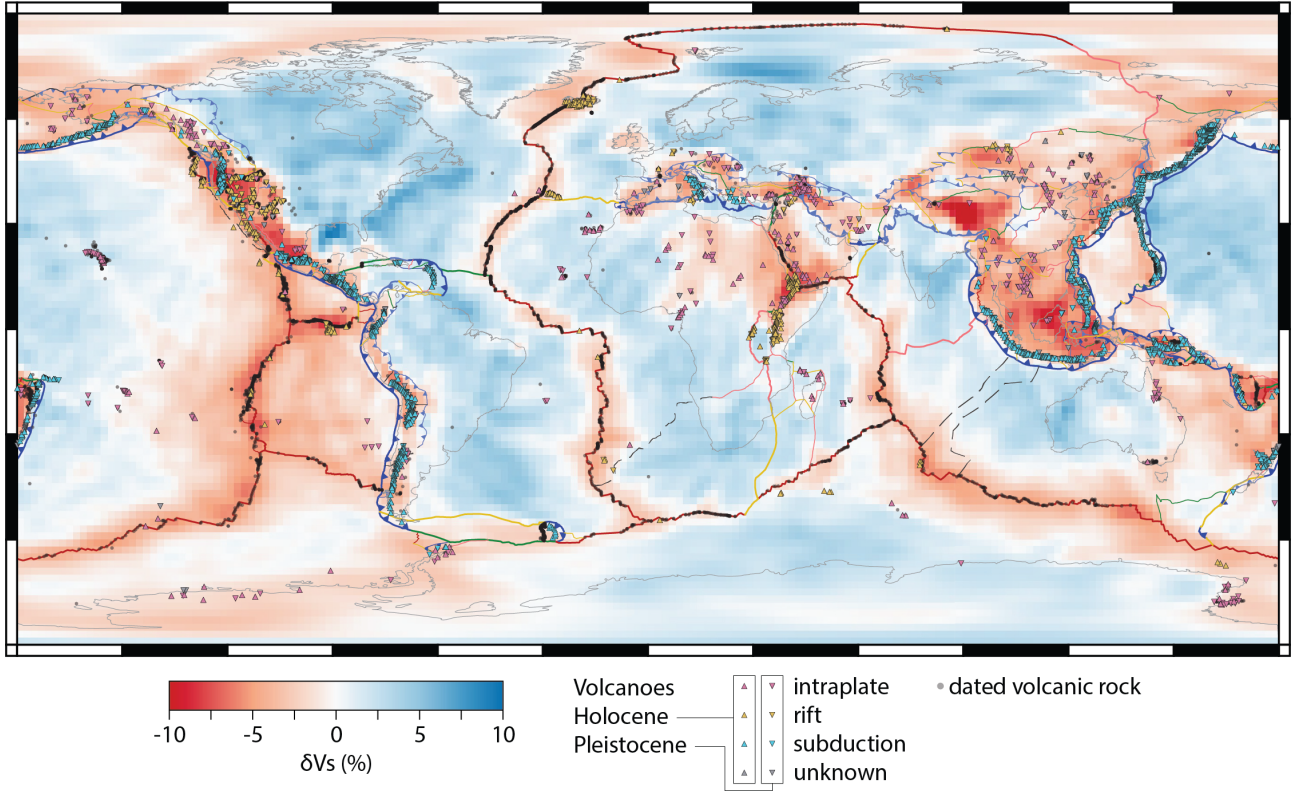


Figure 13: Shear wave tomography at 70 km depth demonstrates a high spatial correlation between negative velocity perturbations and plate boundaries and deformation zones. The shear wave velocity model is by [Debayle et al. \(2016\)](#). Nearly 80% of recently active, Quaternary volcanoes lie within microplates and deformation zones. Volcano locations from [Global Volcanism Program \(2013\)](#). Pleistocene and younger volcanics from [Gard et al. \(2019a\)](#); originally from EarthChem.org affiliated databases.

plate boundary zones begin to lose their negative velocity anomalies. The correlation between plate boundary zones and shallow mantle shear wave velocity anomalies are the result of thinner and warmer lithosphere in actively deforming regions with respect to cold, thick, rigid plate interiors.

Only a few plate boundaries and deformation zones are not clearly associated with negative shear-wave velocity anomalies. The Cordilleran Frontal Thrust, Lesser Antilles Arc, Lwandle Microplate and San Microplate have non-negative seismic anomalies. In the case of Lwandle and San Microplates, the lack of a clear velocity anomaly may be due to the very slow relative velocities between the Microplate and African Plate ([Wedmore et al., 2021](#)). Oceanic intraplate deformation zones do not show clear correlations with negative tomographic anomalies. For example, the Capricorn region between the Indian and Australian Plates, the Macquarie Microplate, and the boundary between North and South America are not clearly delineated by tomography.

Volcanoes also show high correlation with the plate boundary zones as ~80% lie within

deformation zones and microplates (Figure 13). Like earthquakes, there are differences between the distribution of distance from plate boundaries by type (Figure 12). Volcanoes are furthest from subduction zones, with the majority ranging between 130 to 330 km. For transforms and extension zones, >75% lie within 100 km of the boundary. The distribution of volcanoes from spreading centers is more complex because most of the volcanoes identified near these environments are seamounts associated with hotspots rather than flows at ridges. If a full accounting of flows could be made along ridges, it is likely the distribution would indicate most are much closer to the drawn boundaries Rubin (2016). We try to account for this by using dates from a global geochemical dataset (Gard et al., 2019a, and Figure 13), which results in a similar distribution of distances as the volcanic eruption database (Figure 12). The only exception is the distribution of dates from recent volcanic samples, which fall considerably closer to spreading centers than the eruption database similar to earthquakes (Figure 12b).

The correlation between volcanoes and seismic velocities may imply partial melt is common beneath most plate boundary zones. However, there are a few that have minimal volcanism but high seismicity, including Tibet and the Tien Shan Mountains. The Amur, Yangtze and Okhotsk regions also have very little volcanism outside the volcanic arcs on their margins. These regions also have little seismicity in their interiors.

There are a few regions with negative seismic anomalies and/or recently active volcanic centers that do not correspond with plate boundaries. Several of these regions are hotspots associated with mantle plumes (e.g., Hawaii, Reunion, Cape Verde). These regions do not have clear negative velocity anomalies at 70 km depth within the scale of the tomography model (Figure 13). There is a negative shear wave anomaly in the Arctic without volcanics, which may be related to prior rifting and the Eureka Orogeny (Darbyshire, 2005). The Saharan Metacraton has both low shear velocities and volcanism, but little seismicity. There are currently no GPS data from western Egypt, Chad, Sudan or Libya above the seismic anomaly, but GPS data in Nigeria do not indicate active deformation above the negative velocity region. The West Antarctic Rift contains both volcanoes and a negative shear wave anomaly related to renewed extension in the Cenozoic (Winberry and Anandakrishnan, 2004; Gupta et al., 2009; O'Donnell et al., 2019). While there is active volcanism associated with the Marie Byrd and Erebus hotspots, seafloor magnetic anomalies suggest the rift was active as recently as 11 Ma (Granot

945 and Dymant, 2018) and minimal seismicity suggests the region is inactive at present.

946 *4.3.3. Uncertain Plate Boundaries*

947 Many oceanic deformation zones and microplates have relatively uncertain boundaries due to
948 a lack of GPS constraints, significant seismicity and/or distinctive bathymetric features akin to
949 boundaries. The Azores deformation zone, for example, has a well-defined boundary along the
950 northern margin by seismicity. GPS data on individual islands suggest internal deformation
951 (Fernandes et al., 2006; Marques et al., 2013), but the southern boundary is not clear from
952 seismicity. Our best estimate places the southern boundary on the East Azores Fracture Zone
953 due to its clear topographic expression.

954 The Capricorn Plate is a region of diffuse extension between the Indian and Australian
955 Plates (Wiens et al., 1985; Gordon et al., 1990). The region is large, nearly the same size as
956 the Indian Plate, but the eastern and southeastern boundaries are very uncertain (Figure 14).
957 Magnetic anomaly maps of the plate are sparse on the southern boundary (i.e., Wharton Basin).
958 Bathymetry is complicated by several features including the Ninetyeast Ridge, Diamantina
959 Escarpment, Roo Rise, Vening Meinesz Seamounts, and the Raitt Rise. Earthquakes, while
960 indicating extension, are not of sufficient density to clearly delineate the boundaries (Figure 14).
961 Furthermore, the Indian and Australian Plates have relatively high rates of diffuse intraplate
962 seismicity, without clear clustering indicative of rigid plates boundaries.

963 The eastern, western, and northern boundary of the Lwandle Microplate are poorly con-
964 strained. Most authors have drawn the northern boundary as an extension of the Quasama
965 Seismic Axis on the southern end of the Rovuma Microplate to Madagascar and then traversing
966 Madagascar along a constant line of latitude before running along the eastern margin of the
967 island (e.g., Saria et al., 2014). However, there is little to no observed seismicity to constrain
968 this model. A more recent model suggests the northern boundary is constrained by a dextral
969 transform that runs along the Comoros archipelago which is consistent with seismicity and GPS
970 velocities in northern Madagascar (King et al., 2017; Famin et al., 2020; Stamps et al., 2018,
971 2021). For this reason, we prefer the northernmost boundary in our model, and have separated
972 the northern Lwandle region into the Comoros deformation zone.

973 The San Microplate was recently identified from geodetic studies of relative motions in Africa
974 (Njoroge et al., 2015; Wedmore et al., 2021); however, the evidence is currently insufficient to

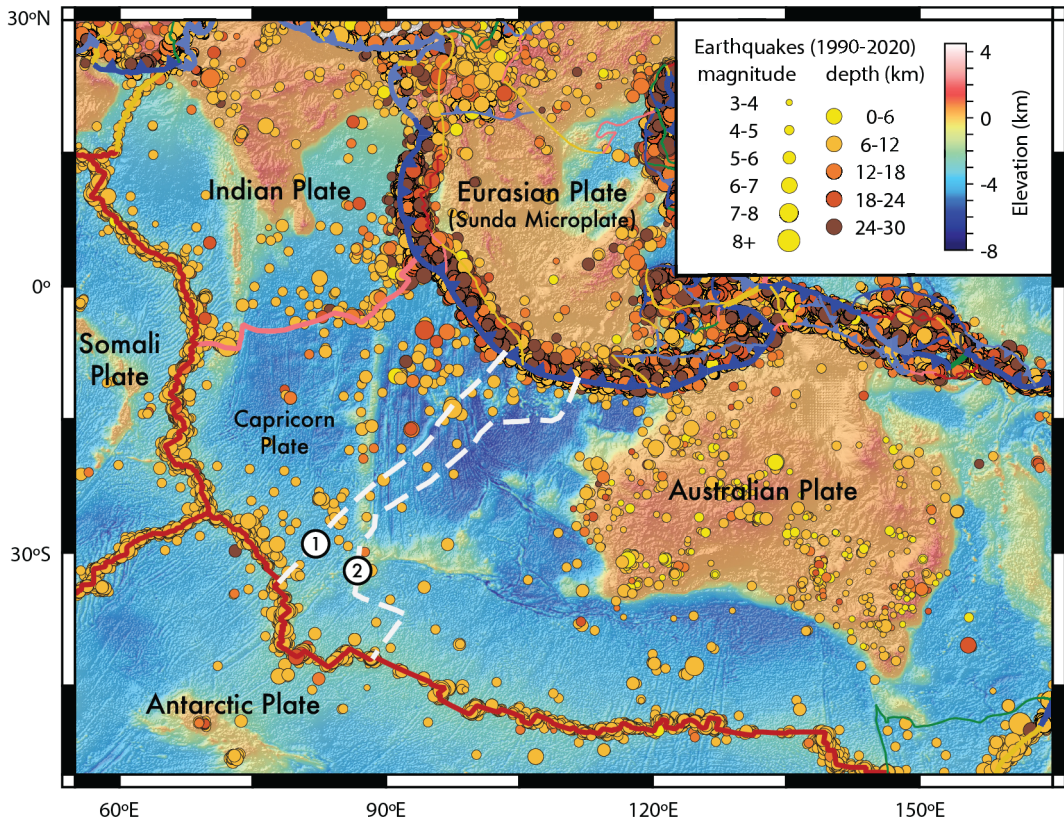


Figure 14: Models of the Capricorn Plate and associated Mid-Indian deformation zone. The white boundaries are a couple of the proposed southern boundaries: 1, (Rathnayake et al., 2019); 2, (Royer and Gordon, 1997).

justify its existence. The microplate shares its eastern boundary with the Lwandle Microplate. The northeastern boundary follows the southwest East African Rift which can be identified by mapped faults and seismicity (Poggi et al., 2017). However, the exact location of the boundary in southwestern Africa is difficult to trace as there is no Quaternary faults, seismicity is not above the intraplate background (Poggi et al., 2017) and there is no clear topographic expression. In the south Atlantic Ocean, Wedmore et al. (2021) infers the Walvis Ridge—a hotspot track (Sager et al., 2021)—marks the boundary. The lack of a clear shear-wave anomaly associated with the northern San Microplate boundary further weakens the case for a microplate boundary (Figure 13). Lastly, relative motions between the San Microplate and the African Plate are $<1 \text{ mm yr}^{-1}$ Njoroge et al. (2015); Wedmore et al. (2021). Such low velocities could result from a far-field long-wavelength glacial isostatic adjustment. As the case is currently weak, we include the San Microplate as part of the African Plate. We retain the polygons should the case be strengthened by future studies and indicate the boundary as inferred.

The boundary between the oceanic portion of the North and South American Plates east of the Lesser Antilles Trench is poorly defined by limited diffuse seismicity. In fact, the low level

990 of seismicity is similar to many intraplate regions not considered deformation zones. The lack
991 of GPS stations in both regions makes it difficult to define the edges of the deformation zone
992 reliably. Given the lack of a clear diffuse region, we draw the boundary as the most prominent
993 feature, the Fifteen-Twenty Fracture Zone, which is consistent with prior interpretations ([Roest](#)
994 and [Collette](#), 1986; [Dixon and Mao](#), 1997; [DeMets et al.](#), 2010).

995 *4.4. Geologic Province Model*

996 The geological province model includes 918 polygons, of which 790 (86%) are continental.
997 Most continental terranes are linear belts with areas that range between 10^4 and 10^6 km 2 . The
998 median province area is 175,000 km 2 , but varies between different continental regions from 10^5
999 and 3×10^5 km 2 (Figure 15a). The distribution of province sizes is largest in South America
1000 and Africa. Part of the reason may be due to the inability to pick out smaller terranes beneath
1001 thick sedimentary cover and relatively few studies with high resolution geophysical data. It is
1002 also due to the number of composite type terranes such as cratons, shields and orogens that are
1003 built from ophiolites, accretionary complexes, and volcanic arcs (Figure 15b). However, some
1004 provinces are naturally larger due to the processes involved in their formation (i.e., passive
1005 margins and wide rifts).

1006 The most common province types are orogenic belts, volcanic arcs and accretionary com-
1007 plexes (Figure 15b). There are many fewer extended terranes, however, passive margins are
1008 generally rifted margins with thick sediment on top. Many ancient rifts are incorporated into
1009 orogenic belts. Where orogenic belts have been separated into their individual constituents,
1010 there is often an accretionary complex and associated arc. However, in many cases only a vol-
1011 canic arc is identified, which may be because the related accretionary complex is commingled
1012 with the volcanic arc and difficult to separate or was destroyed during orogenesis.

1013 *4.4.1. Comparison with Matthews et al. (2016) and Merdith et al. (2021)*

1014 The model by [Matthews et al. \(2016\)](#) was constructed to model plate motions over the past
1015 400 Ma. Given their model timeframe, continental provinces that moved relative to one another
1016 prior to 400 Ma are not typically subdivided. As a result, our model contains a significantly
1017 greater number of terrane divisions. Many of the divisions in the [Matthews et al. \(2016\)](#) model
1018 are also simpler than ours. This simplicity requires fewer polygon vertices, which may make

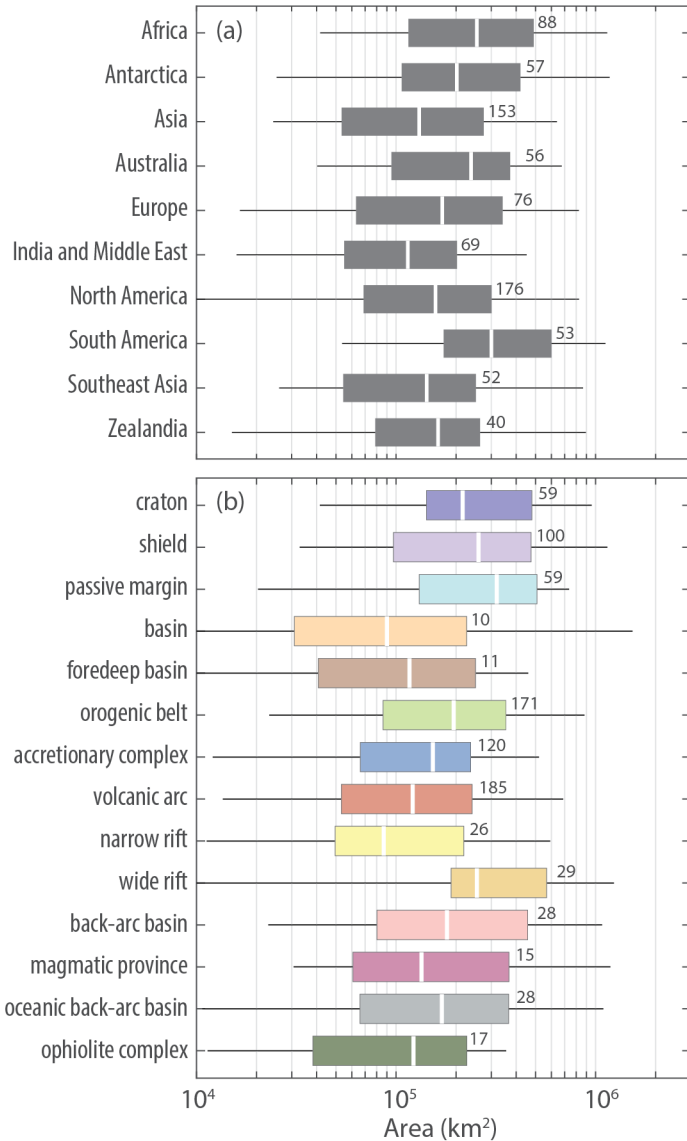


Figure 15: Area of geological provinces for (a) continental regions and by (b) province type. The white bar indicates the median, box enclose the 0.25 to 0.75 quantiles and whiskers extend to the 0.05 and 0.95 quantiles. The number beside the boxes indicates the number of provinces for each region.

1019 computation of plate rotations more rapid, but it compromises accuracy of filtering geologic
1020 data for analysis.

1021 The [Merdith et al. \(2021\)](#) model extends the [Matthews et al. \(2016\)](#) plate motions back
1022 to 1000 Ma, which required the addition of many more province boundaries. The models
1023 for southern Africa, the northwest Cordillera, and the Mongol Orocline are similar to ours.
1024 However, there are significant differences in the number of provinces in Australia, Antarctica,
1025 eastern Europe and the Superior Craton. Many of these differences occur where we include a
1026 finer resolution of terrane boundaries with tectonic histories that converge prior to 1000 Ma.
1027 In light of the agreement with previous reconstruction polygons, the model presented in this
1028 study could be used in the future for plate reconstructions into the Archean.

1029 4.4.2. Comparison with *CrustX* models

1030 We compare our province model with the model by [Laske et al. \(2013\)](#) (Table 6 and Fig-
1031 ure 16). Crust1.0 contains a model of crustal types updated from previous Crust5.1 and
1032 Crust2.0 ([Mooney et al., 1998](#); [Bassin et al., 2000](#); [Artemieva and Mooney, 2001](#); [Mooney,](#)
1033 [2007](#); [Laske et al., 2013](#)). We refer to the multiple generations of the USGS crustal models
1034 as CrustX. Crustal types are defined in [Mooney et al. \(1998\)](#). Most defined crustal types are
1035 similar between the two models. Oceanic crust, and forearc—accretionary complex in this
1036 study—are the only crustal types that have exact equivalencies. However, there are some key
1037 differences in definitions or grouping, with a few types exclusive to one province model or the
1038 other (Table 6).

1039 First, the slight lexical differences (Table 6). [Mooney et al. \(1998\)](#) define Precambrian
1040 regions as shields (exposed) and platforms (sediment covered). The update by [Laske et al.](#)
1041 ([2013](#)) almost entirely redefines the previous Crust5.1 platform regions as shield. We define
1042 cratons as regions with Archean cores and shields as regions with Paleo-Mesoproterozoic belts.
1043 In the thirty-some years since the first iteration of CrustX models, our understanding of Neo-
1044 proterozoic geology has improved sufficiently to classify many of these regions by their tectonic
1045 affiliation. [Mooney et al. \(1998\)](#) defines three types of extended crust: rifts, thinned continent
1046 and extended crust. It appears that only active rifts are defined as rifts. The precise differences
1047 between extended crust and thinned continent are not clear, but thinned continent has been
1048 almost completely removed in Crust1.0. In contrast to CrustX, our model separates rifts into

Table 6: Primary crustal types defined in Crust5.1 ([Mooney et al., 1998](#)) and the similar types from this study.

Crust5.1	This study	Comment
oceanic crust	oceanic crust	created by seafloor-spreading
anomalous o.c.	–	LIPs and hotspots; we suggest superimposing Johansson et al. (2018) if desired
–	ophiolite	generally below the resolution of Crust5.1
shield	craton or shield	Crust5.1 splits into Archean, early-middle Proterozoic, and late Proterozoic; late Proterozoic is classified as orogen or other types in this study
Phanerozoic	–	unknown type of Phanerozoic age
rift	wide or narrow rift	
thinned continent	wide or narrow rift	thinned continent has been effectively removed from Crust1.0
extended crust	wide or narrow rift	unclear how this differs from thinned continent
transition	passive margin	Crust5.1 tile that covers oceanic and continental crust
shelf transition	passive margin	Crust5.1 tile that covers oceanic and continental crust
continental shelf	passive margin or back-arc basin	orogens in this study are divided into other types if possible
ogen	ogenetic belt	
platform	craton, shield, basin (rarely) or orogen	generally sediment covered craton/shield in crust5.1, applied inconsistently; Crust1.0 only contains platform in the West Siberian Basin and Arabia
–	foredeep basin	
continental plateau	–	not clear how this is defined, these are mixed crustal types
–	magmatic province	
continental arcs	volcanic arc	most arcs are below the resolution of Crust5.1
island arcs	volcanic arc	most arcs are below the resolution of Crust5.1
forearc	accretionary complex	not displayed in Mooney et al. (1998) Figure 1A

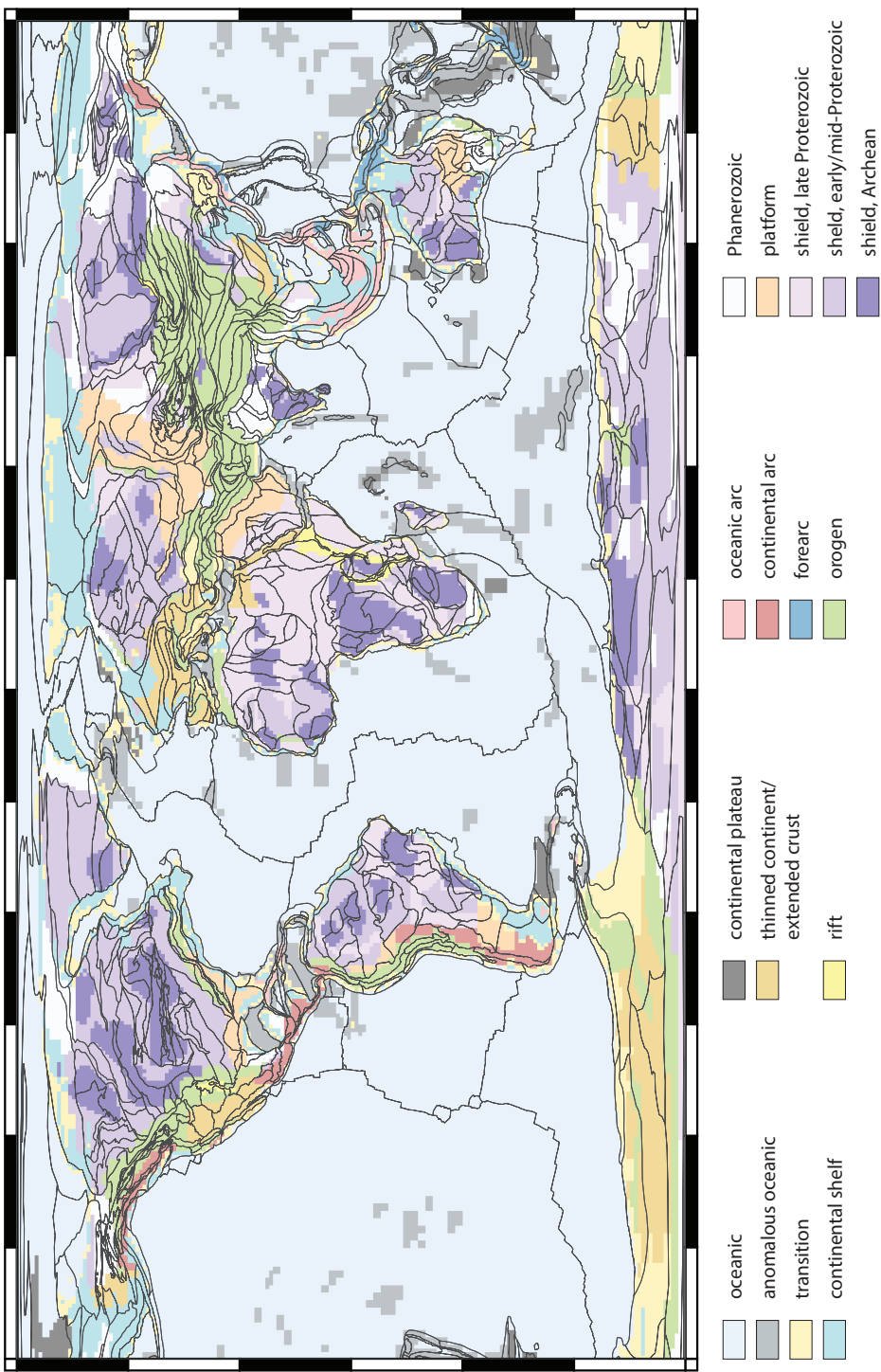


Figure 16: Crust1.0 model from [Laske et al. \(2013\)](#), with crustal types defined by [Mooney et al. \(1998\)](#). Geological province boundaries from this study are superimposed.

1049 narrow and wide rifts. Narrow rifts tend to occur in cold/strong Precambrian lithosphere (e.g.,
1050 East African Rift, Baikal Rift) whereas wide-rifts tend to occur in weak/warm lithosphere at
1051 the time of rifting (e.g., North American Basin and Range). Orogen and orogenic belt are
1052 defined similarly, though we break orogenic belts into other crustal types (e.g., ophiolite, ac-
1053 cretionary complex and volcanic arc) if a province largely retains its distinctive characteristics.
1054 [Mooney et al. \(1998\)](#) separates volcanic arcs into continental and island whereas we do not.
1055 Trace element patterns are very similar between oceanic and continental arcs, with continental
1056 arcs more fractionated and consequently more enriched in light trace elements ([Kelemen et al.,](#)
1057 [2007](#)).

1058 There are a number of larger differences between our model and CrustX (Table 6). Transi-
1059 tional crust and continental shelf in the CrustX model are generally defined as passive margins
1060 in our study, but the CrustX definitions also includes regions we define as continental back-arcs
1061 in our model (Figures 7 and 16). We also define oceanic back-arcs as regions with subduction
1062 modified spreading that occurs in the hinterland of a volcanic arc that are not included in the
1063 CrustX. Curiously, the CrustX models includes oceanic LIPs (anomalous oceanic crust) but not
1064 continental LIPs (Columbia River Basalts, Deccan Traps, Parana-Entedeka Basalts, Siberian
1065 Traps, etc.) except for a few that sit below sea-level (e.g., Campbell Plateau, Ninetyeast Ridge,
1066 and Seychelles). As previously discussed in Section 3.2.1, we do not include LIPs as part of our
1067 model. As CrustX was developed for making crustal corrections to tomography it makes sense
1068 that CrustX includes LIPs whereas our tectonic model does not. However, ophiolite complexes
1069 are not included in CrustX, but are within our model when they are large enough to be resolved
1070 (Figure 7). Magmatic provinces, also excluded from CrustX, are a bit of an enigma. They are a
1071 few regions of predominantly magmatic orogen, not classified as LIPs, and which do not appear
1072 to be related to volcanic arcs. While there are some significant differences, a CrustX-like model
1073 can be reproduced by combining elements of our geologic province model, the LIP model by
1074 [Johansson et al. \(2018\)](#), and a sediment cover by [Laske and Masters \(1997\)](#) or [Straume et al.](#)
1075 [\(2019\)](#).

1076 The visual differences between our models are considerable, though there is some broad
1077 agreement (Figures 7 and 16). Some of these differences are related to the precision of province
1078 boundaries, which are often one to two pixels inside or outside of Crust1.0 crustal types. Some of

1079 the other clear differences are the classification of late Proterozoic regions (shields in Crust1.0)
1080 classified by their tectonic affiliation. Likewise, many orogens are also classified by more specific
1081 tectonic settings where possible. Although our model is likely a more accurate representation of
1082 many province types since it incorporates many recent studies, we anticipate it will be improved
1083 as new geochronological sampling and geoscientific studies expand our understanding.

1084 *4.4.3. Last Orogeny*

1085 To ensure that our orogenic model is reasonable (Figures 8 and 9), we have computed kernel
1086 density estimates (KDE) for both magmatic crystallization dates and metamorphic dates for
1087 each orogen (Figure 17). The dates are mostly derived from U–Pb, ^{207}Pb – ^{206}Pb , and U–Th–Pb
1088 analyses of zircon and monazite. The zircon dates can provide constraints for both igneous and
1089 metamorphic events whereas most monazite dates record metamorphic events in the datasets
1090 we used (Eglington, 2004; Puetz, 2018; Brown and Johnson, 2018; Gard et al., 2019a). Other
1091 isotopic dating systems (e.g., ^{40}Ar – ^{39}Ar , K–Ar, and Rb–Sr) may record lower closure tempera-
1092 tures and can correspond to less significant heating events and are therefore generally excluded
1093 from the dataset except where the dates match the regional higher temperature metamorphism
1094 or in younger systems where U–Th–Pb lose precision.

1095 The largest age peak for metamorphic KDEs always falls within the range of dates attributed
1096 to an orogen as discussed in Section 3.2.2. It is important to note that these dates were not
1097 used to define the orogen, but undoubtedly many of these orogen models are based in part on
1098 geochronology. In Figure 8, one can see the spatial correspondence between metamorphic dates
1099 and our orogen interpretation. In a few cases, there are smaller-magnitude metamorphic date
1100 peaks that record P-T conditions of previous orogenic events. For example, in the Canadian
1101 Cordillera Frontal Thrust Belt a few dates are associated with the Wyoming Craton (ca. 1780
1102 Ma; Cheney et al., 2004b,a) and not the more recent Cordilleran deformation (Figure 8). These
1103 older metamorphic events are still evident because Cordilleran deformation reaches relatively
1104 shallow levels in these regions and has not reset the isotopic systems associated with the older
1105 events.

1106 Very few orogens have significant age peaks younger than the assigned orogen. The excep-
1107 tions include the Rodinian Orogeny which in some cases includes some Gondwana-associated
1108 dates, particularly in Antarctica, and the Circum-Nunalian terranes, which include some

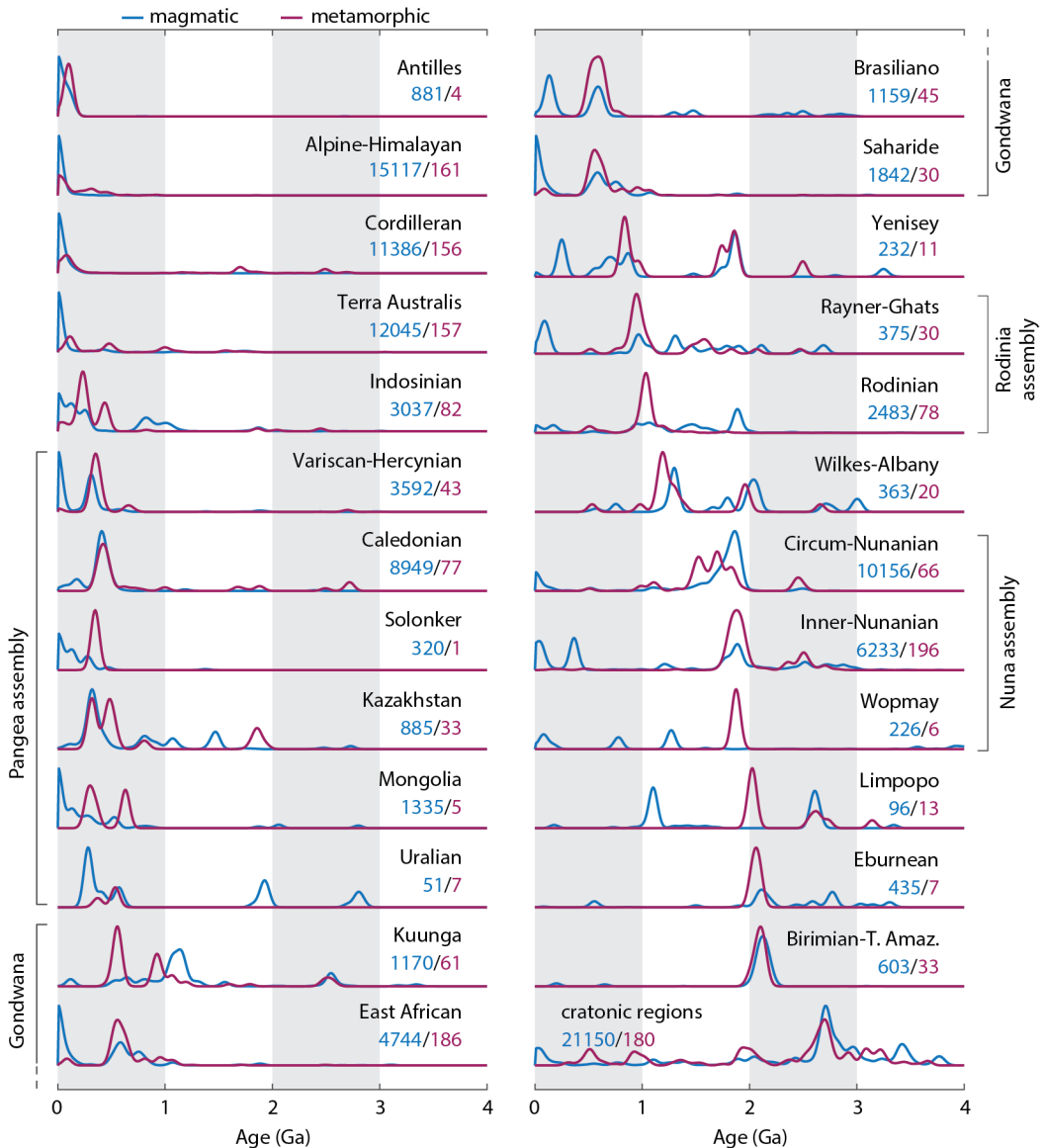


Figure 17: Kernel density estimates for magmatic crystallization dates (blue, [Gard et al. \(2019a\)](#)) and metamorphic dates (violet, [Brown and Johnson \(2018\)](#) updated; [Eglington \(2004\)](#)). A list of metamorphic dates are given in the Supplemental Material. No dates for the Scotian Orogeny are available in the database.

1109 Rodinia-associated overprinting (Figure 17)—specifically in North America where metamorphic
1110 conditions are poorly sampled (Figure 8). These discrepancies between the orogenic model and
1111 observed metamorphic conditions may indicate some refinement of the province model may be
1112 necessary.

1113 The magmatic dates are noisier, often indicating several episodes of magmatism, which
1114 attests to the multi-generational history to the growth of many provinces (Figure 17). There
1115 are a surprising number of provinces which have magmatic peaks near the present day that lie in
1116 generally much older orogens. In the East African Orogen, the younger ages are associated with
1117 the East African Rift. In the Saharides and Trans Hudson Orogen, these younger magmatic
1118 ages are the result of Cenozoic intraplate magmatism, which does not appear to be associated
1119 with active tectonics. In many regions with younger volcanism, the geodynamic process that
1120 has created the melts does not appear to have reset metamorphic conditions or alternatively
1121 the depths at which metamorphism has occurred have not yet been exhumed.

1122 While magmatic dates appear to be less reliable for identifying the last orogen event, there
1123 is often a peak in the KDE that corresponds with the metamorphic peak. The Limpopo Orogen
1124 is a clear exception where no magmatic peak is observed during the orogenic event. The missing
1125 magmatic peak at ca. 2.0 Ga is the reason the Limpopo orogen was originally interpreted as a
1126 ca. 2.7 Ga event, rather than a younger intracontinental orogen (Barton and van Reenen, 1992;
1127 Yin et al., 2019). The only other orogen with missing magmatic dates is the Wopmay Orogen
1128 in northwest Canada, however, this orogen is poorly exposed so there are very few data from
1129 the terranes that comprise it.

1130 The KDEs for the cratonic regions display significant magmatic and metamorphic activity
1131 prior to 2.5 Ga, with a few minor metamorphic and igneous peaks. Many of these small
1132 younger (<2.5 Ga) metamorphic peaks do not appear to correspond with magmatism, which
1133 may indicate minor degrees of intracratonic deformation as orogens occur around them. We
1134 suggest this observation is consistent with a persistent mechanically strong lithosphere able
1135 to resist deformation in most cases. The young magmatic peak within cratonic regions is
1136 common across most orogens. As most of these regions are intraplate several questions arise
1137 regarding the lack of widespread intraplate volcanism in the past. Are intraplate volcanics
1138 easily eroded and therefore poorly preserved? If not, is there a sampling bias, i.e., petrologists

1139 and geochemists vastly oversample present-day intraplate volcanism, or are they generally too
1140 small and distributed in the past to easily recognize and thus ignored?

1141 *4.4.4. Uncertain Province Boundaries*

1142 Perhaps the poorest geologically characterized region is Antarctica due to the lack of out-
1143 crops. Most geological province information about Antarctica comes from regions near the
1144 coast typically combined with constraints from conjugate terranes on now-distant continents
1145 (e.g., [Boger, 2011](#); [Flowerdew et al., 2013](#); [Goodge et al., 2017](#); [Maritati et al., 2019](#); [Rup-](#)
1146 [pel et al., 2020](#)). Due to the nature of these peripheral constraints, province boundaries are
1147 more uncertain into the subglacial interior and are typically guided by geophysical fields such
1148 as gravity and magnetics following linear trends ([Aitken et al., 2014](#); [Maritati et al., 2016](#)).
1149 Because of the uncertainties, it has resulted in a myriad of province models that can change
1150 significantly as additional geological data are added and higher resolution geophysical models
1151 are produced. Very few models include interior provinces that do not reach the coast because of
1152 the lack of geological control (cf., [Ferraccioli et al., 2011](#)), however new multivariate approaches
1153 to mapping lithospheric boundaries suggest significant interior complexity characterizes East
1154 Antarctica ([Stål et al., 2019](#)).

1155 Our Antarctic province model is derived from several geophysical constraints (Table 3). As
1156 with other continents, magnetic anomalies are often the best constraint on province bound-
1157 aries in the upper crust (Figure 18a). Geochronology is important for defining provinces and
1158 identifying boundaries in areas of outcrop, which are mostly concentrated near the coast. The
1159 PetroChron Antarctica database is a compilation of geochronology and other geological data of
1160 Antarctica ([Sanchez et al., 2021](#)), that will surely continue to improve our insights into the pre-
1161 cise positioning of Antarctic province boundaries. Our model includes a few interior provinces
1162 that we interpret as cratonic or shield terranes due to the lithospheric characteristics, though
1163 they are relatively large. These terranes are ringed by orogens at the edges of the continent,
1164 similar to many other continental shields (e.g., Kaapvaal, Congo, and Siberian Cratons).

1165 Most other poorly resolved regions include those covered by thick sedimentary cover: Patag-
1166 onia, Parana Basin, Saudi Arabian Platform, North Africa, and West Siberian Basin. In these
1167 regions the provinces tend to be much larger than the average and there are multiple in-
1168 terpretations for their divisions. These models are difficult to independently assess because

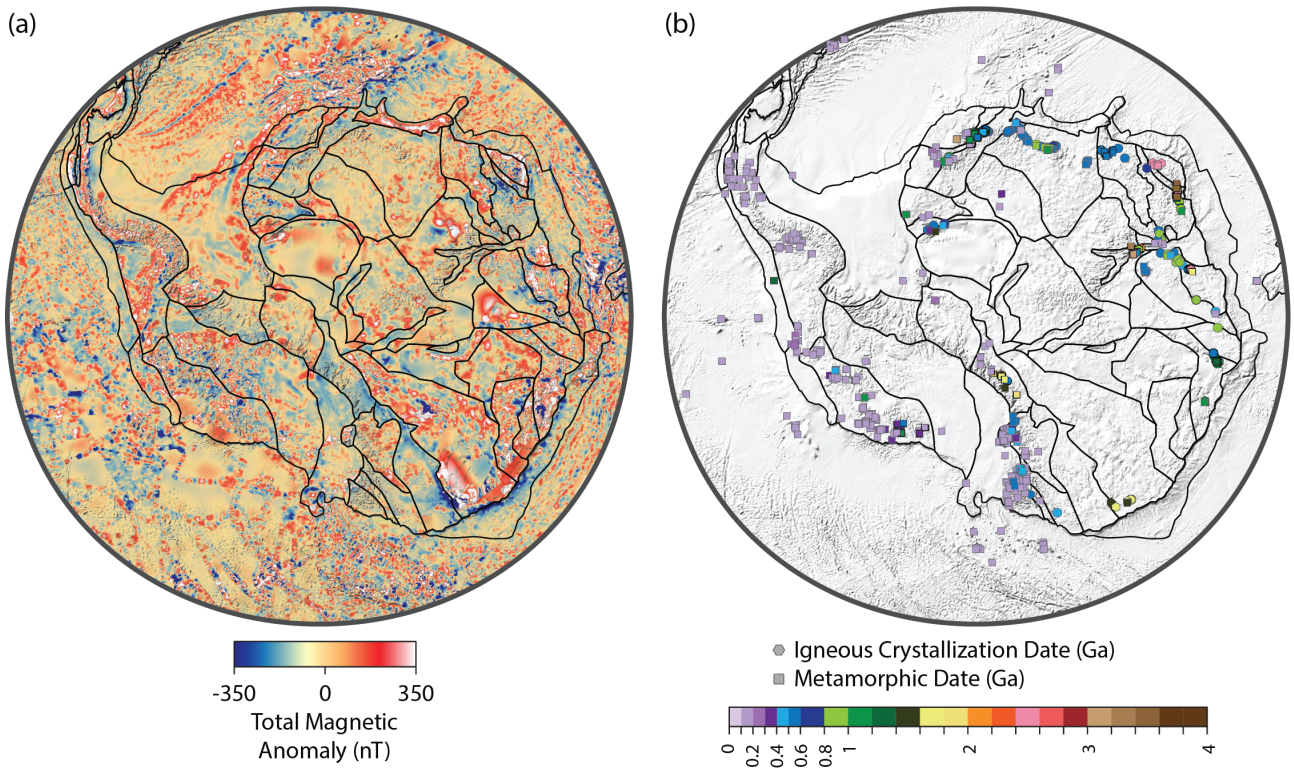


Figure 18: Magnetic (a) and geochronologic (b) constraints on the Antarctic province model. Magnetic data from ADMAP2 (Golynsky et al., 2018) and EMAG2_V3 (Meyer and Saltus, 2016) to fill gaps. Igneous crystallization dates from Gard et al. (2019a) and Puetz (2018) and metamorphic dates from Brown and Johnson (2018), updated, and DateView, (Eglinton, 2004).

the geophysical data in many of these regions is relatively poor. For example, the Saharan Metacraton and Tuareg Shield have considerably different interpretations for their evolution. The Tuareg Shield is constructed of a set of imbricated arc terranes. Most models show little to no association with the Saharan Metacraton, which is interpreted as a set of Archean cores with reworked subcontinental lithosphere (Liégeois et al., 2013; Sobh et al., 2020). This interpretation is based on thermophysical modeling using multiple geophysical data, but the data are relatively low resolution. An alternative explanation developed using geochronological and geochemical data suggests the Tuareg Shield, Arabian–Nubian Shield and portions of the Saharan Metacraton were a single volcanic arc system that was broken in multiple segments, reorganized and then accreted to the core of the metacraton, deforming it in the process in the Neoproterozoic (Liégeois, 2018; Sengör et al., 2020; Blades et al., 2021).

4.5. Future Improvements

There are a number of improvements that can be made to the province definitions in future versions. Higher resolution geologic maps could be incorporated that have better lithological data and finer age resolution in the Precambrian, especially the Archean. Likewise, higher

1184 resolution magnetic data will be very useful for improving terrane boundaries, especially when
1185 the resolution is \sim 10 km pixel spacing. Most global geophysical datasets are available at too
1186 low a resolution to precisely resolve many terrane boundaries.

1187 Province types that do not provide information about the tectonic construction of the crust
1188 (basin, shield, and craton), should be replaced in future versions. Doing so may require im-
1189 proved geologic models of Precambrian regions, which may require the addition of new tectonic
1190 settings that are unique to the early Earth such as granite-greenstone belts. Likewise, orogenic
1191 belts could also be deconstructed into the types of terranes that build them, i.e., separating out
1192 arcs and accretionary margins could help improve models of crustal growth and composition.

1193 Although we currently only ascribe the last orogenic event to provinces, many regions have
1194 experienced multiple orogenic events throughout their history. Adding this history to the at-
1195 tribute tables would provide a more complete view of an individual province's chronological his-
1196 tory, which could be paired with information about the changing tectonic environments. Such
1197 a model would require a more sophisticated analysis of global geochemical and geochronological
1198 data. This process would be tedious to perform on a province by province scale so an automated
1199 approach will be warranted and could include recent machine-learning based approaches to pre-
1200 dicting tectonic environments (e.g., [Tang et al., 2020](#); [Tetley et al., 2020](#)). These improvements
1201 would place valuable constraints on plate reconstruction models.

1202 Constructing the province models can include a community-driven approach that is updated
1203 by individuals or small groups with expertise in specific regions. To that end, we have set
1204 up a GitHub project page where individuals can download the shapefiles, update them, and
1205 upload their changes along with a description, references, and rationale for the changes. The
1206 changes can then be evaluated and incorporated into the model if deemed credible. Thus, one
1207 would not need to wait for a formally published reference before using the improved maps
1208 (https://github.com/dhasterok/global_tectonics).

1209 5. Summary

1210 We have produced a set of plate and geologic province maps that can be used to improve spa-
1211 tial analysis of geoscientific data. The plate model boundaries are validated against earthquake
1212 locations, active fault traces, and GPS motions and shows good correlation with shear wave
1213 velocities at 70 km depth and active volcanism. The geological province model is constructed

1214 from a collage of published models and refined using a wide-variety geophysical and geological
1215 data. The most useful data were found to be aeromagnetic anomalies when the models are high
1216 resolution. The province model has not been independently validated at this point, but relies
1217 on the accuracy of the original studies. However, the last orogeny is validated using metamor-
1218 phic and igneous dates. The plate and province polygons are drawn so that the boundaries are
1219 seamless between the files and additionally include an ocean–continent boundary and a plate
1220 boundary type.

1221 The maps are available in a shapefile format that can be easily interpreted by many modern
1222 computer languages and have advantages over raster maps for geographically selecting data
1223 for various types of analysis. The maps can also be used as a data standard for prescribing
1224 spatial metadata in global databases. Because the models are available on GitHub, the geologic
1225 community can submit updates and fixes to improve their accuracy.

1226 Data Availability

1227 Plate and province models produced in this study are available at the GitHub repository,
1228 https://github.com/dhasterok/global_tectonics. The models can be found in shapefile
1229 format suitable for GIS programs, KML for programs such as GoogleEarth, and GMT format for
1230 Generic Mapping Tools. The models are also available in the global tectonics library on Zenodo,
1231 <http://doi.org/10.5281/zenodo.5093930>, which includes additional global geophysical and
1232 geochronological datasets that are useful for research and educational applications.

1233 Acknowledgements

1234 The authors thank the reviewers Robert J. Stern and Donald F. Argus, and the editor,
1235 Douwe van Hinsbergen, who provided constructive reviews that helped improve this manuscript.
1236 The authors would like to thank Sabin Zahirovic and Sarah Stamps for suggestions related to
1237 earlier versions of the plate and province model. Xianzhi Cao was kind enough to share his
1238 new plate reconstruction and Yebo Liu provided GPlates files for the Siderian period.

1239 Funding

1240 This work was partially funded by the Australian Government through the Australian Re-
1241 search Council’s Discovery Projects funding scheme (project DP180104074) to DH, JH, and

1242 MH. JH's contributions were also supported by the Australian Research Council Special Re-
1243 search Initiative for Antarctic Gateway Partnership (SR140300001) and Australian Centre for
1244 Excellence in Antarctic Science (SR200100008). SG is supported by an Australian Research
1245 Council Future Fellowship (FT210100906). The views expressed herein are those of the authors
1246 and are not necessarily those of the Australian Government or Australian Research Council.
1247 MG was supported by an Australian Government Research Training Program Scholarship.

1248 References

- 1249 Abdullah, R., Rosenbaum, G., 2018. Devonian crustal stretching in the northern Tasmanides
1250 (Australia) and implications for orocinal bending. *Journal of Geophysical Research: Solid*
1251 *Earth* doi:[10.1029/2018jb015724](https://doi.org/10.1029/2018jb015724).
- 1252 Aitken, A.R.A., Young, D.A., Ferraccioli, F., Betts, P.G., Greenbaum, J.S., Richter, T.G.,
1253 Roberts, J.L., Blankenship, D.D., Siegert, M.J., 2014. The subglacial geology of Wilkes Land,
1254 East Antarctica. *Geophysical Research Letters* 41, 2390–2400. doi:[10.1002/2014gl059405](https://doi.org/10.1002/2014gl059405).
- 1255 Allen, R., Collier, J., Stewart, A., Henstock, T., Goes, S., and, A.R., 2019. The role of arc
1256 migration in the development of the Lesser Antilles: A new tectonic model for the Cenozoic
1257 evolution of the eastern Caribbean. *Geology* 47, 891–895. doi:[10.1130/g46708.1](https://doi.org/10.1130/g46708.1).
- 1258 Almeida, M.E., Macambira, M.J., Oliveira, E.C., 2007. Geochemistry and zircon geochronology
1259 of the I-type high-K calc-alkaline and S-type granitoid rocks from southeastern Roraima,
1260 Brazil: Orosirian collisional magmatism evidence (1.97–1.96Ga) in central portion of Guyana
1261 Shield. *Precambrian Research* 155, 69–97. doi:[10.1016/j.precamres.2007.01.004](https://doi.org/10.1016/j.precamres.2007.01.004).
- 1262 Amante, C., Eakins, B., 2009. ETOPO1 1 Arc-Minute Global Relief Model: Procedures, Data
1263 Sources and Analysis. Technical Memorandum NESDIS NGDC-24. NOAA. doi:[10.7289/V5C8276M](https://doi.org/10.7289/V5C8276M).
- 1265 Amato, J.M., Boullion, A.O., Serna, A.M., Sanders, A.E., Farmer, G.L., Gehrels, G.E.,
1266 Wooden, J.L., 2008. Evolution of the Mazatzal province and the timing of the Mazatzal
1267 orogeny: Insights from U-Pb geochronology and geochemistry of igneous and metasedimentary
1268 rocks in southern New Mexico. *Geological Society of America Bulletin* 120, 328–346.
1269 doi:[10.1130/b26200.1](https://doi.org/10.1130/b26200.1).
- 1270 An, M., Wiens, D.A., Zhao, Y., Feng, M., Nyblade, A.A., Kanao, M., Li, Y., Maggi, A.,
1271 Lévéque, J.J., 2015. S -velocity model and inferred Moho topography beneath the Antarctic
1272 Plate from Rayleigh waves. *Journal of Geophysical Research: Solid Earth* 120, 359–383.
1273 doi:[10.1002/2014jb011332](https://doi.org/10.1002/2014jb011332).
- 1274 An, W., Hu, X., Garzanti, E., Wang, J.G., Liu, Q., 2021. New precise dating of the India-Asia
1275 collision in the Tibetan Himalaya at 61 Ma. *Geophysical Research Letters* 48. doi:[10.1029/2020gl090641](https://doi.org/10.1029/2020gl090641).
- 1277 Anderson, J., Kelsey, D., Hand, M., Collins, W., 2013. Conductively driven, high-thermal
1278 gradient metamorphism in the Anmatjira Range, Arunta region, central Australia. *Journal*
1279 *of Metamorphic Petrology* 31, 1003–1026. doi:[10.1111/jmg.12054](https://doi.org/10.1111/jmg.12054).
- 1280 ANSS, 2020. Comprehensive earthquake catalog (comcat),
1281 <https://earthquake.usgs.gov/earthquakes/search/>, downloaded 26 dec. 2020.

- 1282 Arboit, F., Collins, A.S., Morley, C.K., King, R., Amrouch, K., 2016. Detrital zircon analysis
1283 of the southwest Indochina terrane, central Thailand: Unravelling the Indosinian orogeny.
1284 Geological Society of America Bulletin 128, 1024–1043. doi:[10.1130/b31411.1](https://doi.org/10.1130/b31411.1).
- 1285 Aronoff, R.F., Andronicos, C.L., Vervoort, J.D., Hunter, R.A., 2016. Redefining the meta-
1286 morphic history of the oldest rocks in the southern rocky mountains. Geological Society of
1287 America Bulletin 128, 1207–1227. doi:[10.1130/b31455.1](https://doi.org/10.1130/b31455.1).
- 1288 Artemieva, I., 2006. Global $1^\circ \times 1^\circ$ thermal model TC1 for the continental lithosphere: im-
1289 plications for lithosphere secular evolution. Tectonophysics 416, 245–277. doi:[10.1016/j.tecto.2005.11.022](https://doi.org/10.1016/j.tecto.2005.11.022).
- 1290 Artemieva, I., Mooney, W., 2001. Thermal thickness and evolution of Precambrian lithosphere: a
1291 global study. J. Geophys. Res. 106, 16387–16414.
- 1292 Artemieva, I.M., 2019. Lithosphere structure in Europe from thermal isostasy. Earth-Science
1293 Reviews 188, 454–468. doi:[10.1016/j.earscirev.2018.11.004](https://doi.org/10.1016/j.earscirev.2018.11.004).
- 1294 Atwater, T., Stock, J., 1998. Pacific-North America Plate tectonics of the Neogene southwest-
1295 ern United States: An update. International Geology Review 40, 375–402. doi:[10.1080/00206819809465216](https://doi.org/10.1080/00206819809465216).
- 1296 Australia, G., 2004. Magnetic Anomaly Map of Australia. Technical Report Fourth Edition.
1297 Geoscience Australia. Canberra. doi:[10.4225/25/56258E723A032](https://doi.org/10.4225/25/56258E723A032).
- 1298 Balmino, G., Vales, N., Bonvalot, S., Briais, A., 2011. Spherical harmonic modelling to ultra-
1299 high degree of bouguer and isostatic anomalies. Journal of Geodesy 86, 499–520. doi:[10.1007/s00190-011-0533-4](https://doi.org/10.1007/s00190-011-0533-4).
- 1300 Baltybaev, S., Yurchenko, A., Lobach-Zhuchenko, S., Balagansky, V., Galankina, O., Morozov,
1301 M., Bogomolov, E., 2017. Conditions of metamorphism of garnet-bearing aluminous gneisses
1302 in the Orekhov–Pavlograd zone of the Ukrainian Shield. Russian Geology and Geophysics
1303 58, 1333–1348. doi:[10.1016/j.rgg.2017.11.002](https://doi.org/10.1016/j.rgg.2017.11.002).
- 1304 Baranov, A., Tenzer, R., Bagherbandi, M., 2017. Combined gravimetric–seismic crustal model
1305 for Antarctica. Surveys in Geophysics 39, 23–56. doi:[10.1007/s10712-017-9423-5](https://doi.org/10.1007/s10712-017-9423-5).
- 1306 Barbosa, J., Peucat, J., Martin, H., Dasilva, F., Demoraes, A., Correagomes, L., Sabate,
1307 P., Marinho, M., Fanning, C., 2008. Petrogenesis of the late-orogenic Bravo granite and
1308 surrounding high-grade country rocks in the Palaeoproterozoic orogen of Itabuna-Salvador-
1309 Curaçá block, Bahia, Brazil. Precambrian Research 167, 35–52. doi:[10.1016/j.precamres.2008.06.002](https://doi.org/10.1016/j.precamres.2008.06.002).
- 1310 Barnes, C.J., Walczak, K., Janots, E., Schneider, D., Majka, J., 2020. Timing of Paleozoic Ex-
1311 humation and Deformation of the High-Pressure Vestgötabreen Complex at the Motalafjella
1312 Nunatak, Svalbard. Minerals 10, 125. doi:[10.3390/min10020125](https://doi.org/10.3390/min10020125).
- 1313 Barton, J., van Reenen, D., 1992. When was the Limpopo Orogeny? Precambrian Research
1314 55, 7–16. doi:[10.1016/0301-9268\(92\)90010-1](https://doi.org/10.1016/0301-9268(92)90010-1).
- 1315 Bassin, C., Laske, G., Masters, G., 2000. The current limits of resolution for surface wave
1316 tomography in North America (F897), in: Eos Transactions, American Geophysical Union.
1317 p. 48.

- 1322 Battaglia, M., Murray, M.H., Serpelloni, E., Bürgmann, R., 2004. The Adriatic region: An in-
1323 dependent microplate within the Africa-Eurasia collision zone. *Geophysical Research Letters*
1324 31, L09605. doi:[10.1029/2004gl019723](https://doi.org/10.1029/2004gl019723).
- 1325 Begg, G., Griffin, W., Natapov, L., O'Reilly, S.Y., Grand, S., O'Neill, C., Hronsky, J., Djomani,
1326 Y.P., Swain, C., Deen, T., Bowden, P., 2009. The lithospheric architecture of Africa: Seismic
1327 tomography, mantle petrology, and tectonic evolution. *Geosphere* 5, 23–50. URL: <https://doi.org/10.1130%2Fges00179.1>. doi:[10.1130/GES00179.1](https://doi.org/10.1130/GES00179.1).
- 1329 Berman, R., Pehrsson, S., Davis, W., Ryan, J., Qui, H., Ashton, K., 2013a. The Arrowsmith
1330 orogeny: Geochronological and thermobarometric constraints on its extent and tectonic set-
1331 ting in the Rae craton, with implications for pre-Nuna supercontinent reconstruction. *Precam-
1332 brian Research* 232, 44–69. doi:[10.1016/j.precamres.2012.10.015](https://doi.org/10.1016/j.precamres.2012.10.015).
- 1333 Berman, R., Sanborn-Barrie, M., Rayner, N., Whalen, J., 2013b. The tectonometamorphic
1334 evolution of Southampton Island, Nunavut: Insight from petrologic modeling and in situ
1335 SHRIMP geochronology of multiple episodes of monazite growth. *Precambrian Research*
1336 232, 140–166. doi:[10.1016/j.precamres.2012.08.011](https://doi.org/10.1016/j.precamres.2012.08.011).
- 1337 Berndt, C., Planke, S., Teagle, D., Huismans, R., Torsvik, T., Frieling, J., Jones, M.T., Jerram,
1338 D.A., Tegner, C., Faleide, J.I., Coxall, H., Hong, W.L., 2019. Northeast Atlantic breakup
1339 volcanism and consequences for Paleogene climate change – MagellanPlus Workshop report.
1340 *Scientific Drilling* 26, 69–85. doi:[10.5194/sd-26-69-2019](https://doi.org/10.5194/sd-26-69-2019).
- 1341 Betts, P., Giles, D., 2006. The 1800–1100 Ma tectonic evolution of Australia. *Precambrian
1342 Research* 144, 92–125. doi:[10.1016/j.precamres.2005.11.006](https://doi.org/10.1016/j.precamres.2005.11.006).
- 1343 Betts, P., Giles, D., Schaefer, B., 2008. Comparing 1800–1600 Ma accretionary and basin pro-
1344 cesses in Australia and Laurentia: Possible geographic connections in Columbia. *Precambrian
1345 Research* 166, 81–92. doi:[10.1016/j.precamres.2007.03.007](https://doi.org/10.1016/j.precamres.2007.03.007).
- 1346 Bhowmik, S.K., 2019. The current status of orogenesis in the Central Indian Tectonic Zone: A
1347 view from its southern margin. *Geological Journal* 54, 2912–2934. doi:[10.1002/gj.3456](https://doi.org/10.1002/gj.3456).
- 1348 Bird, P., 2003. An updated digital model of plate boundaries. *Geochemistry, Geophysics,
1349 Geosystems* 4. doi:[10.1029/2001gc000252](https://doi.org/10.1029/2001gc000252).
- 1350 Bispo-Santos, F., D'Agrella-Filho, M.S., Pacca, I.I., Janikian, L., Trindade, R.I., Elming, S.A.,
1351 Silva, J.A., Barros, M.A., Pinho, F.E., 2008. Columbia revisited: Paleomagnetic results from
1352 the 1790 Ma colider volcanics (SW Amazonian Craton, Brazil). *Precambrian Research* 164,
1353 40–49. doi:[10.1016/j.precamres.2008.03.004](https://doi.org/10.1016/j.precamres.2008.03.004).
- 1354 Bjorkman, K.E., 2017. 40 crust-mantle evolution of the Western Superior Craton: implications
1355 for Archaean granite-greenstone petrogenesis and geodynamics. Ph.D. thesis. University of
1356 Western Australia. doi:[10.4225/23/5A39C88A2F559](https://doi.org/10.4225/23/5A39C88A2F559).
- 1357 Blades, M.L., Collins, A.S., Foden, J., Payne, J.L., Stüwe, K., Abu-Alam, T., Makroum,
1358 F., Hassan, M., 2021. Age and hafnium isotope evolution of Sudanese Butana and Chad
1359 illuminates the Stenian to Ediacaran evolution of the south and east Sahara. *Precambrian
1360 Research* 362, 106323. doi:[10.1016/j.precamres.2021.106323](https://doi.org/10.1016/j.precamres.2021.106323).
- 1361 Blayney, T., Dupont-Nivet, G., Najman, Y., Proust, J.N., Meijer, N., Roperch, P., Sobel, E.R.,
1362 Millar, I., Guo, Z., 2019. Tectonic evolution of the Pamir recorded in the western Tarim
1363 Basin (China): Sedimentologic and magnetostratigraphic analyses of the Aertashi section.
1364 *Tectonics* 38, 492–515. doi:[10.1029/2018tc005146](https://doi.org/10.1029/2018tc005146).

- 1365 Bogdanova, S., Gorbatschev, R., Skridlaite, G., Soesoo, A., Taran, L., Kurlovich, D., 2015.
1366 Trans-Baltic Palaeoproterozoic correlations towards the reconstruction of supercontinent
1367 Columbia/Nuna. *Precambrian Research* 259, 5–33. doi:[10.1016/j.precamres.2014.11.023](https://doi.org/10.1016/j.precamres.2014.11.023).
- 1369 Boger, S.D., 2011. Antarctica — Before and after Gondwana. *Gondwana Research* 19, 335–371.
1370 doi:[10.1016/j.gr.2010.09.003](https://doi.org/10.1016/j.gr.2010.09.003).
- 1371 Bowring, S.A., Podosek, F.A., 1989. Nd isotopic evidence from Wopmay Orogen for 2.0–2.4
1372 Ga crust in western North America. *Earth and Planetary Science Letters* 94, 217–230.
1373 doi:[10.1016/0012-821x\(89\)90141-6](https://doi.org/10.1016/0012-821x(89)90141-6).
- 1374 Brandl, P.A., Regelous, M., Beier, C., Haase, K.M., 2013. High mantle temperatures following
1375 rifting caused by continental insulation. *Nature Geoscience* 6, 391–394. URL: <https://doi.org/10.1038%2Fngeo1758>, doi:[10.1038/ngeo1758](https://doi.org/10.1038/ngeo1758).
- 1377 Breton, E.L., Handy, M.R., Molli, G., Ustaszewski, K., 2017. Post-20 Ma motion of the
1378 Adriatic Plate: New constraints from surrounding orogens and implications for crust-mantle
1379 decoupling. *Tectonics* 36, 3135–3154. doi:[10.1002/2016tc004443](https://doi.org/10.1002/2016tc004443).
- 1380 Brown, D.A., Morrissey, L.J., Goodge, J.W., Hand, M., 2021. Absence of evidence for Palaeo-
1381 proterozoic eclogite-facies metamorphism in East Antarctica: no record of subduction orogen-
1382 egenesis during Nuna development. *Scientific Reports* 11. doi:[10.1038/s41598-021-86184-4](https://doi.org/10.1038/s41598-021-86184-4).
- 1383 Brown, M., Johnson, T., 2018. Secular change in metamorphism and the onset of global plate
1384 tectonics. *American Mineralogist* 103, 181–196. doi:[10.2138/am-2018-6166](https://doi.org/10.2138/am-2018-6166).
- 1385 Bruhn, R., Sauber, J.M., Cotton, M.M., Pavlis, T.L., Burgess, E.W., Ruppert, N.A., Forster,
1386 R., 2012. Plate margin deformation and active tectonics along the northern edge of the
1387 Yakutat Terrane in the Saint Elias Orogen, Alaska, and Yukon, Canada. *Geosphere* 8, 1384–
1388 1407. doi:[10.1130/ges00807.1](https://doi.org/10.1130/ges00807.1).
- 1389 Burgett, C., Zaw, K., Meffre, S., Lai, C.K., Khositanont, S., Chaodumrong, P., Udchachon,
1390 M., Ekins, S., Halpin, J., 2014. The configuration of Greater Gondwana—Evidence from
1391 LA ICPMS, U–Pb geochronology of detrital zircons from the Palaeozoic and Mesozoic of
1392 Southeast Asia and China. *Gondwana Research* 26, 31–51. doi:[10.1016/j.gr.2013.05.020](https://doi.org/10.1016/j.gr.2013.05.020).
- 1393 Buslov, M.M., Saphonova, I.Y., Watanabe, T., Obut, O.T., Fujiwara, Y., Iwata, K., Semakov,
1394 N.N., Sugai, Y., Smirnova, L.V., Kazansky, A.Y., 2001. Evolution of the Paleo-Asian Ocean
1395 (Altai-Sayan Region, Central Asia) and collision of possible Gondwana-derived terranes with
1396 the southern marginal part of the Siberian continent. *Geosciences Journal* 5, 203–224. doi:[10.1007/bf02910304](https://doi.org/10.1007/bf02910304).
- 1398 Cai, J., Liu, F., Liu, P., Liu, C., Wang, F., Shi, J., 2015. Silica-undersaturated spinel gran-
1399 ulites in the Daqingshan complex of the Khondalite Belt, North China Craton: Petrology
1400 and quantitative P–T–X constraints. *Precambrian Research* 266, 119–136. doi:[10.1016/j.precamres.2015.05.005](https://doi.org/10.1016/j.precamres.2015.05.005).
- 1402 Cao, X., Flamet, N., Collins, A., Pisarevksy, S., Müller, D., Hasterok, D., in prep. Earth's
1403 tectonic and plate boundary evolution over 1.8 billion years. *Earth Science Reviews* .
- 1404 Capitanio, F.A., Faccenna, C., Zlotnik, S., Stegman, D.R., 2011. Subduction dynamics and
1405 the origin of Andean orogeny and the Bolivian orocline. *Nature* 480, 83–86. doi:[10.1038/nature10596](https://doi.org/10.1038/nature10596).

- 1407 de Carvalho Filgueiras, B., de Oliveira, C.G., de Sousa, I.M.C., Cordeiro, P., 2020. Further
1408 evidence of Rhyacian arc magmatism in the basement of the Brasília Belt, western São
1409 Francisco pericraton. *Journal of South American Earth Sciences* 103, 102739. doi:[10.1016/j.jsames.2020.102739](https://doi.org/10.1016/j.jsames.2020.102739).
- 1411 Catalán, J.R.M., Schulmann, K., Ghienne, J.F., 2021. The Mid-Variscan Allochthon: Keys
1412 from correlation, partial retrodeformation and plate-tectonic reconstruction to unlock the
1413 geometry of a non-cylindrical belt. *Earth-Science Reviews* 220, 103700. doi:[10.1016/j.earscirev.2021.103700](https://doi.org/10.1016/j.earscirev.2021.103700).
- 1415 Cave, B., Perkins, W., Lilly, R., 2022. Linking uplift and mineralisation at the Mount Novit
1416 Zn-Pb-Ag Deposit, Northern Australia: Evidence from geology, U-Pb geochronology and
1417 sphalerite geochemistry. *Geoscience Frontiers* 13, 101347. doi:[10.1016/j.gsf.2021.101347](https://doi.org/10.1016/j.gsf.2021.101347).
- 1418 Cawood, P.A., 2005. Terra Australis Orogen: Rodinia breakup and development of the Pacific
1419 and Iapetus margins of Gondwana during the Neoproterozoic and Paleozoic. *Earth-Science
1420 Reviews* 69, 249–279. doi:[10.1016/j.earscirev.2004.09.001](https://doi.org/10.1016/j.earscirev.2004.09.001).
- 1421 Cawood, P.A., Wang, W., Zhao, T., Xu, Y., Mulder, J.A., Pisarevsky, S.A., Zhang, L., Gan,
1422 C., He, H., Liu, H., Qi, L., Wang, Y., Yao, J., Zhao, G., Zhou, M.F., Zi, J.W., 2020.
1423 Deconstructing South China and consequences for reconstructing Nuna and Rodinia. *Earth-
1424 Science Reviews* 204, 103169. doi:[10.1016/j.earscirev.2020.103169](https://doi.org/10.1016/j.earscirev.2020.103169).
- 1425 Chacko, T., De, S.K., Creaser, R.A., Muehlenbachs, K., 2000. Tectonic setting of the Taltson
1426 magmatic zone at 1.9–2.0 Ga: a granitoid-based perspective. *Canadian Journal of Earth
1427 Sciences* 37, 1597–1609. doi:[10.1139/e00-029](https://doi.org/10.1139/e00-029).
- 1428 Charrier, R., Ramos, V.A., Tapia, F., Sagripanti, L., 2014. Tectono-stratigraphic evolution of
1429 the Andean Orogen between 31 and 37°S (Chile and Western Argentina). *Geological Society,
1430 London, Special Publications* 399, 13–61. doi:[10.1144/sp399.20](https://doi.org/10.1144/sp399.20).
- 1431 Charvet, J., Shu, L., Laurent-Charvet, S., Wang, B., Faure, M., Cluzel, D., Chen, Y., Jong,
1432 K.D., 2011. Palaeozoic tectonic evolution of the Tianshan belt, NW China. *Science China
1433 Earth Sciences* 54, 166–184. doi:[10.1007/s11430-010-4138-1](https://doi.org/10.1007/s11430-010-4138-1).
- 1434 Chattopadhyay, S., Upadhyay, D., Nanda, J.K., Mezger, K., Pruseth, K.L., Berndt, J., 2015.
1435 Proto-India was a part of Rodinia: Evidence from Grenville-age suturing of the Eastern
1436 Ghats Province with the Paleoarchean Singhbhum Craton. *Precambrian Research* 266, 506–
1437 529. doi:[10.1016/j.precamres.2015.05.030](https://doi.org/10.1016/j.precamres.2015.05.030).
- 1438 Chaúque, F., Cordani, U., Jamal, D., 2019. Geochronological systematics for the Chimoio-
1439 Macossa frontal nappe in central Mozambique: Implications for the tectonic evolution of
1440 the southern part of the Mozambique belt. *Journal of African Earth Sciences* 150, 47–67.
1441 doi:[10.1016/j.jafrearsci.2018.10.013](https://doi.org/10.1016/j.jafrearsci.2018.10.013).
- 1442 Cheney, J.T., Brady, J.B., Tierney, K.A., DeGraff, K.A., Mohlman, H.K., Frisch, J.D., Hatch,
1443 C.E., Steiner, M.L., Carmichael, S.K., Fisher, R.G., Tuit, C.B., Steffen, K.J., Cady, P.,
1444 Lowell, J., Archuleta, L.L., Hirst, J., Wegmann, K.W., Monteleone, B., 2004a. Proterozoic
1445 metamorphism of the Tobacco Root Mountains, Montana, in: *Precambrian Geology of the
1446 Tobacco Root Mountains, Montana*. Geological Society of America, pp. 105–129. doi:[10.1130/0-8137-2377-9.105](https://doi.org/10.1130/0-8137-2377-9.105).

- 1448 Cheney, J.T., Webb, A.A.G., Coath, C.D., McKeegan, K.D., 2004b. In situ ion microprobe
1449 $^{207}\text{Pb}/^{206}\text{Pb}$ dating of monazite from Precambrian metamorphic suites, Tobacco Root Mountains,
1450 Montana, in: Precambrian Geology of the Tobacco Root Mountains, Montana. Geological Society of America, pp. 151–179. doi:[10.1130/0-8137-2377-9.151](https://doi.org/10.1130/0-8137-2377-9.151).
- 1452 Cherepanova, Y., Artemieva, I.M., Thybo, H., Chemia, Z., 2013. Crustal structure of the
1453 Siberian craton and the West Siberian basin: An appraisal of existing seismic data. Tectono-
1454 physics 609, 154–183. doi:[10.1016/j.tecto.2013.05.004](https://doi.org/10.1016/j.tecto.2013.05.004).
- 1455 Chew, D., Magna, T., Kirkland, C., Miskovic, A., Cardona, A., Spikings, R., Schaltegger, U.,
1456 2008. Detrital zircon fingerprint of the Proto-Andes: Evidence for a Neoproterozoic active
1457 margin? Precambrian Research 167, 186–200. doi:[10.1016/j.precamres.2008.08.002](https://doi.org/10.1016/j.precamres.2008.08.002).
- 1458 Chew, D.M., Schaltegger, U., Kosler, J., Whitehouse, M.J., Gutjahr, M., Spikings, R.A.,
1459 Miskovic, A., 2007. U-Pb geochronologic evidence for the evolution of the Gondwanan
1460 margin of the north-central Andes. Geological Society of America Bulletin 119, 697–711.
1461 doi:[10.1130/b26080.1](https://doi.org/10.1130/b26080.1).
- 1462 Chiarenzelli, J., Aspler, L., Villeneuve, M., Lewry, J., 1998. Early Proterozoic evolution of the
1463 Saskatchewan Craton and its allochthonous cover, Trans-Hudson Orogen. The Journal of
1464 Geology 106, 247–268. doi:[10.1086/516020](https://doi.org/10.1086/516020).
- 1465 Ciborowski, T.J.R., Kerr, A.C., Ernst, R.E., McDonald, I., Minifie, M.J., Harlan, S.S., Mil-
1466 lar, I.L., 2015. The early Proterozoic Matachewan large igneous province: Geochemistry,
1467 petrogenesis, and implications for Earth evolution. Journal of Petrology 56, 1459–1494.
1468 doi:[10.1093/petrology/egv038](https://doi.org/10.1093/petrology/egv038).
- 1469 Clark, C., Collins, A.S., Timms, N.E., Kinny, P.D., Chetty, T., Santosh, M., 2009. SHRIMP
1470 U–Pb age constraints on magmatism and high-grade metamorphism in the Salem Block,
1471 southern India. Gondwana Research 16, 27–36. doi:[10.1016/j.gr.2008.11.001](https://doi.org/10.1016/j.gr.2008.11.001).
- 1472 Clark, D., Hensen, B., Kinny, P., 2000. Geochronological constraints for a two-stage history of
1473 the Albany–Fraser Orogen, Western Australia. Precambrian Research 102, 155–183. doi:[10.1016/s0301-9268\(00\)00063-2](https://doi.org/10.1016/s0301-9268(00)00063-2).
- 1475 Collins, A.S., Blades, M.L., Merdith, A.S., 2021a. The Arabian–Nubian Shield within the
1476 Neoproterozoic plate tectonic circuit, in: The Geology of the Arabian-Nubian Shield. Springer
1477 International Publishing, pp. 195–202. doi:[10.1007/978-3-030-72995-0_8](https://doi.org/10.1007/978-3-030-72995-0_8).
- 1478 Collins, A.S., Blades, M.L., Merdith, A.S., Foden, J.D., 2021b. Closure of the Proterozoic
1479 Mozambique Ocean was instigated by a late Tonian plate reorganization event. Communications
1480 Earth & Environment 2. doi:[10.1038/s43247-021-00149-z](https://doi.org/10.1038/s43247-021-00149-z).
- 1481 Collins, A.S., Fitzsimons, I.C.W., Hulscher, B., Razakamanana, T., 2003. Structure of the
1482 eastern margin of the East African Orogen in central Madagascar. Precambrian Research
1483 123, 111–133. doi:[10.1016/s0301-9268\(03\)00064-0](https://doi.org/10.1016/s0301-9268(03)00064-0).
- 1484 Collins, A.S., Pisarevsky, S.A., 2005. Amalgamating eastern Gondwana: The evolution of the
1485 Circum-Indian Orogens. Earth-Science Reviews 71, 229–270. doi:[10.1016/j.earscirev.2005.02.004](https://doi.org/10.1016/j.earscirev.2005.02.004).
- 1487 Collins, A.S., Reddy, S.M., Buchan, C., Mruma, A., 2004. Temporal constraints on Palaeoproterozoic eclogite formation and exhumation (Usagaran Orogen, Tanzania). Earth and
1488 Planetary Science Letters 224, 175–192. doi:[10.1016/j.epsl.2004.04.027](https://doi.org/10.1016/j.epsl.2004.04.027).

- 1490 Collins, A.S., Windley, B.F., 2002. The tectonic evolution of central and northern Madagascar
1491 and its place in the final assembly of Gondwana. *The Journal of Geology* 110, 325–339.
1492 doi:[10.1086/339535](https://doi.org/10.1086/339535).
- 1493 Colpron, M., Nelson, J., 2011. A Digital Atlas of Terranes for the Northern Cordillera. Technical
1494 Report. Yukon Geological Survey. Whitehorse, Canada. Accessed 11 November, 2017.
- 1495 Condie, K.C., Pisarevsky, S.A., Puetz, S.J., 2021. LIPs, orogens and supercontinents: The
1496 ongoing saga. *Gondwana Research* 96, 105–121. doi:[10.1016/j.gr.2021.05.002](https://doi.org/10.1016/j.gr.2021.05.002).
- 1497 Condie, K.C., Rosen, O.M., 1994. Laurentia-Siberia connection revisited. *Geology* 22, 168.
1498 doi:[10.1130/0091-7613\(1994\)022<0168:lscr>2.3.co;2](https://doi.org/10.1130/0091-7613(1994)022<0168:lscr>2.3.co;2).
- 1499 Cook, F.A., 2011. Multiple arc development in the Paleoproterozoic Wopmay Orogen, North-
1500 west Canada, in: *Frontiers in Earth Sciences*. Springer Berlin Heidelberg, pp. 403–427.
1501 doi:[10.1007/978-3-540-88558-0_14](https://doi.org/10.1007/978-3-540-88558-0_14).
- 1502 Cooray, P., 1994. The Precambrian of Sri Lanka: a historical review. *Precambrian Research*
1503 66, 3–18. doi:[10.1016/0301-9268\(94\)90041-8](https://doi.org/10.1016/0301-9268(94)90041-8).
- 1504 Corrigan, D., Pehrsson, S., Wodicka, N., de Kemp, E., 2009. The Palaeoproterozoic Trans-
1505 Hudson Orogen: a prototype of modern accretionary processes. *Geological Society, London,*
1506 *Special Publications* 327, 457–479. doi:[10.1144/sp327.19](https://doi.org/10.1144/sp327.19).
- 1507 Cutts, K., Hand, M., Kelsey, D., 2011. Evidence for early Mesoproterozoic (ca. 1590Ma)
1508 ultrahigh-temperature metamorphism in southern Australia. *Lithos* 124, 1–16. doi:[10.1016/j.lithos.2010.10.014](https://doi.org/10.1016/j.lithos.2010.10.014).
- 1509 Daczko, N.R., Halpin, J.A., Fitzsimons, I.C.W., Whittaker, J.M., 2018. A cryptic
1510 Gondwana-forming orogen located in Antarctica. *Scientific Reports* 8. doi:[10.1038/s41598-018-26530-1](https://doi.org/10.1038/s41598-018-26530-1).
- 1511 D'Agrella-Filho, M.S., Cordani, U.G., 2016. The Paleomagnetic Record of the São Francisco-
1512 Congo Craton, in: *São Francisco Craton, Eastern Brazil*. Springer International Publishing,
1513 pp. 305–320. doi:[10.1007/978-3-319-01715-0_16](https://doi.org/10.1007/978-3-319-01715-0_16).
- 1514 Daly, J., Balagansky, V., Timmerman, M., Whitehouse, M., de Jong, K., Guise, P., Bogdanova,
1515 S., Gorbatschev, R., Bridgwater, D., 2001. Ion microprobe U-Pb zircon geochronology and
1516 isotopic evidence for a trans-crustal suture in the Lapland–Kola Orogen, northern Fennoscandian
1517 Shield. *Precambrian Research* 105, 289–314. doi:[10.1016/s0301-9268\(00\)00116-9](https://doi.org/10.1016/s0301-9268(00)00116-9).
- 1518 Daniel, C.G., Pfeifer, L.S., Jones, J.V., McFarlane, C.M., 2013. Detrital zircon evidence for
1519 non-Laurentian provenance, Mesoproterozoic (ca. 1490–1450 Ma) deposition and orogenesis
1520 in a reconstructed orogenic belt, northern New Mexico, USA: Defining the Picuris orogeny.
1521 *Geological Society of America Bulletin* 125, 1423–1441. doi:[10.1130/b30804.1](https://doi.org/10.1130/b30804.1).
- 1522 Darbyshire, F.A., 2005. Upper mantle structure of Arctic Canada from Rayleigh wave dispersion.
1523 *Tectonophysics* 405, 1–23. doi:[10.1016/j.tecto.2005.02.013](https://doi.org/10.1016/j.tecto.2005.02.013).
- 1524 Darbyshire, F.A., Bastow, I.D., Petrescu, L., Gilligan, A., Thompson, D.A., 2017. A tale of two
1525 orogens: Crustal processes in the Proterozoic Trans-Hudson and Grenville Orogens, eastern
1526 Canada. *Tectonics* 36, 1633–1659. doi:[10.1002/2017tc004479](https://doi.org/10.1002/2017tc004479).
- 1527 Dasgupta, S., Bose, S., Das, K., 2013. Tectonic evolution of the Eastern Ghats Belt, India.
1528 *Precambrian Research* 227, 247–258. doi:[10.1016/j.precamres.2012.04.005](https://doi.org/10.1016/j.precamres.2012.04.005).

- 1531 Davison, I., Pindell, J., Hull, J., 2020. The Basins, Orogens and Evolution of the southern
1532 Gulf of Mexico and northern Caribbean. Geological Society, London, Special Publications ,
1533 SP504–2020–218doi:[10.1144/sp504-2020-218](https://doi.org/10.1144/sp504-2020-218).
- 1534 Davy, B., 2006. Bollons Seamount and early New Zealand-Antarctic seafloor spreading. Geo-
1535 chemistry, Geophysics, Geosystems 7, Q06021. doi:[10.1029/2005gc001191](https://doi.org/10.1029/2005gc001191).
- 1536 De Roever, E., Lafon, J.M., Delor, C., Cocherie, A., Rossi, P., Guerrrot, C., Potrel, A., 2003.
1537 The Bakhuis ultrahigh-temperature granulite belt (Suriname): I. Petrological and geochrono-
1538 logical evidence for a counterclockwise P-T path at 2.07–2.05 Ga. Géol. France 2-3-4, 175–
1539 205.
- 1540 Debayle, E., Dubuffet, F., Durand, S., 2016. An automatically updated S-wave model of the
1541 upper mantle and the depth extent of azimuthal anisotropy. Geophysical Research Letters
1542 43, 674–682. doi:[10.1002/2015gl067329](https://doi.org/10.1002/2015gl067329).
- 1543 Debayle, E., Dubuffet, F., Durand, S., 2019. Data Services Products: 3D2018_08Sv, a global
1544 Sv wave upper mantle model updated until August 2018. Technical Report. Incorporated
1545 Research Institutions for Seismology (IRIS). doi:[10.17611/DP/EMC3D201808S](https://doi.org/10.17611/DP/EMC3D201808S).
- 1546 DeMets, C., Gordon, R.G., Argus, D.F., 2010. Geologically current plate motions. Geophysical
1547 Journal International 181, 1–80. doi:[10.1111/j.1365-246x.2009.04491.x](https://doi.org/10.1111/j.1365-246x.2009.04491.x).
- 1548 DeMets, C., Gordon, R.G., Argus, D.F., Stein, S., 1990. Current plate motions. Geophysical
1549 Journal International 101, 425–478. doi:[10.1111/j.1365-246x.1990.tb06579.x](https://doi.org/10.1111/j.1365-246x.1990.tb06579.x).
- 1550 DeMets, C., Márquez-Azúa, B., Cabral-Cano, E., 2014. A new GPS velocity field for the Pacific
1551 Plate – Part 2: implications for fault slip rates in western California. Geophysical Journal
1552 International 199, 1900–1909. doi:[10.1093/gji/ggu347](https://doi.org/10.1093/gji/ggu347).
- 1553 DeMets, C., Wiggins-Grandison, M., 2007. Deformation of Jamaica and motion of the Gonâve
1554 microplate from GPS and seismic data. Geophysical Journal International 168, 362–378.
1555 doi:[10.1111/j.1365-246x.2006.03236.x](https://doi.org/10.1111/j.1365-246x.2006.03236.x).
- 1556 Derbeko, I., 2013. The region of matching of Central-Asian Mobile Belt and Pacific Mobile
1557 Belt. International Journal of Geosciences 04, 605–610. doi:[10.4236/ijg.2013.43055](https://doi.org/10.4236/ijg.2013.43055).
- 1558 Dew, R.E., Collins, A.S., Morley, C.K., King, R.C., Evans, N.J., Glorie, S., 2021. Coupled
1559 detrital zircon U-Pb and Hf analysis of the Sibumasu Terrane: From Gondwana to north-
1560 west Thailand. Journal of Asian Earth Sciences 211, 104709. doi:[10.1016/j.jseaes.2021.104709](https://doi.org/10.1016/j.jseaes.2021.104709).
- 1562 Dickinson, W.R., 2004. Evolution of the North American Cordillera. Annual Review of Earth
1563 and Planetary Sciences 32, 13–45. doi:[10.1146/annurev.earth.32.101802.120257](https://doi.org/10.1146/annurev.earth.32.101802.120257).
- 1564 Dilek, Y., 2006. Collision tectonics of the Mediterranean region: Causes and consequences, in:
1565 Postcollisional Tectonics and Magmatism in the Mediterranean Region and Asia. Geological
1566 Society of America, pp. 1–13. doi:[10.1130/2006.2409\(01\)](https://doi.org/10.1130/2006.2409(01)).
- 1567 Dilek, Y., Furnes, H., 2014. Ophiolites and their origins. Elements 10, 93–100. doi:[10.2113/gselements.10.2.93](https://doi.org/10.2113/gselements.10.2.93).
- 1569 Dillon, W.P., Schlee, J.S., Klitgord, K.D., 1988. The development of the continental margin
1570 of eastern North America—conjugate continental margin to West Africa. Journal of African
1571 Earth Sciences (and the Middle East) 7, 361–367. doi:[10.1016/0899-5362\(88\)90080-2](https://doi.org/10.1016/0899-5362(88)90080-2).

- 1572 Dixon, T.H., Mao, A., 1997. A GPS estimate of relative motion between North and South
1573 America. *Geophysical Research Letters* 24, 535–538. doi:[10.1029/97gl100284](https://doi.org/10.1029/97gl100284).
- 1574 Dixon, T.H., Miller, M., Farina, F., Wang, H., Johnson, D., 2000. Present-day motion of the
1575 Sierra Nevada block and some tectonic implications for the Basin and Range province, North
1576 American Cordillera. *Tectonics* 19, 1–24. doi:[10.1029/1998tc001088](https://doi.org/10.1029/1998tc001088).
- 1577 Djeutchou, C., de Kock, M.O., Wabo, H., Gaitán, C.E., Söderlund, U., Gumsley, A.P., 2021.
1578 Late Paleoproterozoic mafic magmatism and the Kalahari craton during Columbia assembly.
1579 *Geology* 49, 1375–1380. doi:[10.1130/g48811.1](https://doi.org/10.1130/g48811.1).
- 1580 Dong, X., Yang, D., Niu, F., Liu, S., Tong, P., 2021. Adjoint traveltime tomography unravels
1581 a scenario of horizontal mantle flow beneath the North China craton. *Scientific Reports* 11.
1582 doi:[10.1038/s41598-021-92048-8](https://doi.org/10.1038/s41598-021-92048-8).
- 1583 Donskaya, T., Gladkochub, D., Pisarevsky, S., Poller, U., Mazukabzov, A., Bayanova, T., 2009.
1584 Discovery of Archaean crust within the Akitkan orogenic belt of the Siberian craton: New
1585 insight into its architecture and history. *Precambrian Research* 170, 61–72. doi:[10.1016/j.precamres.2008.12.003](https://doi.org/10.1016/j.precamres.2008.12.003).
- 1587 Doumbia, S., Pouclet, A., Kouamelan, A., Peucat, J., Vidal, M., Delor, C., 1998. Petroge-
1588 nesis of juvenile-type Birimian (Paleoproterozoic) granitoids in Central Côte-d'Ivoire, West
1589 Africa: geochemistry and geochronology. *Precambrian Research* 87, 33–63. doi:[10.1016/s0301-9268\(97\)00201-5](https://doi.org/10.1016/s0301-9268(97)00201-5).
- 1591 Dovzhikova, E., Pease, V., Remizov, D., 2004. Neoproterozoic island arc magmatism beneath
1592 the pechora basin, NW russia. *GFF* 126, 353–362. doi:[10.1080/11035890401264353](https://doi.org/10.1080/11035890401264353).
- 1593 Ducea, M.N., Saleeby, J.B., Bergantz, G., 2015. The architecture, chemistry, and evolution of
1594 continental magmatic arcs. *Annual Review of Earth and Planetary Sciences* 43, 299–331.
1595 doi:[10.1146/annurev-earth-060614-105049](https://doi.org/10.1146/annurev-earth-060614-105049).
- 1596 Duclaux, G., Rolland, Y., Ruffet, G., Ménot, R.P., Guillot, S., Peucat, J.J., Fanning, M., Rey,
1597 Pêcher, A., 2008. Superimposed Neoarchaean and Paleoproterozoic tectonics in the Terre
1598 Adélie Craton (East Antarctica): Evidence from Th–U–Pb ages on monazite and 40Ar/39Ar
1599 ages. *Precambrian Research* 167, 316–338. doi:[10.1016/j.precamres.2008.09.009](https://doi.org/10.1016/j.precamres.2008.09.009).
- 1600 Dunkley, D.J., Hokada, T., Shiraishi, K., Hiroi, Y., Nogi, Y., Motoyoshi, Y., 2020. Geological
1601 subdivision of the lützow-holm complex in east antarctica: From the neoarchean to the
1602 neoproterozoic. *Polar Science* 26, 100606. doi:[10.1016/j.polar.2020.100606](https://doi.org/10.1016/j.polar.2020.100606).
- 1603 Eagles, G., 2016. Tectonic reconstructions of the southernmost Andes and the Scotia Sea during
1604 the opening of the Drake Passage, in: *Geodynamic Evolution of the Southernmost Andes*.
1605 Springer International Publishing, pp. 75–108. doi:[10.1007/978-3-319-39727-6_4](https://doi.org/10.1007/978-3-319-39727-6_4).
- 1606 Eagles, G., Gloaguen, R., Ebinger, C., 2002. Kinematics of the Danakil microplate. *Earth and*
1607 *Planetary Science Letters* 203, 607–620. doi:[10.1016/s0012-821x\(02\)00916-0](https://doi.org/10.1016/s0012-821x(02)00916-0).
- 1608 Ebbing, J., Dilixiati, Y., Haas, P., Ferraccioli, F., Scheiber-Enslin, S., 2021. East Antarctica
1609 magnetically linked to its ancient neighbours in Gondwana. *Scientific Reports* 11. doi:[10.1038/s41598-021-84834-1](https://doi.org/10.1038/s41598-021-84834-1).
- 1611 Edel, J.B., Casini, L., Oggiano, G., Rossi, P., Schulmann, K., 2014. Early Permian 90° clockwise
1612 rotation of the Maures–Estérel–Corsica–Sardinia block confirmed by new palaeomagnetic
1613 data and followed by a Triassic 60° clockwise rotation. *Geological Society, London, Special*
1614 *Publications* 405, 333–361. doi:[10.1144/sp405.10](https://doi.org/10.1144/sp405.10).

- 1615 Eglinton, B.M., 2004. DateView: a windows geochronology database. Computers & Geosciences 30, 847–858. doi:[10.1016/j.cageo.2004.06.002](https://doi.org/10.1016/j.cageo.2004.06.002).
- 1616
- 1617 Egydio-Silva, M., Vauchez, A., Fossen, H., Cavalcante, G.C.G., Xavier, B.C., 2018. Connecting
1618 the Araçuaí and Ribeira belts (SE – Brazil): Progressive transition from contractional to
1619 transpressive strain regime during the Brasiliiano orogeny. Journal of South American Earth
1620 Sciences 86, 127–139. doi:[10.1016/j.jsames.2018.06.005](https://doi.org/10.1016/j.jsames.2018.06.005).
- 1621 Eizenhöfer, P.R., Zhao, G., Zhang, J., Sun, M., 2014. Final closure of the Paleo-Asian Ocean
1622 along the Solonker Suture Zone: Constraints from geochronological and geochemical data of
1623 Permian volcanic and sedimentary rocks. Tectonics 33, 441–463. doi:[10.1002/2013tc003357](https://doi.org/10.1002/2013tc003357).
- 1624 Elliot, D.H., Fanning, C.M., Hulett, S.R., 2015. Age provinces in the Antarctic craton: Evi-
1625 dence from detrital zircons in Permian strata from the Beardmore Glacier region, Antarctica.
1626 Gondwana Research 28, 152–164. doi:[10.1016/j.gr.2014.03.013](https://doi.org/10.1016/j.gr.2014.03.013).
- 1627 Elliott, J., Freymueller, J.T., 2020. A block model of present-day kinematics of Alaska and West-
1628 ern Canada. Journal of Geophysical Research: Solid Earth 125. doi:[10.1029/2019jb018378](https://doi.org/10.1029/2019jb018378).
- 1629 Elming, S.Å., D'Agrella-Filho, M.S., Page, L.M., Tohver, E., Trindade, R.I.F., Pacca, I.I.G.,
1630 Geraldes, M.C., Teixeira, W., 2009. A palaeomagnetic and $^{40}\text{Ar}/^{39}\text{Ar}$ study of late Precam-
1631 brian sills in the SW part of the Amazonian craton: Amazonia in the Rodinia reconstruction.
1632 Geophysical Journal International 178, 106–122. doi:[10.1111/j.1365-246x.2009.04149.x](https://doi.org/10.1111/j.1365-246x.2009.04149.x).
- 1633 Elming, S.Å., Salminen, J., Pesonen, L.J., 2021. Paleo-Mesoproterozoic Nuna supercycle, in:
1634 Ancient Supercontinents and the Paleogeography of Earth. Elsevier, pp. 499–548. doi:[10.1016/b978-0-12-818533-9.00001-1](https://doi.org/10.1016/b978-0-12-818533-9.00001-1).
- 1635
- 1636 England, P., Molnar, P., 1997. Active Deformation of Asia: From Kinematics to Dynamics.
1637 Science 278, 647–650. doi:[10.1126/science.278.5338.647](https://doi.org/10.1126/science.278.5338.647).
- 1638 Ennih, N., Liégeois, J.P., 2008. The boundaries of the West African craton, with special
1639 reference to the basement of the Moroccan metacratonic Anti-Atlas belt. Geological Society,
1640 London, Special Publications 297, 1–17. doi:[10.1144/sp297.1](https://doi.org/10.1144/sp297.1).
- 1641 Ernst, R., Bleeker, W., 2010. Large igneous provinces (LIPs), giant dyke swarms, and mantle
1642 plumes: Significance for breakup events within Canada and adjacent regions from 2.5 Ga to
1643 the Present. Canadian Journal of Earth Sciences 47, 695–739. doi:[10.1139/e10-025](https://doi.org/10.1139/e10-025).
- 1644 Ernst, R.E., Hamilton, M.A., Söderlund, U., Hanes, J.A., Gladkochub, D.P., Okrugin, A.V.,
1645 Kolotilina, T., Mekhonoshin, A.S., Bleeker, W., LeCheminant, A.N., Buchan, K.L., Cham-
1646 berlain, K.R., Didenko, A.N., 2016. Long-lived connection between southern Siberia and
1647 northern Laurentia in the Proterozoic. Nature Geoscience 9, 464–469. doi:[10.1038/ngeo2700](https://doi.org/10.1038/ngeo2700).
- 1648 Eude, A., Roddaz, M., Brichau, S., Brusset, S., Calderon, Y., Baby, P., Soula, J.C., 2015.
1649 Controls on timing of exhumation and deformation in the northern Peruvian eastern Andean
1650 wedge as inferred from low-temperature thermochronology and balanced cross section.
1651 Tectonics 34, 715–730. doi:[10.1002/2014tc003641](https://doi.org/10.1002/2014tc003641).
- 1652 Evenstar, L.A., Stuart, F.M., Hartley, A.J., Tattitch, B., 2015. Slow Cenozoic uplift of the
1653 western Andean Cordillera indicated by cosmogenic ^3He in alluvial boulders from the Pacific
1654 Planation Surface. Geophysical Research Letters 42, 8448–8455. doi:[10.1002/2015gl065959](https://doi.org/10.1002/2015gl065959).

- 1655 Famin, V., Michon, L., Bourhane, A., 2020. The Comoros Archipelago: a right-lateral transform
1656 boundary between the Somalia and Lwandle plates. *Tectonophysics* 789, 228539. doi:[10.1016/j.tecto.2020.228539](https://doi.org/10.1016/j.tecto.2020.228539).
- 1658 Fergusson, C., Henderson, R., 2015. Early Palaeozoic continental growth in the Tasmanides
1659 of northeast Gondwana and its implications for Rodinia assembly and rifting. *Gondwana
1660 Research* 28, 933–953. doi:[10.1016/j.gr.2015.04.001](https://doi.org/10.1016/j.gr.2015.04.001).
- 1661 Fernandes, R., Bastos, L., Miranda, J., Lourenço, N., Ambrosius, B., Noomen, R., Simons,
1662 W., 2006. Defining the plate boundaries in the Azores region. *Journal of Volcanology and
1663 Geothermal Research* 156, 1–9. doi:[10.1016/j.jvolgeores.2006.03.019](https://doi.org/10.1016/j.jvolgeores.2006.03.019).
- 1664 Ferraccioli, F., Finn, C.A., Jordan, T.A., Bell, R.E., Anderson, L.M., Damaske, D., 2011.
1665 East Antarctic rifting triggers uplift of the Gamburtsev Mountains. *Nature* 479, 388–392.
1666 doi:[10.1038/nature10566](https://doi.org/10.1038/nature10566).
- 1667 Fershtater, G.B., 2012. The main features of the Uralian Paleozoic magmatism and the
1668 epioceanic nature of the orogen. *Mineralogy and Petrology* 107, 39–52. doi:[10.1007/s00710-012-0218-6](https://doi.org/10.1007/s00710-012-0218-6).
- 1670 Filatova, N.I., Khain, V.E., 2008. Development of the Verkhoyansk-Kolyma orogenic system as
1671 a result of interaction of adjacent continental and oceanic plates. *Geotectonics* 42, 258–285.
1672 doi:[10.1134/s001685210804002x](https://doi.org/10.1134/s001685210804002x).
- 1673 Fischer, K.M., 2002. Waning buoyancy in the crustal roots of old mountains. *Nature* 417,
1674 933–936. doi:[10.1038/nature00855](https://doi.org/10.1038/nature00855).
- 1675 Fitzsimons, I., 2000. Grenville-age basement provinces in East Antarctica: Evidence for
1676 three separate collisional orogens. *Geology* 28, 879. doi:[10.1130/0091-7613\(2000\)28<879:gbpiea>2.0.co;2](https://doi.org/10.1130/0091-7613(2000)28<879:gbpiea>2.0.co;2).
- 1678 Fitzsimons, I.C.W., 2003. Proterozoic basement provinces of southern and southwestern Aus-
1679 tralia, and their correlation with Antarctica. *Geological Society, London, Special Publications*
1680 206, 93–130. doi:[10.1144/gsl.sp.2003.206.01.07](https://doi.org/10.1144/gsl.sp.2003.206.01.07).
- 1681 Fletcher, H.J., Freymueller, J.T., 1999. New GPS constraints on the motion of the Yakutat
1682 Block. *Geophysical Research Letters* 26, 3029–3032. doi:[10.1029/1999gl1005346](https://doi.org/10.1029/1999gl1005346).
- 1683 Flowerdew, M.J., Tyrrell, S., Boger, S.D., Fitzsimons, I.C.W., Harley, S.L., Mikhalsky, E.V.,
1684 Vaughan, A.P.M., 2013. Pb isotopic domains from the Indian Ocean sector of Antarctica:
1685 implications for past Antarctica–India connections. *Geological Society, London, Special Pub-
1686 lications* 383, 59–72. doi:[10.1144/sp383.3](https://doi.org/10.1144/sp383.3).
- 1687 Fossen, H., Cavalcante, G.C., de Almeida, R.P., 2017. Hot versus cold orogenic behavior:
1688 Comparing the Araçuaí-West Congo and the Caledonian Orogenes. *Tectonics* 36, 2159–2178.
1689 doi:[10.1002/2017tc004743](https://doi.org/10.1002/2017tc004743).
- 1690 Foster, D., Goscombe, B., 2013. Continental growth and recycling in convergent oro-
1691 gens with large turbidite fans on oceanic crust. *Geosciences* 3, 354–388. doi:[10.3390/geosciences3030354](https://doi.org/10.3390/geosciences3030354).
- 1693 Foulger, G.R., Doré, T., Emeleus, C.H., Franke, D., Geoffroy, L., Gernigon, L., Hey, R.,
1694 Holdsworth, R.E., Hole, M., Höskuldsson, Á., Julian, B., Kusznir, N., Martinez, F., Mc-
1695 Caffrey, K.J., Natland, J.H., Peace, A.L., Petersen, K., Schiffer, C., Stephenson, R., Stoker,
1696 M., 2020. The Iceland Microcontinent and a continental Greenland-Iceland-Faroe Ridge.
1697 *Earth-Science Reviews* 206, 102926. doi:[10.1016/j.earscirev.2019.102926](https://doi.org/10.1016/j.earscirev.2019.102926).

- 1698 French, J.E., Heaman, L.M., Chacko, T., Srivastava, R.K., 2008. 1891–1883Ma Southern
1699 Bastar–Cuddapah mafic igneous events, India: A newly recognized large igneous province.
1700 Precambrian Research 160, 308–322. doi:[10.1016/j.precamres.2007.08.005](https://doi.org/10.1016/j.precamres.2007.08.005).
- 1701 Fretwell, P., Pritchard, H.D., Vaughan, D.G., Bamber, J.L., Barrand, N.E., Bell, R., Bianchi,
1702 C., Bingham, R.G., Blankenship, D.D., Casassa, G., Catania, G., Callens, D., Conway, H.,
1703 Cook, A.J., Corr, H.F.J., Damaske, D., Damm, V., Ferraccioli, F., Forsberg, R., Fujita, S.,
1704 Gim, Y., Gogineni, P., Griggs, J.A., Hindmarsh, R.C.A., Holmlund, P., Holt, J.W., Jacobel,
1705 R.W., Jenkins, A., Jokat, W., Jordan, T., King, E.C., Kohler, J., Krabill, W., Riger-Kusk,
1706 M., Langley, K.A., Leitchenkov, G., Leuschen, C., Luyendyk, B.P., Matsuoka, K., Mouginot,
1707 J., Nitsche, F.O., Nogi, Y., Nost, O.A., Popov, S.V., Rignot, E., Rippin, D.M., Rivera,
1708 A., Roberts, J., Ross, N., Siegert, M.J., Smith, A.M., Steinhage, D., Studinger, M., Sun,
1709 B., Tinto, B.K., Welch, B.C., Wilson, D., Young, D.A., Xiangbin, C., Zirizzotti, A., 2013.
1710 Bedmap2: improved ice bed, surface and thickness datasets for Antarctica. The Cryosphere
1711 7, 375–393. doi:[10.5194/tc-7-375-2013](https://doi.org/10.5194/tc-7-375-2013).
- 1712 Freymueller, J.T., 2010. Active tectonics of plate boundary zones and the continuity of plate
1713 boundary deformation from Asia to North America. Current Science 99, 1719–1732. URL:
1714 <http://www.jstor.org/stable/24073495>, doi:[10.2307/24073495](https://doi.org/10.2307/24073495).
- 1715 Fritz, H., Abdelsalam, M., Ali, K., Bingen, B., Collins, A., Fowler, A., Ghebreab, W., Hauzen-
1716 berger, C., Johnson, P., Kusky, T., Macey, P., Muhongo, S., Stern, R., Viola, G., 2013.
1717 Orogen styles in the East African Orogen: A review of the Neoproterozoic to Cambrian tec-
1718 tonic evolution. Journal of African Earth Sciences 86, 65–106. doi:[10.1016/j.jafrearsci.2013.06.004](https://doi.org/10.1016/j.jafrearsci.2013.06.004).
- 1720 Funck, T., Erlendsson, Ö., Geissler, W.H., Gradmann, S., Kimbell, G.S., McDermott, K.,
1721 Petersen, U.K., 2016. A review of the NE Atlantic conjugate margins based on seismic
1722 refraction data. Geological Society, London, Special Publications 447, 171–205. doi:[10.1144/sp447.9](https://doi.org/10.1144/sp447.9).
- 1724 Furlanetto, F., Thorkelson, D.J., Gibson, H.D., Marshall, D.D., Rainbird, R.H., Davis, W.J.,
1725 Crowley, J.L., Vervoort, J.D., 2013. Late Paleoproterozoic terrane accretion in northwestern
1726 Canada and the case for circum-Columbian orogenesis. Precambrian Research 224, 512–528.
1727 doi:[10.1016/j.precamres.2012.10.010](https://doi.org/10.1016/j.precamres.2012.10.010).
- 1728 Furman, T., 2007. Geochemistry of East African Rift basalts: An overview. Journal of African
1729 Earth Sciences 48, 147–160. doi:[10.1016/j.jafrearsci.2006.06.009](https://doi.org/10.1016/j.jafrearsci.2006.06.009).
- 1730 Fyffe, L.R., Johnson, S.C., Staal, C.R.V., 2012. A review of Proterozoic to Early Paleo-
1731 zoic lithotectonic terranes in New Brunswick, Canada and their tectonic evolution dur-
1732 ing Penobscot, Taconic, Salinic and Acadian Orogenesis. Atlantic Geology 47, 211–248.
1733 doi:[10.4138/atlgeol.2011.010](https://doi.org/10.4138/atlgeol.2011.010).
- 1734 Gaina, C., van Hinsbergen, D.J.J., Spakman, W., 2015. Tectonic interactions between India
1735 and Arabia since the Jurassic reconstructed from marine geophysics, ophiolite geology, and
1736 seismic tomography. Tectonics 34, 875–906. doi:[10.1002/2014tc003780](https://doi.org/10.1002/2014tc003780).
- 1737 Gaina, C., Müller, R.D., Roest, W.R., Symonds, P., 1998. The opening of the Tasman Sea:
1738 A gravity anomaly animation. Earth Interactions 2, 1–23. doi:[10.1175/1087-3562\(1998\)002<0001:toots>2.3.co;2](https://doi.org/10.1175/1087-3562(1998)002<0001:toots>2.3.co;2).

- 1740 Gallais, F., Fujie, G., Boston, B., Hackney, R., Kodaira, S., Miura, S., Nakamura, Y., Kaiho,
1741 Y., 2019. Crustal structure across the Lord Howe Rise, northern Zealandia, and rifting of the
1742 eastern Gondwana margin. *Journal of Geophysical Research: Solid Earth* 124, 3036–3056.
1743 doi:[10.1029/2018jb016798](https://doi.org/10.1029/2018jb016798).
- 1744 Gao, P., Zheng, Y.F., Zhao, Z.F., 2017. Triassic granites in South China: A geochemical
1745 perspective on their characteristics, petrogenesis, and tectonic significance. *Earth-Science
1746 Reviews* 173, 266–294. doi:[10.1016/j.earscirev.2017.07.016](https://doi.org/10.1016/j.earscirev.2017.07.016).
- 1747 García Casco, A., Torres-Roldán, R., Iturrealde-Vinent, M.A., Millán Trujillo, G., K. E. Nuñez
1748 Cambra, C. Lázaro, A.R., 2006. High pressure metamorphism of eclogites in Cuba. *Geologica
1749 Acta* 4, 63–88. doi:[10.1344/105.000000358](https://doi.org/10.1344/105.000000358).
- 1750 Gard, M., Hasterok, D., Halpin, J., 2019a. Global whole-rock geochemical database compilation.
1751 *Earth System Science Data* 11, 1553–1566. doi:[10.5194/essd-11-1553-2019](https://doi.org/10.5194/essd-11-1553-2019).
- 1752 Gard, M., Hasterok, D., Hand, M., Cox, G., 2019b. Variations in continental heat production
1753 from 4 Ga to the present: Evidence from geochemical data. *Lithos* 342-343, 391–406. doi:[10.1016/j.lithos.2019.05.034](https://doi.org/10.1016/j.lithos.2019.05.034).
- 1755 Gardiner, N., Searle, M., Morley, C., Whitehouse, M., Spencer, C., Robb, L., 2016. The closure
1756 of Palaeo-Tethys in Eastern Myanmar and Northern Thailand: New insights from zircon U–
1757 Pb and Hf isotope data. *Gondwana Research* 39, 401–422. doi:[10.1016/j.gr.2015.03.001](https://doi.org/10.1016/j.gr.2015.03.001).
- 1758 Gardner, R.L., Daczko, N.R., Halpin, J.A., Whittaker, J.M., 2015. Discovery of a microcon-
1759 tinent (Gulden Draak Knoll) offshore Western Australia: Implications for East Gondwana
1760 reconstructions. *Gondwana Research* 28, 1019–1031. doi:[10.1016/j.gr.2014.08.013](https://doi.org/10.1016/j.gr.2014.08.013).
- 1761 Garrity, C.P., Soller, D.R., 2009. Database of the Geologic Map of North America: Adapted
1762 from the map by J.C. Reed, Jr. and others (2005). Digital Data Series 424. US Geological
1763 Survey. doi:[10.3133/ds424](https://doi.org/10.3133/ds424).
- 1764 Ge, R., Zhu, W., Wilde, S.A., He, J., Cui, X., Wang, X., Bihai, Z., 2014. Neoproterozoic
1765 to Paleozoic long-lived accretionary orogeny in the northern Tarim Craton. *Tectonics* 33,
1766 302–329. doi:[10.1002/2013tc003501](https://doi.org/10.1002/2013tc003501).
- 1767 Gee, D.G., Stephenson, R.A., 2006. The European lithosphere: an introduction. *Geological
1768 Society, London, Memoirs* 32, 1–9. doi:[10.1144/gsl.mem.2006.032.01.01](https://doi.org/10.1144/gsl.mem.2006.032.01.01).
- 1769 Geognostics, 2021. OZ SEEBASE® 2021 (March 2021), <https://www.geognostics.com/oz-seebase-2021>. Technical Report. Geognostics Australia Pty Ltd.
- 1771 Geological Survey of India, 2006. Gravity Map Series of India. Technical Report. National
1772 Geophysical Research Institute and Geological Survey of India. Hyderabad, India.
- 1773 Gifford, J.N., Mueller, P.A., Foster, D.A., Mogk, D.W., 2018. Extending the realm of Archean
1774 crust in the Great Falls tectonic zone: Evidence from the Little Rocky Mountains, Montana.
1775 *Precambrian Research* 315, 264–281. doi:[10.1016/j.precamres.2018.07.021](https://doi.org/10.1016/j.precamres.2018.07.021).
- 1776 Gion, A.M., Williams, S.E., Müller, R.D., 2017. A reconstruction of the Eurekan Orogeny
1777 incorporating deformation constraints. *Tectonics* 36, 304–320. doi:[10.1002/2015tc004094](https://doi.org/10.1002/2015tc004094).
- 1778 Gladkochub, D., Donskaya, T., Fedorovsky, V., Mazukabzov, A., Larionov, A., Sergeev, S.,
1779 2010. The Olkhon metamorphic terrane in the Baikal region: An Early Paleozoic collage
1780 of Neoproterozoic active margin fragments. *Russian Geology and Geophysics* 51, 447–460.
1781 doi:[10.1016/j.rgg.2010.04.001](https://doi.org/10.1016/j.rgg.2010.04.001).

- 1782 Glen, R., Belousova, E., Griffin, W., 2016. Different styles of modern and ancient non-collisional
1783 orogens and implications for crustal growth: a Gondwanaland perspective. Canadian Journal
1784 of Earth Sciences 53, 1372–1415. doi:[10.1139/cjes-2015-0229](https://doi.org/10.1139/cjes-2015-0229).
- 1785 Global Volcanism Program, 2013. Volcanoes of the World, v. 4.7.3. Venzke, E (ed.). Technical
1786 Report. Smithsonian Institution. doi:[10.5479/si.GVP.VOTW4-2013](https://doi.org/10.5479/si.GVP.VOTW4-2013). downloaded 12 Septem-
1787 ber 2018.
- 1788 Glorie, S., Grave, J.D., 2016. Exhuming the Meso-Cenozoic Kyrgyz Tianshan and Siberian
1789 Altai-Sayan: A review based on low-temperature thermochronology. Geoscience Frontiers 7,
1790 155–170. doi:[10.1016/j.gsf.2015.04.003](https://doi.org/10.1016/j.gsf.2015.04.003).
- 1791 Golynsky, A.V., 2007. Magnetic anomalies in East Antarctica and surrounding regions: a
1792 window on major tectonic provinces and their boundaries, in: Cooper, A., Raymond, C.
1793 (Eds.), Antarctica: A Keystone in a Changing World – Online Proceedings of the 10th
1794 ISAES. US Geological Survey. volume 2007. doi:[10.3133/of2007-1047.srp006](https://doi.org/10.3133/of2007-1047.srp006).
- 1795 Golynsky, A.V., Ferraccioli, F., Hong, J.K., Golynsky, D.A., von Frese, R.R.B., Young, D.A.,
1796 Blankenship, D.D., Holt, J.W., Ivanov, S.V., Kiselev, A.V., Masolov, V.N., Eagles, G., Gohl,
1797 K., Jokat, W., Damaske, D., Finn, C., Aitken, A., Bell, R.E., Armadillo, E., Jordan, T.A.,
1798 Greenbaum, J.S., Bozzo, E., Caneva, G., Forsberg, R., Ghidella, M., Galindo-Zaldivar, J.,
1799 Bohoyo, F., Martos, Y.M., Nogi, Y., Quartini, E., Kim, H.R., Roberts, J.L., 2018. New
1800 magnetic anomaly map of the Antarctic. Geophysical Research Letters 45, 6437–6449. doi:[10.1029/2018gl078153](https://doi.org/10.1029/2018gl078153).
- 1802 Gómez-Tapias, J., Schobbenhaus, C., Montes-Ramírez, N., 2019. Geological Map Of South
1803 America At a Scale of 1: 5M. Technical Report. Commission for the Geological Map of the
1804 World. doi:[10.32685/10.143.2019.929](https://doi.org/10.32685/10.143.2019.929).
- 1805 Goodge, J.W., Fanning, C., Bennett, V.C., 2001. U–Pb evidence of ~1.7 Ga crustal tec-
1806 tonism during the Nimrod Orogeny in the Transantarctic Mountains, Antarctica: im-
1807 plications for Proterozoic plate reconstructions. Precambrian Research 112, 261–288.
1808 doi:[10.1016/s0301-9268\(01\)00193-0](https://doi.org/10.1016/s0301-9268(01)00193-0).
- 1809 Goodge, J.W., Fanning, C.M., Brecke, D.M., Licht, K.J., Palmer, E.F., 2010. Continuation
1810 of the Laurentian Grenville Province across the Ross Sea Margin of East Antarctica. The
1811 Journal of Geology 118, 601–619. doi:[10.1086/656385](https://doi.org/10.1086/656385).
- 1812 Goodge, J.W., Fanning, C.M., Fisher, C.M., Vervoort, J.D., 2017. Proterozoic crustal evolu-
1813 tion of central East Antarctica: Age and isotopic evidence from glacial igneous clasts, and
1814 links with Australia and Laurentia. Precambrian Research 299, 151–176. doi:[10.1016/j.precamres.2017.07.026](https://doi.org/10.1016/j.precamres.2017.07.026).
- 1816 Gordon, R., 1998. The plate tectonic approximation: Plate nonrigidity, diffuse plate boundaries,
1817 and global plate reconstructions. Annual Review of Earth and Planetary Sciences 26, 615–
1818 642. doi:[10.1146/annurev.earth.26.1.615](https://doi.org/10.1146/annurev.earth.26.1.615).
- 1819 Gordon, R.G., DeMets, C., Argus, D.F., 1990. Kinematic constraints on distributed lithospheric
1820 deformation in the equatorial Indian Ocean from present motion between the Australian and
1821 Indian Plates. Tectonics 9, 409–422. doi:[10.1029/tc009i003p00409](https://doi.org/10.1029/tc009i003p00409).
- 1822 Goscombe, B., Foster, D.A., Gray, D., Wade, B., 2020. Assembly of central Gondwana along
1823 the Zambezi Belt: Metamorphic response and basement reactivation during the Kuunga
1824 Orogeny. Gondwana Research 80, 410–465. doi:[10.1016/j.gr.2019.11.004](https://doi.org/10.1016/j.gr.2019.11.004).

- 1825 Goutorbe, B., Poort, J., Lucaleau, F., Raillard, S., 2011. Global heat flow trends resolved from
1826 multiple geological and geophysical proxies. *Geophys. J. Int.* 187, 1405–1419. doi:[10.1111/j.1365-246X.2011.05228.x](https://doi.org/10.1111/j.1365-246X.2011.05228.x).
- 1828 Granot, R., Dymant, J., 2018. Late Cenozoic unification of East and West Antarctica. *Nature Communications* 9. doi:[10.1038/s41467-018-05270-w](https://doi.org/10.1038/s41467-018-05270-w).
- 1830 Grenholm, M., 2019. The global tectonic context of the ca. 2.27–1.96 Ga Birimian Orogen –
1831 Insights from comparative studies, with implications for supercontinent cycles. *Earth-Science Reviews* 193, 260–298. doi:[10.1016/j.earscirev.2019.04.017](https://doi.org/10.1016/j.earscirev.2019.04.017).
- 1833 Grenholm, M., Jessell, M., Thébaud, N., 2019. A geodynamic model for the Paleoproterozoic
1834 (ca. 2.27–1.96 Ga) Birimian Orogen of the southern West African Craton – Insights into
1835 an evolving accretionary-collisional orogenic system. *Earth-Science Reviews* 192, 138–193.
1836 doi:[10.1016/j.earscirev.2019.02.006](https://doi.org/10.1016/j.earscirev.2019.02.006).
- 1837 de Gromard, R.Q., Kirkland, C.L., Howard, H.M., Wingate, M.T., Jourdan, F., McInnes, B.I.,
1838 Danišk, M., Evans, N.J., McDonald, B.J., Smithies, R.H., 2019. When will it end? Long-
1839 lived intracontinental reactivation in central Australia. *Geoscience Frontiers* 10, 149–164.
1840 doi:[10.1016/j.gsf.2018.09.003](https://doi.org/10.1016/j.gsf.2018.09.003).
- 1841 Gupta, S., Zhao, D., Rai, S., 2009. Seismic imaging of the upper mantle under the Erebus
1842 hotspot in Antarctica. *Gondwana Research* 16, 109–118. doi:[10.1016/j.gr.2009.01.004](https://doi.org/10.1016/j.gr.2009.01.004).
- 1843 Hall, J.W., Glorie, S., Reid, A.J., Boone, S.C., Collins, A.S., Gleadow, A., 2018. An apatite
1844 U–Pb thermal history map for the northern Gawler Craton, South Australia. *Geoscience
1845 Frontiers* 9, 1293–1308. doi:[10.1016/j.gsf.2017.12.010](https://doi.org/10.1016/j.gsf.2017.12.010).
- 1846 Halls, H.C., Li, J., Davis, D., Hou, G., Zhang, B., Qian, X., 2000. A precisely dated Proterozoic
1847 palaeomagnetic pole from the North China craton, and its relevance to palaeocontinental
1848 reconstruction. *Geophysical Journal International* 143, 185–203. doi:[10.1046/j.1365-246x.2000.00231.x](https://doi.org/10.1046/j.1365-246x.2000.00231.x).
- 1850 Halpin, J.A., Daczko, N.R., Clarke, G.L., Murray, K.R., 2013. Basin analysis in polymeta-
1851 morphic terranes: An example from east Antarctica. *Precambrian Research* 231, 78–97.
1852 doi:[10.1016/j.precamres.2013.03.015](https://doi.org/10.1016/j.precamres.2013.03.015).
- 1853 Halpin, J.A., Daczko, N.R., Kobler, M.E., Whittaker, J.M., 2017. Strike-slip tectonics during
1854 the Neoproterozoic–Cambrian assembly of East Gondwana: Evidence from a newly discov-
1855 ered microcontinent in the Indian Ocean (Batavia Knoll). *Gondwana Research* 51, 137–148.
1856 doi:[10.1016/j.gr.2017.08.002](https://doi.org/10.1016/j.gr.2017.08.002).
- 1857 Halpin, J.A., Reid, A.J., 2016. Earliest Paleoproterozoic high-grade metamorphism and oro-
1858 genesis in the Gawler Craton, South Australia: The southern cousin in the Rae family?
1859 *Precambrian Research* 276, 123–144. doi:[10.1016/j.precamres.2016.02.001](https://doi.org/10.1016/j.precamres.2016.02.001).
- 1860 Hand, M., Reid, A., Jagodzinski, L., 2007. Tectonic Framework and Evolution of the Gawler
1861 Craton, Southern Australia. *Economic Geology* 102, 1377–1395. doi:[10.2113/gsecongeo.102.8.1377](https://doi.org/10.2113/gsecongeo.102.8.1377).
- 1863 Hanson, R.E., 2003. Proterozoic geochronology and tectonic evolution of southern Africa.
1864 Geological Society, London, Special Publications 206, 427–463. doi:[10.1144/gsl.sp.2003.206.01.20](https://doi.org/10.1144/gsl.sp.2003.206.01.20).

- 1866 Hardy, N., 1991. Tectonic evolution of the easternmost Panama basin: Some new data and in-
1867 ferences. *Journal of South American Earth Sciences* 4, 261–269. doi:[10.1016/0895-9811\(91\)90035-j](https://doi.org/10.1016/0895-9811(91)90035-j).
- 1869 Harley, S.L., Fitzsimons, I.C.W., Zhao, Y., 2013. Antarctica and supercontinent evolution:
1870 historical perspectives, recent advances and unresolved issues. *Geological Society, London,*
1871 *Special Publications* 383, 1–34. doi:[10.1144/sp383.9](https://doi.org/10.1144/sp383.9).
- 1872 Harley, S.L., Kelly, N.M., 2007. Chapter 3.2 Ancient Antarctica: The Archaean of the
1873 East Antarctic Shield, in: *Earth's Oldest Rocks*. Elsevier, pp. 149–186. doi:[10.1016/s0166-2635\(07\)15032-5](https://doi.org/10.1016/s0166-2635(07)15032-5).
- 1875 Hartlaub, R.P., Heaman, L.M., Chacko, T., Ashton, K.E., 2007. Circa 2.3-Ga Magmatism of
1876 the Arrowsmith Orogeny, Uranium City Region, Western Churchill Craton, Canada. *The*
1877 *Journal of Geology* 115, 181–195. doi:[10.1086/510641](https://doi.org/10.1086/510641).
- 1878 Hartmann, J., Moosdorf, N., 2012a. Global Lithological Map Database v1.0 (gridded to
1879 0.5° spatial resolution), supplement to: Hartmann, Jens; Moosdorf, Nils (2012): The
1880 new global lithological map database GLiM: A representation of rock properties at the
1881 Earth surface. *Geochemistry, Geophysics, Geosystems*, 13, Q12004. Technical Report.
1882 doi:[10.1594/PANGAEA.788537](https://doi.org/10.1594/PANGAEA.788537).
- 1883 Hartmann, J., Moosdorf, N., 2012b. The new global lithological map database GLiM: A rep-
1884 resentation of rock properties at the Earth surface. *Geochemistry, Geophysics, Geosystems*
1885 13, Q12004. doi:[10.1029/2012gc004370](https://doi.org/10.1029/2012gc004370).
- 1886 Hasterok, D., Chapman, D., 2007. Continental thermal isostasy II: Applications to North
1887 America. *J. Geophys. Res.* 112, B06415. doi:[10.1029/2006JB004664](https://doi.org/10.1029/2006JB004664).
- 1888 Hauksson, E., Kanamori, H., Stock, J., Cormier, M.H., Legg, M., 2013. Active Pacific
1889 North America Plate boundary tectonics as evidenced by seismicity in the oceanic litho-
1890 sphere offshore Baja California, Mexico. *Geophysical Journal International* 196, 1619–1630.
1891 doi:[10.1093/gji/ggt467](https://doi.org/10.1093/gji/ggt467).
- 1892 He, Z.Y., Klemd, R., Yan, L.L., Lu, T.Y., Zhang, Z.M., 2018. Mesoproterozoic juvenile
1893 crust in microcontinents of the Central Asian Orogenic Belt: evidence from oxygen and
1894 hafnium isotopes in zircon10.3389/feart.2020.00363. *Scientific Reports* 8. doi:[10.1038/s41598-018-23393-4](https://doi.org/10.1038/s41598-018-23393-4).
- 1896 Henderson, B., Collins, A.S., Payne, J., Forbes, C., Saha, D., 2014. Geologically constraining
1897 India in Columbia: The age, isotopic provenance and geochemistry of the protoliths of the
1898 Ongole Domain, Southern Eastern Ghats, India. *Gondwana Research* 26, 888–906. doi:[10.1016/j.gr.2013.09.002](https://doi.org/10.1016/j.gr.2013.09.002).
- 1900 Hickey-Vargas, R., Savov, I.P., Bizimis, M., Ishii, T., Fujioka, K., 2006. Origin of diverse
1901 geochemical signatures in igneous rocks from the West Philippine Basin: Implications for
1902 tectonic models, in: *Back-Arc Spreading Systems: Geological, Biological, Chemical, and*
1903 *Physical Interactions*. American Geophysical Union, pp. 287–303. doi:[10.1029/166gm15](https://doi.org/10.1029/166gm15).
- 1904 Hildebrand, R.S., Hoffman, P.F., Bowring, S.A., 2009. The Calderian orogeny in Wopmay
1905 orogen (1.9 Ga), northwestern Canadian Shield. *Geological Society of America Bulletin* 122,
1906 794–814. doi:[10.1130/b26521.1](https://doi.org/10.1130/b26521.1).

- 1907 Hinsbergen, D.J.J.V., Buiter, S.J.H., Torsvik, T.H., Gaina, C., Webb, S.J., 2011. The forma-
1908 tion and evolution of Africa from the Archaean to Present: introduction. Geological Soci-
1909 ety, London, Special Publications 357, 1–8. URL: <https://doi.org/10.1144%2Fsp357.1>,
1910 doi:[10.1144/SP357.1](https://doi.org/10.1144/SP357.1).
- 1911 Holm, D., Schneider, D., Rose, S., Mancuso, C., McKenzie, M., Foland, K., Hodges, K., 2007.
1912 Proterozoic metamorphism and cooling in the southern Lake Superior region, North America
1913 and its bearing on crustal evolution. *Precambrian Research* 157, 106–126. doi:[10.1016/j.precamres.2007.02.012](https://doi.org/10.1016/j.precamres.2007.02.012).
- 1915 Horner-Johnson, B.C., Gordon, R.G., Argus, D.F., 2007. Plate kinematic evidence for the
1916 existence of a distinct plate between the Nubian and Somalian plates along the Southwest
1917 Indian Ridge. *Journal of Geophysical Research* 112. doi:[10.1029/2006jb004519](https://doi.org/10.1029/2006jb004519).
- 1918 Horner-Johnson, B.C., Gordon, R.G., Cowles, S.M., Argus, D.F., 2005. The angular velocity of
1919 Nubia relative to Somalia and the location of the Nubia-Somalia-Antarctica triple junction.
1920 *Geophysical Journal International* 162, 221–238. doi:[10.1111/j.1365-246x.2005.02608.x](https://doi.org/10.1111/j.1365-246x.2005.02608.x).
- 1921 Howard, H., Smithies, R., Kirkland, C., Kelsey, D., Aitken, A., Wingate, M., de Gromard,
1922 R.Q., Spaggiari, C., Maier, W., 2015. The burning heart—the Proterozoic geology and
1923 geological evolution of the west Musgrave Region, central Australia. *Gondwana Res.* 27,
1924 64–94. doi:[10.1016/j.gr.2014.09.001](https://doi.org/10.1016/j.gr.2014.09.001).
- 1925 Hu, X., Garzanti, E., Wang, J., Huang, W., An, W., Webb, A., 2016. The timing of India-
1926 Asia collision onset – Facts, theories, controversies. *Earth-Science Reviews* 160, 264–299.
1927 doi:[10.1016/j.earscirev.2016.07.014](https://doi.org/10.1016/j.earscirev.2016.07.014).
- 1928 Hyndman, R.D., 2019. Origin of regional barrovian metamorphism in hot backarcs prior to
1929 orogeny deformation. *Geochemistry, Geophysics, Geosystems* 20, 460–469. doi:[10.1029/2018gc007650](https://doi.org/10.1029/2018gc007650).
- 1931 Ibañez-Mejia, M., Ruiz, J., Valencia, V.A., Cardona, A., Gehrels, G.E., Mora, A.R., 2011.
1932 The Putumayo Orogen of Amazonia and its implications for Rodinia reconstructions: New
1933 U-Pb geochronological insights into the Proterozoic tectonic evolution of northwestern South
1934 America. *Precambrian Research* 191, 58–77. doi:[10.1016/j.precamres.2011.09.005](https://doi.org/10.1016/j.precamres.2011.09.005).
- 1935 Isbell, J.L., Biakov, A.S., Vedernikov, I.L., Davydov, V.I., Gulbranson, E.L., Fedorchuk, N.D.,
1936 2016. Permian diamictites in northeastern Asia: Their significance concerning the bipo-
1937 larity of the late Paleozoic ice age. *Earth-Science Reviews* 154, 279–300. doi:[10.1016/j.earscirev.2016.01.007](https://doi.org/10.1016/j.earscirev.2016.01.007).
- 1939 Ivanov, A.V., Demonterova, E.I., Gladkochub, D.P., Donskaya, T.V., 2014. The Tuva–Mongolia
1940 Massif and the Siberian Craton – are they the same? A comment on ‘Age and provenance
1941 of the Ergunahe Group and the Wubinaobao Formation, northeastern Inner Mongolia, NE
1942 China: implications for tectonic setting of the Erguna Massif’ by Zhang et al. *International
1943 Geology Review* 56, 954–958. doi:[10.1080/00206814.2014.905999](https://doi.org/10.1080/00206814.2014.905999).
- 1944 Jacobs, J., Elburg, M., Läufer, A., Kleinhanns, I.C., Henjes-Kunst, F., Estrada, S., Ruppel,
1945 A.S., Damaske, D., Montero, P., Bea, F., 2015. Two distinct Late Mesoproterozoic/Early
1946 Neoproterozoic basement provinces in central/eastern Dronning Maud Land, East Antarctica:
1947 The missing link, 15–21°E. *Precambrian Research* 265, 249–272. doi:[10.1016/j.precamres.2015.05.003](https://doi.org/10.1016/j.precamres.2015.05.003).

- 1949 Janoušek, V., Jiang, Y., Buriánek, D., Schulmann, K., Hanzl, P., Soejono, I., Kröner, A.,
1950 Altanbaatar, B., Erban, V., Lexa, O., Ganchuluun, T., Košler, J., 2018. Cambrian–
1951 Ordovician magmatism of the Ikh-Mongol Arc System exemplified by the Khantaishir Mag-
1952 matic Complex (Lake Zone, south-central Mongolia). *Gondwana Research* 54, 122–149.
1953 doi:[10.1016/j.gr.2017.10.003](https://doi.org/10.1016/j.gr.2017.10.003).
- 1954 Jelsma, H.A., McCourt, S., Perritt, S.H., Armstrong, R.A., 2018. The geology and evolution
1955 of the Angolan Shield, Congo Craton, in: *Regional Geology Reviews*. Springer International
1956 Publishing, pp. 217–239. doi:[10.1007/978-3-319-68920-3_9](https://doi.org/10.1007/978-3-319-68920-3_9).
- 1957 Jessop, K., Daczko, N.R., Piazolo, S., 2019. Tectonic cycles of the New England Orogen,
1958 eastern Australia: A Review. *Australian Journal of Earth Sciences* 66, 459–496. doi:[10.1080/08120099.2018.1548378](https://doi.org/10.1080/08120099.2018.1548378).
- 1960 Johansson, Å., 2009. Baltica, Amazonia and the SAMBA connection—1000 million years of
1961 neighbourhood during the Proterozoic? *Precambrian Research* 175, 221–234. doi:[10.1016/j.precamres.2009.09.011](https://doi.org/10.1016/j.precamres.2009.09.011).
- 1963 Johansson, Å., Bingen, B., Huhma, H., Waught, T., Vestergaard, R., Soesoo, A., Skridlaite,
1964 G., Krzeminska, E., Shumlyanskyy, L., Holland, M.E., Holm-Denoma, C., Teixeira, W.,
1965 Faleiros, F.M., Ribeiro, B.V., Jacobs, J., Wang, C., Thomas, R.J., Macey, P.H., Kirkland,
1966 C.L., Hartnady, M.I., Eglington, B.M., Puetz, S.J., Condie, K.C., 2022. A geochronological
1967 review of magmatism along the external margin of Columbia and in the Grenville-age orogens
1968 forming the core of Rodinia. *Precambrian Research*, 106463 doi:[10.1016/j.precamres.2021.106463](https://doi.org/10.1016/j.precamres.2021.106463).
- 1970 Johansson, L., Zahirovic, S., Müller, R.D., 2018. The interplay between the eruption and
1971 weathering of large igneous provinces and the deep-time carbon cycle. *Geophysical Research
1972 Letters* 45, 5380–5389. doi:[10.1029/2017gl076691](https://doi.org/10.1029/2017gl076691).
- 1973 Johnson, P., Andresen, A., Collins, A., Fowler, A., Fritz, H., Ghebreab, W., Kusky, T.,
1974 Stern, R., 2011. Late Cryogenian–Ediacaran history of the Arabian–Nubian Shield: A
1975 review of depositional, plutonic, structural, and tectonic events in the closing stages
1976 of the northern East African Orogen. *Journal of African Earth Sciences* 61, 167–232.
1977 doi:[10.1016/j.jafrearsci.2011.07.003](https://doi.org/10.1016/j.jafrearsci.2011.07.003).
- 1978 Johnson, P.R., 2014. An expanding Arabian-Nubian Shield geochronologic and isotopic
1979 dataset: Defining limits and confirming the tectonic setting of a Neoproterozoic accre-
1980 tionary orogen. *The Open Geology Journal* 8, 3–33. URL: <https://doi.org/10.2174%2F1874262901408010003>, doi:[10.2174/1874262901408010003](https://doi.org/10.2174/1874262901408010003).
- 1982 Johnson, S.P., Thorne, A.M., Tyler, I.M., Korsch, R.J., Kennett, B.L.N., Cutten, H.N., Good-
1983 win, J., Blay, O., Blewett, R.S., Joly, A., Dentith, M.C., Aitken, A.R.A., Holzschuh, J.,
1984 Salmon, M., Reading, A., Heinson, G., Boren, G., Ross, J., Costelloe, R.D., Fomin, T., 2013.
1985 Crustal architecture of the Capricorn Orogen, Western Australia and associated metallogeny.
1986 *Australian Journal of Earth Sciences* 60, 681–705. doi:[10.1080/08120099.2013.826735](https://doi.org/10.1080/08120099.2013.826735).
- 1987 Jordan, T.A., Riley, T.R., Siddoway, C.S., 2020. The geological history and evolution
1988 of West Antarctica. *Nature Reviews Earth & Environment* 1, 117–133. doi:[10.1038/s43017-019-0013-6](https://doi.org/10.1038/s43017-019-0013-6).
- 1990 Juliani, C., de Assis, R.R., Monteiro, L.V.S., Fernandes, C.M.D., da Silva Martins, J.E.Z.,
1991 e Costa, J.R.C., 2021. Gold in Paleoproterozoic (2.1 to 1.77 Ga) Continental Magmatic
1992 Arcs at the Tapajós and Juruena Mineral Provinces (Amazonian Craton, Brazil): A New

- 1993 Frontier for the Exploration of Epithermal–Porphyry and Related Deposits. *Minerals* 11,
1994 714. doi:[10.3390/min11070714](https://doi.org/10.3390/min11070714).
- 1995 Karlstrom, K.E., Åhäll, K.I., Harlan, S.S., Williams, M.L., McLelland, J., Geissman, J.W.,
1996 2001. Long-lived (1.8–1.0 Ga) convergent orogen in southern Laurentia, its extensions to
1997 Australia and Baltica, and implications for refining Rodinia. *Precambrian Research* 111,
1998 5–30. doi:[10.1016/s0301-9268\(01\)00154-1](https://doi.org/10.1016/s0301-9268(01)00154-1).
- 1999 Kazmi, A., Rana, R., 1982. Tectonic map of Pakistan. Technical Report. Geological Survey of
2000 Pakistan.
- 2001 Kelemen, P., Hanghøj, K., Greene, A., 2007. One view of the geochemistry of subduction-
2002 related magmatic arcs, with an emphasis on primitive andesite and lower crust, in: *Treatise*
2003 on *Geochemistry*. Elsevier, pp. 1–70. doi:[10.1016/b0-08-043751-6/03035-8](https://doi.org/10.1016/b0-08-043751-6/03035-8).
- 2004 King, R., Floyd, M., Reilinger, R., Bendick, R., 2017. GPS velocity field (MIT 2016.0a) for the
2005 East African Rift System generated by King et al. doi:[10.1594/IEDA/321764](https://doi.org/10.1594/IEDA/321764).
- 2006 Kirkland, C., Smithies, R., Spaggiari, C., Wingate, M., de Gromard, R.Q., Clark, C., Gardiner,
2007 N., Belousova, E., 2017. Proterozoic crustal evolution of the Eucla basement, Australia:
2008 Implications for destruction of oceanic crust during emergence of Nuna. *Lithos* 278–281,
2009 427–444. doi:[10.1016/j.lithos.2017.01.029](https://doi.org/10.1016/j.lithos.2017.01.029).
- 2010 Kirscher, U., Mitchell, R.N., Liu, Y., Nordsvan, A.R., Cox, G.M., Pisarevsky, S.A., Wang,
2011 C., Wu, L., Murphy, J.B., Li, Z.X., 2020. Paleomagnetic constraints on the duration of the
2012 Australia-Laurentia connection in the core of the Nuna supercontinent. *Geology* 49, 174–179.
2013 doi:[10.1130/g47823.1](https://doi.org/10.1130/g47823.1).
- 2014 Klaver, M., de Roever, E.W., Nanne, J.A., Mason, P.R., Davies, G.R., 2015. Charnockites
2015 and UHT metamorphism in the Bakhuis Granulite Belt, western Suriname: Evidence for two
2016 separate UHT events. *Precambrian Research* 262, 1–19. doi:[10.1016/j.precamres.2015.02.014](https://doi.org/10.1016/j.precamres.2015.02.014).
- 2018 Kleinhanns, I.C., Fullgraf, T., Wilsky, F., Nolte, N., Fliegel, D., Klemd, R., Hansen, B.T.,
2019 2013. U–Pb zircon ages and (isotope) geochemical signatures of the Kamanjab Inlier (NW
2020 Namibia): constraints on Palaeoproterozoic crustal evolution along the southern Congo cra-
2021 ton. *Geological Society, London, Special Publications* 389, 165–195. doi:[10.1144/sp389.1](https://doi.org/10.1144/sp389.1).
- 2022 Klett, T.R., Ahlbrandt, T.S., Schmoker, J.W., Dolton, G.L., 1997. Ranking of the world's oil
2023 and gas provinces by known petroleum volumes. Open-File Report 97-463. US Geological
2024 Survey. [Http://pubs.usgs.gov/of/1997/ofr-97-463/97463.html](http://pubs.usgs.gov/of/1997/ofr-97-463/97463.html).
- 2025 Klier, J.J., 2019. The Marshfield terrane : redefinition of origin through zircon geochronology
2026 and geochemistry. Master's thesis. Ball State University. Wisconsin.
- 2027 Korhonen, F., Saw, A., Clark, C., Brown, M., Bhattacharya, S., 2011. New constraints on UHT
2028 metamorphism in the Eastern Ghats Province through the application of phase equilibria
2029 modelling and in situ geochronology. *Gondwana Research* 20, 764–781. doi:[10.1016/j.gr.2011.05.006](https://doi.org/10.1016/j.gr.2011.05.006).
- 2031 Kozlov, P., Likhanov, I., Reverdatto, V., Zinoviev, S., 2012. Tectonometamorphic evolution of
2032 the Garevka polymetamorphic complex (Yenisei Ridge). *Russian Geology and Geophysics*
2033 53, 1133–1149. doi:[10.1016/j.rgg.2012.09.002](https://doi.org/10.1016/j.rgg.2012.09.002).

- 2034 Kranendonk, M.J.V., Kirkland, C.L., 2013. Orogenic climax of Earth: The 1.2-1.1 Ga Grenvillian superevent. *Geology* 41, 735–738. doi:[10.1130/g34243.1](https://doi.org/10.1130/g34243.1).
- 2035
- 2036 Kreemer, C., Blewitt, G., Klein, E.C., 2014. A geodetic plate motion and Global Strain Rate Model. *Geochemistry, Geophysics, Geosystems* 15, 3849–3889. doi:[10.1002/2014gc005407](https://doi.org/10.1002/2014gc005407).
- 2037
- 2038 Kreemer, C., Holt, W.E., Haines, A.J., 2003. An integrated global model of present-day plate motions and plate boundary deformation. *Geophysical Journal International* 154, 8–34. doi:[10.1046/j.1365-246x.2003.01917.x](https://doi.org/10.1046/j.1365-246x.2003.01917.x).
- 2039
- 2040
- 2041 Kröner, A., 1980. Pan African crustal evolution. *Episodes* 3, 3–8. doi:[10.18814/epiiugs/1980/v3i2/001](https://doi.org/10.18814/epiiugs/1980/v3i2/001).
- 2042
- 2043 Kuhnt, W., Holbourn, A., Hall, R., Zuvela, M., Käse, R., 2004. Neogene history of the Indonesian throughflow, in: *Continent-Ocean Interactions Within East Asian Marginal Seas*. American Geophysical Union, pp. 299–320. doi:[10.1029/149gm16](https://doi.org/10.1029/149gm16).
- 2044
- 2045
- 2046 Kusky, T.M., Windley, B.F., Zhai, M.G., 2007. Tectonic evolution of the North China Block: from orogen to craton to orogen. *Geological Society, London, Special Publications* 280, 1–34. doi:[10.1144/sp280.1](https://doi.org/10.1144/sp280.1).
- 2047
- 2048
- 2049 Kuzmichev, A.B., Sklyarov, E.V., 2016. The precambrian of transangaria, yenisei ridge (siberia): Neoproterozoic microcontinent, grenville-age orogen, or reworked margin of the siberian craton? *Journal of Asian Earth Sciences* 115, 419–441. doi:[10.1016/j.jseaes.2015.10.017](https://doi.org/10.1016/j.jseaes.2015.10.017).
- 2050
- 2051
- 2052
- 2053 Kwékam, M., Talla, V., Fozing, E.M., Kouémo, J.T., Dunkl, I., Njonfang, E., 2020. The pan-african high-k i-type granites from batié complex, west cameroon: Age, origin, and tectonic implications. *Frontiers in Earth Science* 8. doi:[10.3389/feart.2020.00363](https://doi.org/10.3389/feart.2020.00363).
- 2054
- 2055
- 2056 van de Lagemaat, S.H., Swart, M.L., Vaes, B., Kosters, M.E., Boschman, L.M., Burton-Johnson, A., Bijl, P.K., Spakman, W., van Hinsbergen, D.J., 2021. Subduction initiation in the Scotia Sea region and opening of the Drake Passage: When and why? *Earth-Science Reviews* 215, 103551. doi:[10.1016/j.earscirev.2021.103551](https://doi.org/10.1016/j.earscirev.2021.103551).
- 2057
- 2058
- 2059
- 2060 Langmuir, C., Bézos, A., Escrig, S., Parman, S., 2006. Chemical systematics and hydrous melting of the mantle in back-arc basins, in: Christie, D., Fisher, C., Lee, S.M., Givens, S. (Eds.), *Back-Arc Spreading Systems: Geological, Biological, Chemical, and Physical Interactions*. Am. Geophys. Un.. volume 166 of *Geophys. Monogr.*, pp. 87–146. doi:[10.1029/166GM07](https://doi.org/10.1029/166GM07).
- 2061
- 2062
- 2063
- 2064 Laske, G., Masters, G., 1997. A global digital map of sediment thickness. *EOS Trans. AGU* 78, F483.
- 2065
- 2066 Laske, G., Masters, G., Ma, Z., Pasquano, M., 2013. Update on CRUST1.0 - A 1-degree Global Model of Earth's Crust, in: *Geophys. Res. Abstracts*. European Geophysical Union. volume 15, pp. EGU2013–2658.
- 2067
- 2068
- 2069 Leitchenkov, G.L., Antonov, A.V., Luneov, P.I., Lipenkov, V.Y., 2016. Geology and environments of subglacial Lake Vostok. *Philosophical Transactions of the Royal Society A: Mathematical, Physical and Engineering Sciences* 374, 20140302. doi:[10.1098/rsta.2014.0302](https://doi.org/10.1098/rsta.2014.0302).
- 2070
- 2071
- 2072 Lepvrier, C., Maluski, H., Tich, V.V., Leyreloup, A., Thi, P.T., Vuong, N.V., 2004. The Early Triassic Indosinian orogeny in Vietnam (Truong Son Belt and Kontum Massif): implications for the geodynamic evolution of Indochina. *Tectonophysics* 393, 87–118. doi:[10.1016/j.tecto.2004.07.030](https://doi.org/10.1016/j.tecto.2004.07.030).
- 2073
- 2074
- 2075

- 2076 Lesur, V., Hamoudi, M., Choi, Y., Dyment, J., Thébault, E., 2016. Building the second
2077 version of the world digital magnetic anomaly map (WDMAM). *Earth, Planets and Space*
2078 68. doi:[10.1186/s40623-016-0404-6](https://doi.org/10.1186/s40623-016-0404-6).
- 2079 Li, B., Massonne, H.J., Hartmann, L.A., Zhang, J., Luo, T., 2021. Kyanite-garnet granulite
2080 from the Andrelândia nappe system, Brasília belt, registers two late Neoproterozoic metamor-
2081 phic cycles. *Precambrian Research* 355, 106086. doi:[10.1016/j.precamres.2020.106086](https://doi.org/10.1016/j.precamres.2020.106086).
- 2082 Li, J., yan Cai, W., yong Wang, K., Kim, N., lun Liu, H., Lee, G.J., Yoo, B.C., 2019. Initial
2083 decratonization of the eastern North China Craton: New constraints from geochronology,
2084 geochemistry, and Hf isotopic compositions of Mesozoic igneous rocks in the Qingchengzi
2085 district. *Geological Journal* 55, 3796–3820. doi:[10.1002/gj.3635](https://doi.org/10.1002/gj.3635).
- 2086 Li, S.S., Santosh, M., Palin, R.M., 2018. Metamorphism during the Archean–Paleoproterozoic
2087 Transition Associated with Microblock Amalgamation in the Dharwar Craton, India. *Journal*
2088 of Petrology 59, 2435–2462. doi:[10.1093/petrology/egy102](https://doi.org/10.1093/petrology/egy102).
- 2089 Li, Z., Bogdanova, S., Collins, A., Davidson, A., Waele, B.D., Ernst, R., Fitzsimons, I., Fuck,
2090 R., Gladkochub, D., Jacobs, J., Karlstrom, K., Lu, S., Natapov, L., Pease, V., Pisarevsky, S.,
2091 Thrane, K., Vernikovsky, V., 2008. Assembly, configuration, and break-up history of Rodinia:
2092 A synthesis. *Precambrian Research* 160, 179–210. doi:[10.1016/j.precamres.2007.04.021](https://doi.org/10.1016/j.precamres.2007.04.021).
- 2093 Liégeois, J.P., 2018. A new synthetic geological map of the Tuareg Shield: An overview of Its
2094 global structure and geological evolution, in: *The Geology of the Arab World—An Overview*.
2095 Springer International Publishing, pp. 83–107. doi:[10.1007/978-3-319-96794-3_2](https://doi.org/10.1007/978-3-319-96794-3_2).
- 2096 Liégeois, J.P., Abdelsalam, M.G., Ennih, N., Ouabadi, A., 2013. Metacraton: Nature, genesis
2097 and behavior. *Gondwana Research* 23, 220–237. doi:[10.1016/j.gr.2012.02.016](https://doi.org/10.1016/j.gr.2012.02.016).
- 2098 Linde, G.M., Trexler, J.H., Cashman, P.H., Gehrels, G., Dickinson, W.R., 2017. Three-
2099 dimensional evolution of the early Paleozoic western Laurentian margin: New insights from
2100 detrital zircon U-Pb geochronology and Hf isotope geochemistry of the Harmony Formation
2101 of Nevada. *Tectonics* 36, 2347–2369. doi:[10.1002/2017tc004520](https://doi.org/10.1002/2017tc004520).
- 2102 Lister, G.S., Forster, M.A., Rawling, T.J., 2001. Episodicity during orogenesis. *Geological*
2103 Society, London, Special Publications 184, 89–113. doi:[10.1144/gsl.sp.2001.184.01.06](https://doi.org/10.1144/gsl.sp.2001.184.01.06).
- 2104 Liu, F., Zhang, J., Liu, C., 2017. Archean to Paleoproterozoic Evolution of the North China
2105 Craton: Preface. *Precambrian Research* 303, 1–9. doi:[10.1016/j.precamres.2017.11.011](https://doi.org/10.1016/j.precamres.2017.11.011).
- 2106 Liu, M., Shen, Y., 1998. Sierra Nevada uplift: A ductile link to mantle upwelling under the
2107 Basin and Range province. *Geology* 26, 299–302. doi:[10.1130/0091-7613\(1998\)026<0299:snuadl>2.3.co;2](https://doi.org/10.1130/0091-7613(1998)026<0299:snuadl>2.3.co;2).
- 2109 Liu, X., m. Jahn, B., Zhao, Y., Liu, J., Ren, L., 2014. Geochemistry and geochronology of
2110 Mesoproterozoic basement rocks from the Eastern Amery Ice Shelf and southwestern Prydz
2111 Bay, East Antarctica: Implications for a long-lived magmatic accretion in a continental arc.
2112 *American Journal of Science* 314, 508–547. doi:[10.2475/02.2014.03](https://doi.org/10.2475/02.2014.03).
- 2113 Liu, Y., Mitchell, R.N., Li, Z.X., Kirscher, U., Pisarevsky, S.A., Wang, C., 2021. Archean
2114 geodynamics: Ephemeral supercontinents or long-lived supercratons. *Geology* doi:[10.1130/g48575.1](https://doi.org/10.1130/g48575.1).
- 2116 Llubes, M., Seoane, L., Bruinsma, S., Rémy, F., 2018. Crustal thickness of Antarctica estimated
2117 using data from gravimetric satellites. *Solid Earth* 9, 457–467. doi:[10.5194/se-9-457-2018](https://doi.org/10.5194/se-9-457-2018).

- 2118 Loose, D., Schenk, V., 2018. 2.09 Ga old eclogites in the Eburnian-Transamazonian orogen
2119 of southern Cameroon: Significance for Palaeoproterozoic plate tectonics. Precambrian Re-
2120 search 304, 1–11. doi:[10.1016/j.precamres.2017.10.018](https://doi.org/10.1016/j.precamres.2017.10.018).
- 2121 Lowman, P., Yates, J., 2002. Digital tectonic activity map. NASA Goddard Space Flight
2122 Center, <http://denali.gsfc.nasa.gov/dtam/>.
- 2123 Lucaleau, F., 2019. Analysis and mapping of an updated terrestrial heat flow dataset. Geo-
2124 chemistry, Geophysics, Geosystems doi:[10.1029/2019gc008389](https://doi.org/10.1029/2019gc008389).
- 2125 Lund, K., Box, S.E., Holm-Denoma, C.S., Juan, C.A.S., Blakely, R.J., Saltus, R.W., Anderson,
2126 E.D., DeWitt, E., 2015. Basement domain map of the conterminous United States and
2127 Alaska. Data Series 898. U.S. Geological Survey. URL: <https://doi.org/10.3133%2Fds898>,
2128 doi:[10.3133/ds898](https://doi.org/10.3133/ds898).
- 2129 Makkonen, H.V., , and, P.T., 2020. Geology and crystallization conditions of the
2130 särkiniemiinruption and related nickel-copper ore, central finland – implications for depth
2131 of emplacement of 1.88 ga nickel-bearing intrusions. Bulletin of the Geological Society of
2132 Finland 92, 111–130. doi:[10.17741/bgsf/92.2.003](https://doi.org/10.17741/bgsf/92.2.003).
- 2133 Mako, C.A., Williams, M.L., Karlstrom, K.E., Doe, M.F., Powicki, D., Holland, M.E., Gehrels,
2134 G., Pecha, M., 2015. Polyphase proterozoic deformation in the four peaks area, central
2135 arizona, and relevance for the mazatzal orogeny. Geosphere 11, 1975–1995. doi:[10.1130/ges01196.1](https://doi.org/10.1130/ges01196.1).
- 2137 Maritati, A., Aitken, A.R.A., Young, D.A., Roberts, J.L., Blankenship, D.D., Siegert, M.J.,
2138 2016. The tectonic development and erosion of the Knox Subglacial Sedimentary Basin, East
2139 Antarctica. Geophysical Research Letters 43, 10,728–10,737. doi:[10.1002/2016gl071063](https://doi.org/10.1002/2016gl071063).
- 2140 Maritati, A., Halpin, J.A., Whittaker, J.M., Daczko, N.R., 2019. Fingerprinting Protero-
2141 zoic bedrock in interior Wilkes Land, East Antarctica. Scientific Reports 9. doi:[10.1038/s41598-019-46612-y](https://doi.org/10.1038/s41598-019-46612-y).
- 2143 Marques, F., Catalão, J., DeMets, C., Costa, A., Hildenbrand, A., 2013. GPS and tectonic
2144 evidence for a diffuse plate boundary at the Azores Triple Junction. Earth and Planetary
2145 Science Letters 381, 177–187. doi:[10.1016/j.epsl.2013.08.051](https://doi.org/10.1016/j.epsl.2013.08.051).
- 2146 Matte, P., 2001. The Variscan collage and orogeny (480-290 Ma) and the tectonic definition
2147 of the Armorica microplate: a review. Terra Nova 13, 122–128. doi:[10.1046/j.1365-3121.2001.00327.x](https://doi.org/10.1046/j.1365-3121.2001.00327.x).
- 2149 Matthews, K.J., Maloney, K.T., Zahirovic, S., Williams, S.E., Seton, M., Müller, R.D., 2016.
2150 Global plate boundary evolution and kinematics since the late Paleozoic. Global and Plane-
2151 tary Change 146, 226–250. doi:[10.1016/j.gloplacha.2016.10.002](https://doi.org/10.1016/j.gloplacha.2016.10.002).
- 2152 McClusky, S., Reilinger, R., Ogubazghi, G., Amleson, A., Healeb, B., Vernant, P., Sholan,
2153 J., Fisseha, S., Asfaw, L., Bendick, R., Kogan, L., 2010. Kinematics of the southern Red
2154 Sea-Afar Triple Junction and implications for plate dynamics. Geophysical Research Letters
2155 37, L05301. doi:[10.1029/2009gl041127](https://doi.org/10.1029/2009gl041127).
- 2156 McCourt, S., Armstrong, R.A., Jelsma, H., Mapeo, R.B.M., 2013. New U–Pb SHRIMP ages
2157 from the Lubango region, SW Angola: insights into the Palaeoproterozoic evolution of the
2158 Angolan Shield, southern Congo Craton, Africa. Journal of the Geological Society 170,
2159 353–363. URL: <https://doi.org/10.1144%2Fjgs2012-059>, doi:[10.1144/jgs2012-059](https://doi.org/10.1144/jgs2012-059).

- 2160 McKerrow, W.S., MacNiocaill, C., Dewey, J.F., 2000. The Caledonian Orogeny redefined.
2161 Journal of the Geological Society 157, 1149–1154. doi:[10.1144/jgs.157.6.1149](https://doi.org/10.1144/jgs.157.6.1149).
- 2162 McQuarrie, N., van Hinsbergen, D.J., 2013. Retrodeforming the Arabia-Eurasia collision zone:
2163 Age of collision versus magnitude of continental subduction. Geology 41, 315–318. doi:[10.1130/g33591.1](https://doi.org/10.1130/g33591.1).
- 2165 Medaris, L.G., Singer, B.S., Jicha, B.R., Malone, D.H., Schwartz, J.J., Stewart, E.K., Lankveld,
2166 A.V., Williams, M.L., Reiners, P.W., 2021. Early Mesoproterozoic evolution of midcontinent
2167 Laurentia: Defining the geon 14 Baraboo orogeny. Geoscience Frontiers 12, 101174.
2168 doi:[10.1016/j.gsf.2021.101174](https://doi.org/10.1016/j.gsf.2021.101174).
- 2169 Meert, J.G., Lieberman, B.S., 2008. The Neoproterozoic assembly of Gondwana and its rela-
2170 tionship to the Ediacaran–Cambrian radiation. Gondwana Research 14, 5–21. doi:[10.1016/j.gr.2007.06.007](https://doi.org/10.1016/j.gr.2007.06.007).
- 2172 Meert, J.G., Santosh, M., 2017. The Columbia supercontinent revisited. Gondwana Research
2173 50, 67–83. doi:[10.1016/j.gr.2017.04.011](https://doi.org/10.1016/j.gr.2017.04.011).
- 2174 Meert, J.G., Voo, R.V.D., 1997. The assembly of Gondwana 800–550 Ma. Journal of Geody-
2175 namics 23, 223–235. doi:[10.1016/s0264-3707\(96\)00046-4](https://doi.org/10.1016/s0264-3707(96)00046-4).
- 2176 Meredith, A.S., Williams, S.E., Collins, A.S., Tetley, M.G., Mulder, J.A., Blades, M.L., Young,
2177 A., Armistead, S.E., Cannon, J., Zahirovic, S., Müller, R.D., 2021. Extending full-plate
2178 tectonic models into deep time: Linking the Neoproterozoic and the Phanerozoic. Earth-
2179 Science Reviews 214, 103477. doi:[10.1016/j.earscirev.2020.103477](https://doi.org/10.1016/j.earscirev.2020.103477).
- 2180 Meyer, B., Saltus, R., 2016. Emag2: Earth magnetic anomaly grid (2-arc-minute resolution)
2181 version 3. doi:[10.7289/v5h70cvx](https://doi.org/10.7289/v5h70cvx).
- 2182 Mikkola, P., Mönkäre, K., Ahven, M., Huhma, H., 2018. Geochemistry and age of the paleopro-
2183 terozoic makkola suite volcanic rocks in central finland. Development of the Paleoproterozoic
2184 Svecofennian orogeny: new constraints from the southeastern boundary of the Central Fin-
2185 land Granitoid Complex , 85–105doi:[10.30440/bt407.5](https://doi.org/10.30440/bt407.5).
- 2186 Minster, J.B., Jordan, T.H., 1978. Present-day plate motions. Journal of Geophysical Research
2187 83, 5331. doi:[10.1029/jb083ib11p05331](https://doi.org/10.1029/jb083ib11p05331).
- 2188 Mitchell, A., Chung, S.L., Oo, T., Lin, T.H., Hung, C.H., 2012. Zircon U–Pb ages in Myanmar:
2189 Magmatic–metamorphic events and the closure of a neo-Tethys ocean? Journal of Asian
2190 Earth Sciences 56, 1–23. doi:[10.1016/j.jseaes.2012.04.019](https://doi.org/10.1016/j.jseaes.2012.04.019).
- 2191 Mooney, W., 2007. Crust and Lithospheric Structure –Global Crustal Structure, in: Treatise
2192 on Geophysics. Elsevier, pp. 361–417. doi:[10.1016/b978-044452748-6.00011-0](https://doi.org/10.1016/b978-044452748-6.00011-0).
- 2193 Mooney, W., Laske, G., Masters, T., 1998. Crust 5.1: a global crustal model 5° x5°. J. Geophys.
2194 Res. 103, 727–747.
- 2195 Morley, C., Ampaiwan, P., Thanudamrong, S., Kuenphan, N., Warren, J., 2013. Development
2196 of the Khao Khwang Fold and Thrust Belt: Implications for the geodynamic setting of
2197 Thailand and Cambodia during the Indosinian Orogeny. Journal of Asian Earth Sciences 62,
2198 705–719. doi:[10.1016/j.jseaes.2012.11.021](https://doi.org/10.1016/j.jseaes.2012.11.021).
- 2199 Morley, C.K., Searle, M., 2017. Chapter 5 Regional tectonics, structure and evolution of the
2200 Andaman–Nicobar Islands from ophiolite formation and obduction to collision and back-arc
2201 spreading. Geological Society, London, Memoirs 47, 51–74. doi:[10.1144/m47.5](https://doi.org/10.1144/m47.5).

- 2202 Morrissey, L., Payne, J.L., Kelsey, D.E., Hand, M., 2011. Grenvillian-aged reworking in the
2203 North Australian Craton, central Australia: Constraints from geochronology and modelled
2204 phase equilibria. *Precambrian Research* 191, 141–165. doi:[10.1016/j.precamres.2011.09.010](https://doi.org/10.1016/j.precamres.2011.09.010).
- 2205
- 2206 Morrissey, L.J., Barovich, K.M., Hand, M., Howard, K.E., Payne, J.L., 2019. Magmatism
2207 and metamorphism at ca. 1.45 Ga in the northern Gawler Craton: The Australian record
2208 of rifting within Nuna (Columbia). *Geoscience Frontiers* 10, 175–194. doi:[10.1016/j.gsf.2018.07.006](https://doi.org/10.1016/j.gsf.2018.07.006).
- 2209
- 2210 Morrissey, L.J., Hand, M., Kelsey, D.E., 2015. Multi-stage metamorphism in the Rayner–
2211 Eastern Ghats Terrane: P–T– constraints from the northern Prince Charles Mountains, east
2212 Antarctica. *Precambrian Research* 267, 137–163. doi:[10.1016/j.precamres.2015.06.003](https://doi.org/10.1016/j.precamres.2015.06.003).
- 2213 Morrissey, L.J., Hand, M., Kelsey, D.E., 2017. A curious case of agreement between conven-
2214 tional thermobarometry and phase equilibria modelling in granulites: New constraints *P-T*
2215 estimates in the Antarctica segment of the Musgrave-Albany-Fraser-Wilkes Orogen. *Journal*
2216 of Metamorphic Geology 35, 1023–1050. doi:[10.1111/jmg.12266](https://doi.org/10.1111/jmg.12266).
- 2217 Mortimer, N., 2004. New Zealand’s Geological Foundations. *Gondwana Research* 7, 261–272.
2218 doi:[10.1016/s1342-937x\(05\)70324-5](https://doi.org/10.1016/s1342-937x(05)70324-5).
- 2219 Mulder, J.A., Halpin, J.A., Daczko, N.R., Orth, K., Meffre, S., Thompson, J.M., Morrissey,
2220 L.J., 2019. A Multiproxy provenance approach to uncovering the assembly of East Gondwana
2221 in Antarctica. *Geology* 47, 645–649. doi:[10.1130/g45952.1](https://doi.org/10.1130/g45952.1).
- 2222 Mulder, J.A., Karlstrom, K.E., Halpin, J.A., Merdith, A.S., Spencer, C.J., Berry, R.F., Mc-
2223 Donald, B., 2018. Rodinian devil in disguise: Correlation of 1.25–1.10 Ga strata between
2224 Tasmania and Grand Canyon. *Geology* 46, 991–994. doi:[10.1130/g45225.1](https://doi.org/10.1130/g45225.1).
- 2225 Muttoni, G., Kent, D.V., Garzanti, E., Brack, P., Abrahamsen, N., Gaetani, M., 2003. Early
2226 Permian Pangea ‘B’ to Late Permian Pangea ‘A’. *Earth and Planetary Science Letters* 215,
2227 379–394. doi:[10.1016/s0012-821x\(03\)00452-7](https://doi.org/10.1016/s0012-821x(03)00452-7).
- 2228 Naimi-Ghassabian, N., Khatib, M.M., Nazari, H., Heyhat, M.R., 2018. Regional variations
2229 and earthquake frequency–magnitude distribution and fractal dimension in the North of
2230 Central-East Iran Blocks (NCEIB). *Arabian Journal of Geosciences* 11. doi:[10.1007/s12517-018-3506-6](https://doi.org/10.1007/s12517-018-3506-6).
- 2232 Nance, R.D., Gutiérrez-Alonso, G., Keppie, J.D., Linnemann, U., Murphy, J.B., Quesada, C.,
2233 Strachan, R.A., Woodcock, N.H., 2012. A brief history of the Rheic Ocean. *Geoscience*
2234 *Frontiers* 3, 125–135. doi:[10.1016/j.gsf.2011.11.008](https://doi.org/10.1016/j.gsf.2011.11.008).
- 2235 Nedel, I.M., Fuck, R.A., Ruiz, A.S., Matos, R., Ferreira, A.C.D., 2020. U–Pb geochronology and
2236 geochemistry of Grenville-age plutons in the Sunsas Belt - Bolivia, SW Amazonian Craton:
2237 Tectonic and magmatic implications. *Journal of South American Earth Sciences* 104, 102845.
2238 doi:[10.1016/j.jsames.2020.102845](https://doi.org/10.1016/j.jsames.2020.102845).
- 2239 Neill, I., Kerr, A.C., Hastie, A.R., Stanek, K.P., Millar, I.L., 2011. Origin of the Aves Ridge
2240 and Dutch–Venezuelan Antilles: interaction of the Cretaceous ‘Great Arc’ and Caribbean–
2241 Colombian Oceanic Plateau? *Journal of the Geological Society* 168, 333–348. doi:[10.1144/0016-76492010-067](https://doi.org/10.1144/0016-76492010-067).
- 2242

- 2243 Nixon, A., Glorie, S., Collins, A., Blades, M., Simpson, A., Whelan, J., 2022. Inter-cratonic
2244 geochronological and geochemical correlations of the Derim Derim–Galiwinku/Yanliao re-
2245 constructed Large Igneous Province across the North Australian and North China cratons.
2246 *Gondwana Research* 103, 473–486. doi:[10.1016/j.gr.2021.10.027](https://doi.org/10.1016/j.gr.2021.10.027).
- 2247 Njoroge, M., Malservisi, R., Voytenko, D., Hackl, M., 2015. Is Nubia Plate rigid? A geodetic
2248 study of the relative motion of different cratonic areas within Africa, in: REFAG 2014.
2249 Springer International Publishing, pp. 171–180. doi:[10.1007/1345_2015_212](https://doi.org/10.1007/1345_2015_212).
- 2250 O'Donnell, J., Stuart, G., Brisbourne, A., Selway, K., Yang, Y., Nield, G., Whitehouse, P.,
2251 Nyblade, A., Wiens, D., Aster, R., Anandakrishnan, S., Huerta, A., Wilson, T., Winberry,
2252 J., 2019. The uppermost mantle seismic velocity structure of West Antarctica from Rayleigh
2253 wave tomography: Insights into tectonic structure and geothermal heat flow. *Earth and*
2254 *Planetary Science Letters* 522, 219–233. doi:[10.1016/j.epsl.2019.06.024](https://doi.org/10.1016/j.epsl.2019.06.024).
- 2255 Ontario Geological Survey, 2011. 1: 250 000 Scale Bedrock Geology of Ontario-Revision 1.
2256 Miscellaneous Release - Data MRD 126-REV-1. Ontario Geological Survey.
- 2257 Oxman, V.S., 2003. Tectonic evolution of the Mesozoic Verkhoyansk–Kolyma belt (NE Asia).
2258 *Tectonophysics* 365, 45–76. doi:[10.1016/s0040-1951\(03\)00064-7](https://doi.org/10.1016/s0040-1951(03)00064-7).
- 2259 Pant, N.C., Dasgupta, S., 2017. An introduction to the crustal evolution of India and Antarc-
2260 tica: the supercontinent connection. *Geological Society, London, Special Publications* 457,
2261 1–6. doi:[10.1144/sp457.14](https://doi.org/10.1144/sp457.14).
- 2262 Paulsen, T., Encarnación, J., Grunow, A.M., Valencia, V.A., Pecha, M.E., Benowitz, J., Layer,
2263 P., 2020. New ages from the Shackleton Glacier area and their context in the regional
2264 tectonomagmatic evolution of the Ross orogen of Antarctica. *International Geology Review*
2265 63, 1596–1618. doi:[10.1080/00206814.2020.1786737](https://doi.org/10.1080/00206814.2020.1786737).
- 2266 Pawlewicz, M.J., Steinshouer, D.W., Gautier, D.L., 1997. Map showing geology, oil and gas
2267 fields, and geologic provinces of Europe including Turkey. Open-file Report 97-470I. US
2268 Geological Survey. doi:[10.3133/ofr97470i](https://doi.org/10.3133/ofr97470i).
- 2269 Pawley, M.J., Dutch, R.A., Wise, T.W., 2020. The relationship between crustal architecture,
2270 deformation, and magmatism in the Coompana Province, Australia. *Tectonics* 39. doi:[10.1029/2019tc005593](https://doi.org/10.1029/2019tc005593).
- 2272 Payne, J.L., Hand, M., Barovich, K.M., Reid, A., Evans, D.A.D., 2009. Correlations and
2273 reconstruction models for the 2500–1500 Ma evolution of the Mawson Continent. *Geological*
2274 *Society, London, Special Publications* 323, 319–355. doi:[10.1144/sp323.16](https://doi.org/10.1144/sp323.16).
- 2275 Payne, J.L., Morrissey, L.J., Tucker, N.M., Roche, L.K., Szpunar, M.A., Neroni, R., 2021.
2276 Granites and gabbros at the dawn of a coherent Australian continent. *Precambrian Research*
2277 359, 106189. doi:[10.1016/j.precamres.2021.106189](https://doi.org/10.1016/j.precamres.2021.106189).
- 2278 Pease, V., 2021. Eastern Europe: The Timanian and Uralian Orogenes, in: Encyclopedia of
2279 Geology. Elsevier, pp. 302–310. doi:[10.1016/b978-0-08-102908-4.00028-x](https://doi.org/10.1016/b978-0-08-102908-4.00028-x).
- 2280 Pehrsson, S.J., Berman, R.G., Eglington, B., Rainbird, R., 2013. Two Neoarchean supercon-
2281 tinents revisited: The case for a Rae family of cratons. *Precambrian Research* 232, 27–43.
2282 doi:[10.1016/j.precamres.2013.02.005](https://doi.org/10.1016/j.precamres.2013.02.005).

- 2283 Pehrsson, S.J., Buchan, K.L., Eglington, B.M., Berman, R.M., Rainbird, R.H., 2014. Did plate
2284 tectonics shutdown in the Palaeoproterozoic? A view from the Siderian geologic record.
2285 *Gondwana Research* 26, 803–815. doi:[10.1016/j.gr.2014.06.001](https://doi.org/10.1016/j.gr.2014.06.001).
- 2286 Pelletier, J., Broxton, P., Hazenberg, P., Zeng, X., Troch, P., Niu, G., Williams, Z., Brunke,
2287 M., Gochis, D., 2016. Global 1-km Gridded Thickness of Soil, Regolith, and Sedimentary
2288 Deposit Layers. doi:[10.3334/ORNLDAA/1304](https://doi.org/10.3334/ORNLDAA/1304).
- 2289 Peron-Pinvidic, G., Gernigon, L., Gaina, C., Ball, P., 2012. Insights from the Jan Mayen
2290 system in the Norwegian-Greenland sea-I. Mapping of a microcontinent. *Geophysical Journal
2291 International* 191, 385–412. doi:[10.1111/j.1365-246x.2012.05639.x](https://doi.org/10.1111/j.1365-246x.2012.05639.x).
- 2292 Persits, F., Ahlbrandt, T.S., Tuttle, M.L., Charpentier, R.R., Brownfield, M.E., Takahashi,
2293 K.I., 1997a. Maps showing geology, oil and gas fields and geological provinces of Africa.
2294 Open-file Report 97-470A. US Geological Survey. doi:[10.3133/ofr97470a](https://doi.org/10.3133/ofr97470a).
- 2295 Persits, F., Ulmishek, G., Steinshouer, D., 1997b. Maps showing geology, oil and gas fields
2296 and geologic provinces of the former Soviet Union. Open-file Report 97-470E. US Geological
2297 Survey. doi:[10.3133/ofr97470e](https://doi.org/10.3133/ofr97470e).
- 2298 Pesonen, L., Mertanen, S., Veikkolainen, T., 2012. Paleo-Mesoproterozoic Supercontinents —
2299 A Paleomagnetic View. *Geophysica* 48, 5–47.
- 2300 Peucat, J., Ménot, R., Monnier, O., Fanning, C., 1999. The Terre Adélie basement in the
2301 East-Antarctica Shield: geological and isotopic evidence for a major 1.7Ga thermal event:
2302 comparison with the Gawler Craton in South Australia. *Precambrian Research* 94, 205–224.
2303 doi:[10.1016/s0301-9268\(98\)00119-3](https://doi.org/10.1016/s0301-9268(98)00119-3).
- 2304 Peucat, J.J., Barbosa, J.S.F., de Araújo Pinho, I.C., Paquette, J.L., Martin, H., Fanning, C.M.,
2305 de Menezes Leal, A.B., Cruz, S., 2011. Geochronology of granulites from the south Itabuna-
2306 Salvador-Curaçá Block, São Francisco Craton (Brazil): Nd isotopes and U–Pb zircon ages.
2307 *Journal of South American Earth Sciences* 31, 397–413. doi:[10.1016/j.jsames.2011.03.009](https://doi.org/10.1016/j.jsames.2011.03.009).
- 2309 Phillips, G., Kelsey, D.E., Corvino, A.F., Dutch, R.A., 2009. Continental reworking during
2310 overprinting orogenic events, southern Prince Charles Mountains, East Antarctica. *Journal
2311 of Petrology* 50, 2017–2041. doi:[10.1093/petrology/egp065](https://doi.org/10.1093/petrology/egp065).
- 2312 Pierce, E., Hemming, S., Williams, T., van de Flierdt, T., Thomson, S., Reiners, P., Gehrels,
2313 G., Brachfeld, S., Goldstein, S., 2014. A comparison of detrital U–Pb zircon, 40Ar/39Ar
2314 hornblende, 40Ar/39Ar biotite ages in marine sediments off East Antarctica: Implications
2315 for the geology of subglacial terrains and provenance studies. *Earth-Science Reviews* 138,
2316 156–178. doi:[10.1016/j.earscirev.2014.08.010](https://doi.org/10.1016/j.earscirev.2014.08.010).
- 2317 Pilia, S., Rawlinson, N., Cayley, R.A., Bodin, T., Musgrave, R., Reading, A.M., Direen, N.G.,
2318 Young, M.K., 2015. Evidence of micro-continent entrainment during crustal accretion. *Sci-
2319 entific Reports* 5. doi:[10.1038/srep08218](https://doi.org/10.1038/srep08218).
- 2320 Pisarevsky, S.A., Elming, S.Å., Pesonen, L.J., Li, Z.X., 2014. Mesoproterozoic paleogeogra-
2321 phy: Supercontinent and beyond. *Precambrian Research* 244, 207–225. doi:[10.1016/j.precamres.2013.05.014](https://doi.org/10.1016/j.precamres.2013.05.014).
- 2323 Pisarevsky, S.A., Wingate, M.T.D., Harris, L.B., 2003. Late Mesoproterozoic (ca1.2 Ga) palaeo-
2324 magnetism of the Albany-Fraser orogen: no pre-Rodinia Australia-Laurentia connection.
2325 *Geophysical Journal International* 155, F6–F11. doi:[10.1046/j.1365-246x.2003.02074.x](https://doi.org/10.1046/j.1365-246x.2003.02074.x).

- 2326 Poggi, V., Durrheim, R., Tuluka, G.M., Weatherill, G., Gee, R., Pagani, M., Nyblade, A.,
2327 Delvaux, D., 2017. Assessing seismic hazard of the east african rift: a pilot study from
2328 GEM and AfricaArray. *Bulletin of Earthquake Engineering* 15, 4499–4529. doi:[10.1007/s10518-017-0152-4](https://doi.org/10.1007/s10518-017-0152-4).
- 2329
- 2330 Pollastro, R., Persits, F., Steinshouer, D., 1997. Maps showing geology, oil and gas fields, and
2331 geologic provinces of Iran. Open-file report. US Geological Survey. doi:[10.3133/ofr97470g](https://doi.org/10.3133/ofr97470g).
2332 97-470G.
- 2333 Pollastro, R.M., Karshbaum, A.S., Viger, R.J., 1999. Maps showing geology, oil and gas fields
2334 and geologic provinces of the Arabian Peninsula. Open-file Report 97-470B. US Geological
2335 Survey. doi:[10.3133/ofr97470b](https://doi.org/10.3133/ofr97470b).
- 2336 Pourteau, A., Smit, M.A., Li, Z.X., Collins, W.J., Nordsvan, A.R., Volante, S., Li, J., 2018.
2337 1.6 Ga crustal thickening along the final Nuna suture. *Geology* 46, 959–962. doi:[10.1130/g45198.1](https://doi.org/10.1130/g45198.1).
- 2338
- 2339 Profeta, L., Ducea, M.N., Chapman, J.B., Paterson, S.R., Gonzales, S.M.H., Kirsch, M., Pe-
2340 trescu, L., DeCelles, P.G., 2015. Quantifying crustal thickness over time in magmatic arcs.
2341 *Scientific Reports* 5. doi:[10.1038/srep17786](https://doi.org/10.1038/srep17786).
- 2342 Puetz, S.J., 2018. A relational database of global U–Pb ages. *Geoscience Frontiers* 9, 877–891.
2343 doi:[10.1016/j.gsf.2017.12.004](https://doi.org/10.1016/j.gsf.2017.12.004).
- 2344 Pyle, D.G., Christie, D.M., Mahoney, J.J., 1992. Resolving an isotopic boundary within the
2345 Australian-Antarctic discordance. *Earth and Planetary Science Letters* 112, 161–178. doi:[10.1016/0012-821x\(92\)90014-m](https://doi.org/10.1016/0012-821x(92)90014-m).
- 2346
- 2347 Ramos, V., Aleman, A., 2000. Tectonic evolution of the Andes, in: Cordani, U., Milani, E.,
2348 Filho, T., Campos, A. (Eds.), *Tectonic Evolution of South America*. Geological Survey of
2349 Brazil, pp. 635–685.
- 2350 Rathnayake, S., Tenzer, R., Eshagh, M., Pitonák, M., 2019. Gravity maps of the lithospheric
2351 structure beneath the Indian Ocean. *Surveys in Geophysics* 40, 1055–1093. doi:[10.1007/s10712-019-09564-6](https://doi.org/10.1007/s10712-019-09564-6).
- 2352
- 2353 Robertson, A.H.F., Ustaömer, T., Pickett, E.A., Collins, A.S., Andrew, T., Dixon, J.E., 2004.
2354 Testing models of Late Palaeozoic–Early Mesozoic orogeny in Western Turkey: support for
2355 an evolving open-Tethys model. *Journal of the Geological Society* 161, 501–511. doi:[10.1144/0016-764903-080](https://doi.org/10.1144/0016-764903-080).
- 2356
- 2357 Roest, W.R., Collette, B.J., 1986. The Fifteen Twenty Fracture Zone and the North American–
2358 South American plate boundary. *Journal of the Geological Society* 143, 833–843. doi:[10.1144/gsjgs.143.5.0833](https://doi.org/10.1144/gsjgs.143.5.0833).
- 2359
- 2360 da Rosa-Costa, L.T., Lafon, J.M., Cocherie, A., Delor, C., 2008. Electron microprobe u–th–pb
2361 monazite dating of the transamazonian metamorphic overprint on archean rocks from the
2362 amapá block, southeastern guiana shield, northern brazil. *Journal of South American Earth
2363 Sciences* 26, 445–462. doi:[10.1016/j.jsames.2008.05.007](https://doi.org/10.1016/j.jsames.2008.05.007).
- 2364 Royer, J., Gordon, R., 1997. The motion and boundary between the Capricorn and Australian
2365 Plates. *Science* 277, 1268–1274. doi:[10.1126/science.277.5330.1268](https://doi.org/10.1126/science.277.5330.1268).

- 2366 Rubin, K., 2016. Mid-ocean Ridge Magmatism and Volcanism, in: Harff, J., Meschede, M.,
2367 Petersen, S., Thiede, J. (Eds.), Encyclopedia of Marine Geosciences. Springer Netherlands,
2368 pp. 1–28. doi:[10.1007/978-94-007-6238-1_28](https://doi.org/10.1007/978-94-007-6238-1_28).
- 2369 Ruppel, A.S., Jacobs, J., Läufer, A., Ratschbacher, L., Pfänder, J.A., Sonntag, B.L., Krasniqi,
2370 K., Elburg, M., Krohne, N., Damaske, D., Lisker, F., 2020. Protracted late Neoproterozoic
2371 – early Palaeozoic deformation and cooling history of Sør Rondane, East Antarctica, from
2372 40Ar/39Ar and U-Pb geochronology. Geological Magazine 158, 635–655. doi:[10.1017/s0016756820000746](https://doi.org/10.1017/s0016756820000746).
- 2374 Rusmore, M.E., Bogue, S.W., Dodson, K., Farley, K.A., Woodsworth, G.J., 2010. Deformation
2375 of continental crust along a transform boundary, Coast Mountains, British Columbia.
2376 Tectonics 29, TC4007. doi:[10.1029/2009tc002502](https://doi.org/10.1029/2009tc002502).
- 2377 Sager, W.W., Thoram, S., Engfer, D.W., Koppers, A.A.P., Class, C., 2021. Late Cretaceous
2378 Ridge Reorganization, Microplate Formation, and the Evolution of the Rio Grande Rise –
2379 Walvis Ridge Hot Spot Twins, South Atlantic Ocean. Geochemistry, Geophysics, Geosystems
2380 22. doi:[10.1029/2020gc009390](https://doi.org/10.1029/2020gc009390).
- 2381 Saha, A., Sensarma, S., Hazra, A., Ganguly, S., Peketi, A., Doley, B., Mudholkar, A.V., 2020.
2382 Imprints of ancient recycled oceanic lithosphere in heterogeneous Indian Ocean mantle: Evi-
2383 dence from petrogenesis of Carlsberg ridge basalts from Northwest Indian Ocean. Gondwana
2384 Research 86, 60–82. doi:[10.1016/j.gr.2020.05.003](https://doi.org/10.1016/j.gr.2020.05.003).
- 2385 Salminen, J., Pehrsson, S., Evans, D.A., Wang, C., 2021. Neoarchean–Paleoproterozoic super-
2386 cycles, in: Ancient Supercontinents and the Paleogeography of Earth. Elsevier, pp. 465–498.
2387 doi:[10.1016/b978-0-12-818533-9.00014-x](https://doi.org/10.1016/b978-0-12-818533-9.00014-x).
- 2388 Sanchez, G., Halpin, J.A., Gard, M., Hasterok, D., Stål, T., Raimondo, T., Peters, S., Burton-
2389 Johnson, A., 2021. PetroChron Antarctica: A geological database for interdisciplinary use.
2390 Geochemistry, Geophysics, Geosystems 22. doi:[10.1029/2021gc010154](https://doi.org/10.1029/2021gc010154).
- 2391 Sandiford, M., Hand, M., McLaren, S., 2001. Tectonic feedback, intraplate orogeny and the geo-
2392 chemical structure of the crust: a central Australian perspective, in: Miller, J., Holdsworth,
2393 J., Buick, I., Hand, M. (Eds.), Continental Reactivation and Reworking. Geological Society
2394 of London. volume 184 of *Spec. Pub.*, pp. 195–218. doi:[10.1144/gsl.sp.2001.184.01.10](https://doi.org/10.1144/gsl.sp.2001.184.01.10).
- 2395 Santos, J., Rizzotto, G., Potter, P., McNaughton, N., Matos, R., Hartmann, L., Chemale, F.,
2396 Quadros, M., 2008. Age and autochthonous evolution of the Sunsás Orogen in West Amazon
2397 Craton based on mapping and U-Pb geochronology. Precambrian Research 165, 120–152.
2398 doi:[10.1016/j.precamres.2008.06.009](https://doi.org/10.1016/j.precamres.2008.06.009).
- 2399 Saria, E., Calais, E., Stamps, D.S., Delvaux, D., Hartnady, C.J.H., 2014. Present-day kinemat-
2400 ics of the East African Rift. Journal of Geophysical Research: Solid Earth 119, 3584–3600.
2401 doi:[10.1002/2013jb010901](https://doi.org/10.1002/2013jb010901).
- 2402 Savko, K.A., Samsonov, A.V., Sal'nikova, E.B., Kotov, A.B., Bazikov, N.S., 2015. HT/LP
2403 metamorphic zoning in the eastern voronezh crystalline massif: Age and parameters of
2404 metamorphism and its geodynamic environment. Petrology 23, 559–575. doi:[10.1134/s0869591115050045](https://doi.org/10.1134/s0869591115050045).
- 2406 Scheinert, M., Ferraccioli, F., Schwabe, J., Bell, R., Studinger, M., Damaske, D., Jokat, W.,
2407 Aleshkova, N., Jordan, T., Leitchenkov, G., Blankenship, D.D., Damiani, T.M., Young,
2408 D., Cochran, J.R., Richter, T.D., 2016. New antarctic gravity anomaly grid for enhanced

- 2409 geodetic and geophysical studies in antarctica. *Geophysical Research Letters* 43, 600–610.
2410 doi:[10.1002/2015gl067439](https://doi.org/10.1002/2015gl067439).
- 2411 Schenk, C.J., Viger, R.J., Anderson, C.P., 1999. Maps showing geology, oil and gas fields and
2412 geologic provinces of the South America region. Open-file Report 97-470D. US Geological
2413 Survey. doi:[10.3133/ofr97470d](https://doi.org/10.3133/ofr97470d).
- 2414 Schepers, G., van Hinsbergen, D.J.J., Spakman, W., Kosters, M.E., Boschman, L.M., McQuar-
2415 rie, N., 2017. South-American plate advance and forced Andean trench retreat as drivers for
2416 transient flat subduction episodes. *Nature Communications* 8. doi:[10.1038/ncomms15249](https://doi.org/10.1038/ncomms15249).
- 2417 Schmid, S.M., Fügenschuh, B., Kounov, A., Małenco, L., Nievergelt, P., Oberhänsli, R.,
2418 Pleuger, J., Schefer, S., Schuster, R., Tomljenović, B., Ustaszewski, K., van Hinsbergen,
2419 D.J., 2020. Tectonic units of the Alpine collision zone between Eastern Alps and western
2420 Turkey. *Gondwana Research* 78, 308–374. doi:[10.1016/j.gr.2019.07.005](https://doi.org/10.1016/j.gr.2019.07.005).
- 2421 Schultz, M.E., Chacko, T., Heaman, L.M., Sandeman, H.A., Simonetti, A., Creaser, R.A., 2007.
2422 Queen Maud block: A newly recognized Paleoproterozoic (2.4–2.5 Ga) terrane in northwest
2423 Laurentia. *Geology* 35, 707. doi:[10.1130/g23629a.1](https://doi.org/10.1130/g23629a.1).
- 2424 Schweickert, R., Lahren, M., Smith, K., Howle, J., Ichinose, G., 2004. Transtensional deforma-
2425 tion in the Lake Tahoe region, California and Nevada, USA. *Tectonophysics* 392, 303–323.
2426 doi:[10.1016/j.tecto.2004.04.019](https://doi.org/10.1016/j.tecto.2004.04.019).
- 2427 Scrimgeour, I.R., Kinny, P.D., Close, D.F., Edgoose, C.J., 2005. High-T granulites and poly-
2428 metamorphism in the southern Arunta Region, central Australia: Evidence for a 1.64 Ga ac-
2429 cretional event. *Precambrian Research* 142, 1–27. doi:[10.1016/j.precamres.2005.08.005](https://doi.org/10.1016/j.precamres.2005.08.005).
- 2430 Sears, J.W., Price, R.A., 2003. Tightening the Siberian connection to western Laurentia.
2431 Geological Society of America Bulletin 115, 943–953. doi:[10.1130/b25229.1](https://doi.org/10.1130/b25229.1).
- 2432 Sedlock, R.L., Ortega-Gutiérrez, F., Speed, R.C., 1993. Tectonostratigraphic Terranes and
2433 Tectonic Evolution of Mexico. Geological Society of America. doi:[10.1130/spe278](https://doi.org/10.1130/spe278).
- 2434 Sengör, A.M.C., Lom, N., Zabcı, C., Sunal, G., Öner, T., 2020. Reconstructing orogens
2435 without biostratigraphy: The Saharides and continental growth during the final assembly
2436 of Gondwana-Land. *Proceedings of the National Academy of Sciences* 117, 32278–32284.
2437 doi:[10.1073/pnas.2015117117](https://doi.org/10.1073/pnas.2015117117).
- 2438 Sengör, A.M.C., Natal'in, B.A., 1996. Turkik-type orogeny and its role in the making of the
2439 continental crust. *Annual Review of Earth and Planetary Sciences* 24, 263–337. doi:[10.1146/annurev.earth.24.1.263](https://doi.org/10.1146/annurev.earth.24.1.263).
- 2441 Seton, M., Müller, R.D., Zahirovic, S., Williams, S., Wright, N.M., Cannon, J., Whittaker,
2442 J.M., Matthews, K.J., McGirr, R., 2020. A global data set of present-day oceanic crustal
2443 age and seafloor spreading parameters. *Geochemistry, Geophysics, Geosystems* 21. doi:[10.1029/2020gc009214](https://doi.org/10.1029/2020gc009214).
- 2445 Sheppard, S., Occhipinti, S., Nelson, D., 2005. Intracontinental reworking in the Capricorn
2446 Orogen, Western Australia: the 1680–1620 Ma Mangaroon Orogeny. *Australian Journal of
2447 Earth Sciences* 52, 443–460. doi:[10.1080/08120090500134589](https://doi.org/10.1080/08120090500134589).
- 2448 Sheppard, S., Rasmussen, B., Muhling, J.R., Farrell, T.R., Fletcher, I.R., 2007. Grenvillian-
2449 aged orogenesis in the Palaeoproterozoic Gascoyne Complex, Western Australia: 1030–950
2450 Ma reworking of the Proterozoic Capricorn Orogen. *Journal of Metamorphic Geology* 25,
2451 477–494. doi:[10.1111/j.1525-1314.2007.00708.x](https://doi.org/10.1111/j.1525-1314.2007.00708.x).

- 2452 Shi, X., Tapponnier, P., Wang, T., Wei, S., Wang, Y., Wang, X., Jiao, L., 2019. Triple
2453 junction kinematics accounts for the 2016 Mw7.8 Kaikoura earthquake rupture complexity.
2454 Proceedings of the National Academy of Sciences 116, 26367–26375. doi:[10.1073/pnas.1916770116](https://doi.org/10.1073/pnas.1916770116).
- 2455
- 2456 da Silva Schmitt, R., de Araújo Fragoso, R., Collins, A.S., 2018. Suturing Gondwana in the
2457 Cambrian: The orogenic events of the final amalgamation, in: Regional Geology Reviews.
2458 Springer International Publishing, pp. 411–432. doi:[10.1007/978-3-319-68920-3_15](https://doi.org/10.1007/978-3-319-68920-3_15).
- 2459 Sobh, M., Ebbing, J., Mansi, A.H., Götze, H.J., Emry, E.L., Abdelsalam, M.G., 2020. The
2460 lithospheric structure of the saharan metacraton from 3-d integrated geophysical-petrological
2461 modeling. Journal of Geophysical Research: Solid Earth 125. doi:[10.1029/2019jb018747](https://doi.org/10.1029/2019jb018747).
- 2462 Song, D., Xiao, W., Collins, A.S., Glorie, S., Han, C., Li, Y., 2018. Final subduction processes
2463 of the Paleo-Asian Ocean in the Alxa Tectonic Belt (NW China): Constraints from field and
2464 chronological data of Permian arc-related volcano-sedimentary rocks. Tectonics 37, 1658–
2465 1687. doi:[10.1029/2017tc004919](https://doi.org/10.1029/2017tc004919).
- 2466 Song, D., Xiao, W., Windley, B.F., Mao, Q., Ao, S., Wang, H.Y.C., Li, R., 2021. Closure
2467 of the Paleo-Asian Ocean in the Middle-Late Triassic (Ladinian-Carnian): Evidence from
2468 provenance analysis of retroarc sediments. Geophysical Research Letters 48. doi:[10.1029/2021gl094276](https://doi.org/10.1029/2021gl094276).
- 2469
- 2470 Spaggiari, C.V., Smithies, R.H., Kirkland, C.L., Wingate, M.T., England, R.N., Lu, Y.J.,
2471 2018. Buried but preserved: The Proterozoic Arubiddy Ophiolite, Madura Province, Western
2472 Australia. Precambrian Research 317, 137–158. doi:[10.1016/j.precamres.2018.08.025](https://doi.org/10.1016/j.precamres.2018.08.025).
- 2473 St-Onge, M.R., Searle, M.P., Wodicka, N., 2006. Trans-Hudson Orogen of North America and
2474 Himalaya-Karakoram-Tibetan Orogen of Asia: Structural and thermal characteristics of the
2475 lower and upper plates. Tectonics 25, n/a–n/a. doi:[10.1029/2005tc001907](https://doi.org/10.1029/2005tc001907).
- 2476 Stagg, H., Alcock, M., Borissova, I., Moore, A., 2002. Geological framework of the southern
2477 Lord Howe Rise and adjacent areas. Record 2002/25. Geoscience Australia. Canberra.
- 2478 Stål, T., Reading, A.M., Halpin, J.A., Whittaker, J.M., 2019. A multivariate approach for
2479 mapping lithospheric domain boundaries in East Antarctica. Geophysical Research Letters
2480 46, 10404–10416. doi:[10.1029/2019gl083453](https://doi.org/10.1029/2019gl083453).
- 2481 Stampfli, G., Hochard, C., Vérard, C., Wilhem, C., vonRaumer, J., 2013. The formation of
2482 Pangea. Tectonophysics 593, 1–19. doi:[10.1016/j.tecto.2013.02.037](https://doi.org/10.1016/j.tecto.2013.02.037).
- 2483 Stamps, D., Kreemer, C., Fernandes, R., Rajaonarison, T., Rambolamanana, G., 2021. Re-
2484 defining East African Rift System kinematics. Geology 49, 150–155. doi:[10.1130/g47985.1](https://doi.org/10.1130/g47985.1).
- 2485 Stamps, D.S., Saria, E., Kreemer, C., 2018. A geodetic strain rate model for the East African
2486 Rift system. Scientific Reports 8. doi:[10.1038/s41598-017-19097-w](https://doi.org/10.1038/s41598-017-19097-w).
- 2487 Steinshouer, D.W., Qiang, J., McCabe, P.J., Ryder, R.T., 1999. Maps showing geology, oil and
2488 gas fields, and geologic provinces of the Asia Pacific region. Open-file Report 97-470F. US
2489 Geological Survey. doi:[10.3133/ofr97470f](https://doi.org/10.3133/ofr97470f).
- 2490 Stern, R.J., 1994. Arc assembly and continental collision in the Neoproterozoic East African
2491 Orogen: Implications for the consolidation of Gondwanaland. Annual Review of Earth and
2492 Planetary Sciences 22, 319–351. doi:[10.1146/annurev.ea.22.050194.001535](https://doi.org/10.1146/annurev.ea.22.050194.001535).

- 2493 Straume, E.O., Gaina, C., Medvedev, S., Hochmuth, K., Gohl, K., Whittaker, J.M., Fattah,
2494 R.A., Doornenbal, J.C., Hopper, J.R., 2019. GlobSed: Updated total sediment thickness
2495 in the world's oceans. *Geochemistry, Geophysics, Geosystems* 20, 1756–1772. doi:[10.1029/2018gc008115](https://doi.org/10.1029/2018gc008115).
- 2497 Styron, R., Pagani, M., 2020. The GEM global active faults database. *Earthquake Spectra* 36,
2498 160–180. doi:[10.1177/8755293020944182](https://doi.org/10.1177/8755293020944182).
- 2499 Sun, L., Mann, P., Bird, D.E., 2020. Integration of tectonic geomorphology and crustal struc-
2500 ture across the active obliquely collisional zone on the island of Hispaniola, northeastern
2501 Caribbean. Geological Society, London, Special Publications , SP504–2019–242doi:[10.1144/sp504-2019-242](https://doi.org/10.1144/sp504-2019-242).
- 2502 Symeou, V., Homberg, C., Nader, F.H., Darnault, R., Lecomte, J.C., Papadimitriou, N., 2018.
2503 Longitudinal and temporal evolution of the tectonic style along the Cyprus Arc system,
2504 assessed through 2-D reflection seismic interpretation. *Tectonics* 37, 30–47. doi:[10.1002/2017tc004667](https://doi.org/10.1002/2017tc004667).
- 2505 Szwilus, W., Afonso, J.C., Ebbing, J., Mooney, W.D., 2019. Global crustal thickness and ve-
2506 locity structure from geostatistical analysis of seismic data. *Journal of Geophysical Research: Solid Earth* 124, 1626–1652. doi:[10.1029/2018jb016593](https://doi.org/10.1029/2018jb016593).
- 2507 Tagami, T., Hasebe, N., 1999. Cordilleran-type orogeny and episodic growth of continents:
2508 Insights from the circum-pacific continental margins. *Island Arc* 8, 206–217. doi:[10.1046/j.1440-1738.1999.00232.x](https://doi.org/10.1046/j.1440-1738.1999.00232.x).
- 2510 Tamblyn, R., Hasterok, D., Hand, M., Gard, M., 2021. Mantle heating at ca. 2 Ga by continental
2511 insulation: Evidence from granites and eclogites. *Geology* 50, 91–95. doi:[10.1130/g49288.1](https://doi.org/10.1130/g49288.1).
- 2513 Tang, M., Ji, W.Q., Chu, X., Wu, A., Chen, C., 2020. Reconstructing crustal thickness evolution
2514 from europium anomalies in detrital zircons. *Geology* 49, 76–80. doi:[10.1130/g47745.1](https://doi.org/10.1130/g47745.1).
- 2515 Tetley, M.G., Li, Z.X., Matthews, K.J., Williams, S.E., Müller, R.D., 2020. Decoding Earth's
2516 plate tectonic history using sparse geochemical data. *Geoscience Frontiers* 11, 265–276.
2517 doi:[10.1016/j.gsf.2019.05.002](https://doi.org/10.1016/j.gsf.2019.05.002).
- 2518 Thiessen, E.J., Gibson, H.D., Regis, D., Pehrsson, S.J., 2018. Deformation and extensional
2519 exhumation of 1.9 Ga high-pressure granulites along the Wholdaia Lake shear zone, south
2520 Rae craton, Northwest Territories, Canada. *Lithosphere* 10, 641–661. doi:[10.1130/l1704.1](https://doi.org/10.1130/l1704.1).
- 2521 Tiddy, C.J., Betts, P.G., Neumann, M.R., Murphy, F.C., Stewart, J., Giles, D., Sawyer, M.,
2522 Freeman, H., Jourdan, F., 2020. Interpretation of a ca. 1600–1580 Ma metamorphic core
2523 complex in the northern Gawler Craton, Australia. *Gondwana Research* 85, 263–290. doi:[10.1016/j.gr.2020.04.008](https://doi.org/10.1016/j.gr.2020.04.008).
- 2524 Tohver, E., Teixeira, W., van der Pluijm, B., Geraldes, M.C., Bettencourt, J.S., Rizzotto, G.,
2525 2006. Restored transect across the exhumed Grenville orogen of Laurentia and Amazonia,
2526 with implications for crustal architecture. *Geology* 34, 669. doi:[10.1130/g22534.1](https://doi.org/10.1130/g22534.1).
- 2527 Topuz, G., Candan, O., Okay, A.I., von Quadt, A., Othman, M., Zack, T., Wang, J., 2020.
2528 Silurian anorogenic basic and acidic magmatism in Northwest Turkey: Implications for the
2529 opening of the Paleo-Tethys. *Lithos* 356-357, 105302. doi:[10.1016/j.lithos.2019.105302](https://doi.org/10.1016/j.lithos.2019.105302).

- 2533 Torsvik, T.H., Amundsen, H., Hartz, E.H., Corfu, F., Kusznir, N., Gaina, C., Doubrovine,
2534 P.V., Steinberger, B., Ashwal, L.D., Jamtveit, B., 2013. A Precambrian microcontinent in
2535 the Indian Ocean. *Nature Geoscience* 6, 223–227. doi:[10.1038/ngeo1736](https://doi.org/10.1038/ngeo1736).
- 2536 Torsvik, T.H., Andersen, T.B., 2002. The Taimyr fold belt, Arctic Siberia: timing of pre-
2537 fold remagnetisation and regional tectonics. *Tectonophysics* 352, 335–348. doi:[10.1016/s0040-1951\(02\)00274-3](https://doi.org/10.1016/s0040-1951(02)00274-3).
- 2539 Torsvik, T.H., Cocks, L.R.M., 2016. *Earth History and Palaeogeography*. Cambridge University
2540 Press. doi:[10.1017/9781316225523](https://doi.org/10.1017/9781316225523).
- 2541 Tretiakova, I.G., Belousova, E.A., Malkovets, V.G., Griffin, W.L., Piazolo, S., Pearson, N.J.,
2542 O'Reilly, S.Y., Nishido, H., 2017. Recurrent magmatic activity on a lithosphere-scale struc-
2543 ture: Crystallization and deformation in kimberlitic zircons. *Gondwana Research* 42, 126–
2544 132. doi:[10.1016/j.gr.2016.10.006](https://doi.org/10.1016/j.gr.2016.10.006).
- 2545 Tuisku, P., Huhma, H., 2006. Evolution of migmatitic granulite complexes: Implications from
2546 Lapland Granulite Belt, Part II: Isotopic dating. *Bulletin of the Geological Society of Finland*
2547 78, 143–175. doi:[10.17741/bgsf/78.2.003](https://doi.org/10.17741/bgsf/78.2.003).
- 2548 Ueki, K., Hino, H., Kuwatani, T., 2018. Geochemical discrimination and characteristics of
2549 magmatic tectonic settings: A machine-learning-based approach. *Geochemistry, Geophysics,*
2550 *Geosystems* 19, 1327–1347. doi:[10.1029/2017gc007401](https://doi.org/10.1029/2017gc007401).
- 2551 Ustaszewski, K., Kounov, A., Schmid, S.M., Schaltegger, U., Krenn, E., Frank, W., Fügenschuh,
2552 B., 2010. Evolution of the Adria-Europe plate boundary in the northern Dinarides: From
2553 continent-continent collision to back-arc extension. *Tectonics* 29, n/a–n/a. doi:[10.1029/2010tc002668](https://doi.org/10.1029/2010tc002668).
- 2555 Vaes, B., Hinsbergen, D.J.J., Boschman, L.M., 2019. Reconstruction of subduction and back-
2556 arc spreading in the NW Pacific and Aleutian Basin: Clues to causes of Cretaceous and
2557 Eocene plate reorganizations. *Tectonics* 38, 1367–1413. doi:[10.1029/2018tc005164](https://doi.org/10.1029/2018tc005164).
- 2558 Vallini, D.A., Cannon, W.F., Schulz, K.J., McNaughton, N.J., 2007. Thermal history of low
2559 metamorphic grade Paleoproterozoic sedimentary rocks of the Penokean orogen, Lake Su-
2560 perior region: Evidence for a widespread 1786Ma overprint based on xenotime geochronology.
2561 *Precambrian Research* 157, 169–187. doi:[10.1016/j.precamres.2007.02.015](https://doi.org/10.1016/j.precamres.2007.02.015).
- 2562 Vernikovsky, V., Vernikovskaya, A., Wingate, M., Popov, N., Kovach, V., 2007. The 880–
2563 864Ma granites of the Yenisey Ridge, western Siberian margin: Geochemistry, SHRIMP
2564 geochronology, and tectonic implications. *Precambrian Research* 154, 175–191. doi:[10.1016/j.precamres.2006.12.006](https://doi.org/10.1016/j.precamres.2006.12.006).
- 2566 Vernikovsky, V.A., Vernikovskaya, A., Kotov, A., Sal'nikova, E., Kovach, V., 2003. Neopro-
2567 terozoic accretionary and collisional events on the western margin of the Siberian craton:
2568 new geological and geochronological evidence from the Yenisey Ridge. *Tectonophysics* 375,
2569 147–168. doi:[10.1016/s0040-1951\(03\)00337-8](https://doi.org/10.1016/s0040-1951(03)00337-8).
- 2570 Volante, S., Pourteau, A., Collins, W.J., Blereau, E., Li, Z.X., Smit, M., Evans, N.J., Nordsvan,
2571 A.R., Spencer, C.J., McDonald, B.J., Li, J., Günter, C., 2020. Multiple P–T–d–t paths reveal
2572 the evolution of the final Nuna assembly in northeast Australia. *Journal of Metamorphic*
2573 *Geology* 38, 593–627. doi:[10.1111/jmg.12532](https://doi.org/10.1111/jmg.12532).

- 2574 Wan, Y., Liu, D., Dong, C., Liu, S., Wang, S., Yang, E., 2011. U–Th–Pb behavior of zircons
2575 under high-grade metamorphic conditions: A case study of zircon dating of meta-diorite near
2576 Qixia, eastern Shandong. *Geoscience Frontiers* 2, 137–146. doi:[10.1016/j.gsf.2011.02.004](https://doi.org/10.1016/j.gsf.2011.02.004).
- 2578 Wandrey, C.J., Law, B.E., 1998. Maps showing geology, oil and gas fields and geologic provinces
2579 of South Asia. Open-file Report 97-470C. US Geological Survey. doi:[10.3133/ofr97470c](https://doi.org/10.3133/ofr97470c).
- 2580 Wang, C., Li, Z.X., Peng, P., Pisarevsky, S., Liu, Y., Kirscher, U., Nordsvan, A., 2019. Long-
2581 lived connection between the north china and north australian cratons in supercontinent
2582 nuna: paleomagnetic and geological constraints. *Science Bulletin* 64, 873–876. doi:[10.1016/j.scib.2019.04.028](https://doi.org/10.1016/j.scib.2019.04.028).
- 2584 Wang, C.C., Jacobs, J., Elburg, M.A., Läufer, A., Thomas, R.J., Elvevold, S., 2020. Grenville-
2585 age continental arc magmatism and crustal evolution in central Dronning Maud Land (East
2586 Antarctica): Zircon geochronological and Hf–O isotopic evidence. *Gondwana Research* 82,
2587 108–127. doi:[10.1016/j.gr.2019.12.004](https://doi.org/10.1016/j.gr.2019.12.004).
- 2588 Wang, Y., Fan, W., Zhang, G., Zhang, Y., 2013. Phanerozoic tectonics of the South China
2589 Block: Key observations and controversies. *Gondwana Research* 23, 1273–1305. doi:[10.1016/j.gr.2012.02.019](https://doi.org/10.1016/j.gr.2012.02.019).
- 2591 Weber, F., Gauthier-Lafaye, F., Whitechurch, H., Ulrich, M., Albani, A.E., 2016. The 2-Ga
2592 Eburnean Orogeny in Gabon and the opening of the Francevillian intracratonic basins: A
2593 review. *Comptes Rendus Geoscience* 348, 572–586. doi:[10.1016/j.crte.2016.07.003](https://doi.org/10.1016/j.crte.2016.07.003).
- 2594 Wedmore, L.N.J., Biggs, J., Floyd, M., Fagereng, Å., Mdala, H., Chindandali, P., Williams,
2595 J.N., Mphepo, F., 2021. Geodetic constraints on cratonic microplates and broad strain during
2596 rifting of thick southern African lithosphere. *Geophysical Research Letters* 48. doi:[10.1029/2021gl093785](https://doi.org/10.1029/2021gl093785).
- 2598 Weller, O.M., Mottram, C.M., St-Onge, M.R., Möller, C., Strachan, R., Rivers, T., Copley, A.,
2599 2021. The metamorphic and magmatic record of collisional orogens. *Nature Reviews Earth & Environment* 2, 781–799. doi:[10.1038/s43017-021-00218-z](https://doi.org/10.1038/s43017-021-00218-z).
- 2601 Weller, O.M., St-Onge, M.R., 2017. Record of modern-style plate tectonics in the palaeoproterozoic trans-hudson orogen. *Nature Geoscience* 10, 305–311. doi:[10.1038/ngeo2904](https://doi.org/10.1038/ngeo2904).
- 2603 Whalen, J.B., Berman, R.G., Davis, W.J., Sanborn-Barrie, M., Nadeau, L., 2018. Bedrock
2604 geochemistry of the central Thelon Tectonic Zone, Nunavut. Technical Report. doi:[10.4095/306385](https://doi.org/10.4095/306385).
- 2606 Whattam, S.A., Stern, R.J., 2015. Late Cretaceous plume-induced subduction initiation along
2607 the southern margin of the Caribbean and NW South America: The first documented ex-
2608 ample with implications for the onset of plate tectonics. *Gondwana Research* 27, 38–63.
2609 doi:[10.1016/j.gr.2014.07.011](https://doi.org/10.1016/j.gr.2014.07.011).
- 2610 White, L.F., Bailey, I., Foster, G.L., Allen, G., Kelley, S.P., Andrews, J.T., Hogan, K.,
2611 Dowdeswell, J.A., Storey, C.D., 2016. Tracking the provenance of Greenland-sourced,
2612 Holocene aged, individual sand-sized ice rafted debris using the Pb-isotope compositions
2613 of feldspars and $^{40}\text{Ar}/^{39}\text{Ar}$ ages of hornblendes. *Earth and Planetary Science Letters* 433,
2614 192–203. doi:[10.1016/j.epsl.2015.10.054](https://doi.org/10.1016/j.epsl.2015.10.054).
- 2615 Whitmeyer, S., Karlstrom, K.E., 2007. Tectonic model for the Proterozoic growth of North
2616 America. *Geosphere* 3, 220. doi:[10.1130/ges00055.1](https://doi.org/10.1130/ges00055.1).

- 2617 Wiens, D.A., DeMets, C., Gordon, R.G., Stein, S., Argus, D., Engeln, J.F., Lundgren, P.,
2618 Quible, D., Stein, C., Weinstein, S., Woods, D.F., 1985. A diffuse plate boundary model
2619 for Indian Ocean tectonics. *Geophysical Research Letters* 12, 429–432. doi:[10.1029/g1012i007p00429](https://doi.org/10.1029/g1012i007p00429).
- 2621 Wilde, S.A., Zhao, G., Sun, M., 2002. Development of the North China Craton during the late
2622 Archaean and its final amalgamation at 1.8 Ga: some speculations on its position within
2623 a global palaeoproterozoic supercontinent. *Gondwana Research* 5, 85–94. doi:[10.1016/s1342-937x\(05\)70892-3](https://doi.org/10.1016/s1342-937x(05)70892-3).
- 2625 Willner, A.P., Gopon, M., Glodny, J., Puchkov, V.N., Schertl, H.P., 2019. Timanide (Ediacaran-
2626 Early Cambrian) metamorphism at the transition from eclogite to amphibolite facies in the
2627 Beloretsk Complex, SW-Urals, Russia. *Journal of Earth Science* 30, 1144–1165. doi:[10.1007/s12583-019-1249-2](https://doi.org/10.1007/s12583-019-1249-2).
- 2629 Winberry, J.P., Anandakrishnan, S., 2004. Crustal structure of the West Antarctic rift system
2630 and Marie Byrd Land hotspot. *Geology* 32, 977. doi:[10.1130/g20768.1](https://doi.org/10.1130/g20768.1).
- 2631 Windley, B.F., Alexeiev, D., Xiao, W., Kröner, A., Badarch, G., 2007. Tectonic models for
2632 accretion of the Central Asian Orogenic Belt. *Journal of the Geological Society* 164, 31–47.
2633 doi:[10.1144/0016-76492006-022](https://doi.org/10.1144/0016-76492006-022).
- 2634 Wingate, M.T.D., Pisarevsky, S.A., Evans, D.A.D., 2002. Rodinia connections between Aus-
2635 tralia and Laurentia: no SWEAT, no AUSWUS? *Terra Nova* 14, 121–128. doi:[10.1046/j.1365-3121.2002.00401.x](https://doi.org/10.1046/j.1365-3121.2002.00401.x).
- 2637 Wong, B.L., Morrissey, L.J., Hand, M., Fields, C.E., Kelsey, D.E., 2015. Grenvillian-aged
2638 reworking of late Paleoproterozoic crust of the southern North Australian Craton, central
2639 Australia: Implications for the assembly of Mesoproterozoic Australia. *Precambrian Research*
2640 270, 100–123. doi:[10.1016/j.precamres.2015.09.001](https://doi.org/10.1016/j.precamres.2015.09.001).
- 2641 Wu, F.Y., Yang, J.H., Xu, Y.G., Wilde, S.A., Walker, R.J., 2019. Destruction of the North
2642 China Craton in the Mesozoic. *Annual Review of Earth and Planetary Sciences* 47, 173–195.
2643 doi:[10.1146/annurev-earth-053018-060342](https://doi.org/10.1146/annurev-earth-053018-060342).
- 2644 Wu, J.L., Zhang, H.F., Zhai, M.G., Guo, J.H., Liu, L., Yang, W.Q., Wang, H.Z., Zhao, L.,
2645 Jia, X.L., Wang, W., 2016. Discovery of pelitic high-pressure granulite from Manjinggou
2646 of the Huai'an Complex, North China Craton: Metamorphic P-T evolution and geological
2647 implications. *Precambrian Research* 278, 323–336. doi:[10.1016/j.precamres.2016.03.001](https://doi.org/10.1016/j.precamres.2016.03.001).
- 2648 Wynne, P., Bacchin, M., 2009. Index of Gravity Surveys (Second Edition). Geoscience Australia
2649 Record 2009/07. Geoscience Australia. Canberra, Australia.
- 2650 Xiao, W., Windley, B.F., Sun, S., Li, J., Huang, B., Han, C., Yuan, C., Sun, M., Chen, H.,
2651 2015. A Tale of Amalgamation of Three Permo-Triassic Collage Systems in Central Asia:
2652 Oroclines, Sutures, and Terminal Accretion. *Annual Review of Earth and Planetary Sciences*
2653 43, 477–507. doi:[10.1146/annurev-earth-060614-105254](https://doi.org/10.1146/annurev-earth-060614-105254).
- 2654 Xu, Y., Zeyen, H., Hao, T., Santosh, M., Li, Z., Huang, S., Xing, J., 2016. Lithospheric structure
2655 of the North China Craton: Integrated gravity, geoid and topography data. *Gondwana
2656 Research* 34, 315–323. doi:[10.1016/j.gr.2015.03.010](https://doi.org/10.1016/j.gr.2015.03.010).

- 2657 Yang, B., Collins, A.S., Blades, M.L., Munson, T.J., Payne, J.L., Glorie, S., Farkaš, J., 2020.
2658 Tectonic controls on sedimentary provenance and basin geography of the Mesoproterozoic
2659 Wilton package, McArthur Basin, northern Australia. *Geological Magazine* 159, 179–198.
2660 doi:[10.1017/s0016756820001223](https://doi.org/10.1017/s0016756820001223).
- 2661 Yang, J.H., Zhang, M., Wu, F.Y., 2018. Mesozoic decratonization of the North China Craton
2662 by lithospheric delamination: Evidence from Sr-Nd-Hf-Os isotopes of mantle xenoliths of
2663 Cenozoic alkaline basalts in Yangyuan, Hebei Province, China. *Journal of Asian Earth
2664 Sciences* 160, 396–407. doi:[10.1016/j.jseaes.2017.09.002](https://doi.org/10.1016/j.jseaes.2017.09.002).
- 2665 Yin, A., Brandl, G., Kröner, A., 2019. Plate-tectonic processes at ca. 2.0 Ga: Evidence from
2666 >600 km of plate convergence. *Geology* 48, 103–107. doi:[10.1130/g47070.1](https://doi.org/10.1130/g47070.1).
- 2667 Yin, C., Zhao, G., Wei, C., Sun, M., Guo, J., Zhou, X., 2014. Metamorphism and partial
2668 melting of high-pressure pelitic granulites from the qianlishan complex: Constraints on the
2669 tectonic evolution of the khondalite belt in the north china craton. *Precambrian Research*
2670 242, 172–186. doi:[10.1016/j.precamres.2013.12.025](https://doi.org/10.1016/j.precamres.2013.12.025).
- 2671 Zahirovic, S., Seton, M., Müller, R.D., 2014. The Cretaceous and Cenozoic tectonic evolution
2672 of Southeast Asia. *Solid Earth* 5, 227–273. doi:[10.5194/se-5-227-2014](https://doi.org/10.5194/se-5-227-2014).
- 2673 Žák, J., Verner, K., Janoušek, V., Holub, F.V., Kachlík, V., Finger, F., Hajná, J., Tomek, F.,
2674 Vondrovic, L., Trubač, J., 2014. A plate-kinematic model for the assembly of the Bohemian
2675 Massif constrained by structural relationships around granitoid plutons. *Geological Society,
2676 London, Special Publications* 405, 169–196. doi:[10.1144/sp405.9](https://doi.org/10.1144/sp405.9).
- 2677 Zhang, S., Li, Z.X., Evans, D.A., Wu, H., Li, H., Dong, J., 2012. Pre-Rodinia supercontinent
2678 Nuna shaping up: A global synthesis with new paleomagnetic results from North China.
2679 *Earth and Planetary Science Letters* 353-354, 145–155. doi:[10.1016/j.epsl.2012.07.034](https://doi.org/10.1016/j.epsl.2012.07.034).
- 2680 Zhang, S.H., Ernst, R.E., Munson, T.J., Pei, J., Hu, G., Liu, J.M., Zhang, Q.Q., Cai, Y.H.,
2681 Zhao, Y., 2022. Comparisons of the Paleo-Mesoproterozoic large igneous provinces and black
2682 shales in the North China and North Australian cratons. *Fundamental Research* 2, 84–100.
2683 doi:[10.1016/j.fmre.2021.10.009](https://doi.org/10.1016/j.fmre.2021.10.009).
- 2684 Zhang, T., Gordon, R.G., Mishra, J.K., Wang, C., 2017. The Malpelo Plate Hypothesis and
2685 implications for nonclosure of the Cocos-Nazca-Pacific plate motion circuit. *Geophysical
2686 Research Letters* 44, 8213–8218. doi:[10.1002/2017gl073704](https://doi.org/10.1002/2017gl073704).
- 2687 Zhang, Z., Shu, Q., Yang, X., Wu, C., Zheng, C., Xu, J., 2019. Review on the tectonic terranes
2688 associated with metallogenic zones in southeast asia. *Journal of Earth Science* 30, 1–19.
2689 doi:[10.1007/s12583-019-0858-0](https://doi.org/10.1007/s12583-019-0858-0).
- 2690 Zhao, G., Cawood, P.A., Li, S., Wilde, S.A., Sun, M., Zhang, J., He, Y., Yin, C., 2012.
2691 Amalgamation of the North China Craton: Key issues and discussion. *Precambrian Research*
2692 222-223, 55–76. doi:[10.1016/j.precamres.2012.09.016](https://doi.org/10.1016/j.precamres.2012.09.016).
- 2693 Zhao, G., Cawood, P.A., Wilde, S.A., Sun, M., 2002. Review of global 2.1–1.8 Ga orogens:
2694 implications for a pre-Rodinia supercontinent. *Earth-Science Reviews* 59, 125–162. doi:[10.1016/S0012-8252\(02\)00073-9](https://doi.org/10.1016/S0012-8252(02)00073-9).
- 2696 Zhao, G., Li, S., Sun, M., Wilde, S.A., 2011. Assembly, accretion, and break-up of the Palaeo-
2697 Mesoproterozoic Columbia supercontinent: record in the North China Craton revisited. *International
2698 Geology Review* 53, 1331–1356. doi:[10.1080/00206814.2010.527631](https://doi.org/10.1080/00206814.2010.527631).

2699 wei Zhou, H., Murphy, M.A., 2005. Tomographic evidence for wholesale underthrusting of
2700 India beneath the entire Tibetan plateau. Journal of Asian Earth Sciences 25, 445–457.
2701 doi:[10.1016/j.jseaes.2004.04.007](https://doi.org/10.1016/j.jseaes.2004.04.007).

2702 Zi, J.W., Sheppard, S., Muhling, J.R., Rasmussen, B., 2021. Refining the Paleoproterozoic tectonothermal history of the Penokean Orogen: New U-Pb age constraints from the
2703 Pembine-Wausau terrane, Wisconsin, USA. GSA Bulletin doi:[10.1130/b36114.1](https://doi.org/10.1130/b36114.1).
2704